STUDI STABILITAS LERENG EFEK DARI INTENSITAS HUJAN TERHADAP PENINGKATAN KADAR AIR DAN INDEK KECAIRAN TANAH DENGAN PEMODELAN LABORATORIUM

DISERTASI

Oleh:

<u>Nofrizal</u>
NIM.1830922013

Promotor:

Prof.Dr.Eng.Fauzan, S.T, M.Sc (Eng)
Prof. Abdul Hakam, M.T, Ph.D
Prof.Dr.Bambang Istijono, M.E

PROGRAM STUDI DOKTOR TEKNIK SIPIL
DEPARTEMEN TEKNIK SIPIL
FAKULTAS TEKNIK
UNIVERSITAS ANDALAS

2026

PERSETUJUAN UJIAN TERTUTUP

Yang bertanda tangan dibawah ini komisi pembimbing di Program Studi Doktor Teknik Sipil Departemen Teknik Sipil Universitas Andalas :

Nama Promotor : **Prof.Dr.Eng.Fauzan, S.T, M.Sc (Eng)**

Nama Ko-promotor 1 : **Prof. Abdul Hakam, M.T, Ph.D**

Nama Ko-promotor 2 : **Prof.Dr.Bambang Istijono, M.E**

Sebagai Promotor dan Ko-promotor dari mahasiswa berikut:

Nama : Nofrizal

NIM : 1830922013

Dengan judul disertasi sebagai berikut :

Studi Stabilitas Lereng Efek Dari Intensitas Hujan Terhadap Peningkatan Kadar Air Dan Indek Kecairan Tanah Dengan Pemodelan Laboratorium

Menyatakan bahwa Disertasi mahasiswa tersebut telah disetujui dan dapat dilakukan **Ujian tertutup**

Padang, 27Januari 2026

PROMOTOR

Prof. Dr.Eng. Ir. Fauzan, S.T., M.Sc(Eng).
NIP. 197406121998021002

KO-PROMOTOR 1

Prof. Ir. Abdul Hakam, M.T., Ph.D.
NIP. 196812261992031002

KO-PROMOTOR 2

Prof. Dr. Bambang Istijono, M.E.
NIP. 195205141976031005

Diketahui,
Ketua Departemen Teknik Sipil

Ir. Sabril Haris HG, S.T., M.T., Ph.D.
NIP. 197610012000121003

ABSTRAK

Kegagalan lereng atau longsoran tanah merupakan salah satu bencana geoteknik yang sering terjadi, terutama di wilayah tropis dengan intensitas curah hujan tinggi seperti Indonesia. Salah satu faktor utama penyebab ketidakstabilan lereng adalah peningkatan kadar air tanah yang menyebabkan perubahan sifat fisik dan mekanik tanah, terutama terhadap kohesi dan kekuatan geser. Masalah utama yang ingin diselesaikan dalam penelitian ini adalah bagaimana hubungan antara sudut geometri lereng, kadar air tanah, dan indeks kecairan tanah (Liquidity Index/LI) dalam mempengaruhi kestabilan lereng, serta bagaimana parameter Likuid Indek tanah dapat digunakan sebagai indikator prediksi dini terhadap potensi longsor. Penelitian ini bertujuan untuk menganalisis pengaruh peningkatan kadar air tanah terhadap nilai Liquid Limit (LL) dan indeks kecairan tanah pada kestabilan lereng melalui pemodelan laboratorium. Metodologi yang digunakan meliputi pengambilan sampel tanah dari lokasi bencana longsor di kawasan Talamau, Pasaman, kemudian dilakukan uji laboratorium untuk memperoleh parameter-parameter tanah seperti Atterberg Limit (LL, PL, PI), kadar air, dan nilai Liquidity Index (LI), serta melakukan simulasi keruntuhan lereng dalam skala laboratorium dengan variasi sudut kemiringan lereng 30°, 45°, 60°, dan 90°. Hasil penelitian menunjukkan bahwa peningkatan kadar air tanah sebagai respons dari curah hujan secara langsung meningkatkan nilai LI; ketika kadar air mendekati atau melampaui LL, tanah masuk ke dalam kondisi cair (LI > 1), kehilangan kohesi, dan sangat berpotensi mengalami kelongsoran dalam bentuk longsoran aliran (flow slide). Nilai LI yang tinggi ditemukan pada lereng curam (60° dan 90°), yang menunjukkan bahwa geometri lereng berpengaruh signifikan terhadap percepatan kegagalan. Penelitian ini juga berhasil memetakan grafik hubungan antara kadar air tanah dan nilai LI terhadap potensi keruntuhan lereng untuk setiap variasi sudut lereng, yang memperkuat peran LI sebagai indikator kuantitatif untuk sistem peringatan dini longsor. Kontribusi utama dari penelitian ini adalah memberikan pemahaman baru tentang hubungan dinamis antara kadar air, geometri lereng, dan indeks kecairan tanah serta pemanfaatannya sebagai alat prediksi keruntuhan lereng berbasis data laboratorium. Validasi dilakukan melalui pengulangan eksperimen, perbandingan dengan literatur terdahulu, dan korelasi hasil dengan model teoritis keruntuhan tanah. Hasil validasi menunjukkan konsistensi dan keandalan parameter LI dalam berbagai kondisi geometri dan kejenuhan tanah, sehingga mendukung rekomendasi penggunaan nilai LI > 1 sebagai batas kritis ketidakstabilan lereng. Penelitian ini memberikan dasar ilmiah bagi strategi mitigasi bencana longsor dan pemantauan risiko lereng berbasis perubahan kadar air tanah dan parameter indeks kecairan.

Kata Kunci : Kadar air tanah, Indek kecairan tanah, dan Kegagalan lereng

KATA PENGANTAR

Penulis mengucapkan puji syukur kepada Tuhan Yang Maha Kuasa yang telah memberikan berkat-Nya kepada penulis sehingga penulis dapat menyelesaikan penulisan laporan disertasi pada ujian tertutup yang berjudul : **“Studi Stabilitas Lereng Efek Dari Intensitas Hujan Terhadap Peningkatan Kadar Air Dan Indek Kecairan Tanah Dengan Pemodelan Laboratorium”**. Ujian tertutup Disertasi ini merupakan salah satu rangkaian dari studi pada Program Doktor Teknik Sipil Universitas andalas.

Pada kesempatan ini penulis ingin menyampaikan terimakasih kepada semua pihak yang telah memberikan dukungan moril maupun materil sehingga dalam penulisan laporan Ujian tertutup disertasi ini dapat diselesaikan. Ucapan terima kasih yang tulus penulis tujukan kepada Bapak Prof. Dr.Eng. Fauzan, S.T, M.Sc (Eng), selaku Promotor, dan Bapak Prof. Abdul Hakam, M.T, Ph.D, selaku Ko Pomotor – 1, dan Bapak Prof.Dr. Bambang Istijono, M.E, selaku Ko Promotor – 2, atas segala bimbingan dan motivasi yang diberikan. Laporan ujian tertutup disertasi ini masih banyak kekurangannya, oleh karena itu penulis mengharapkan kritik, saran, dan masukan yang membangun guna kesempurnaan dari segala kekurangannya.

Padang, Januari 2026

Penulis,

DAFTAR PUBLIKASI

Pablis :

Nofrizal, Fauzan, Hakam.A, Istijono.B[3], & Aprijal (2025).Analysis of The Effect Of Rainfal Intensity And Slope Steepnes On Landslide Disaster. Accepted to Civil and Envoromental Engineering Journal.(Scopus Q3) : **https://sciendo.com/article/10.2478/cee-2025-0073**

Accepted:

Nofrizal , Fauzan, Hakam.A, Istijono.B , Setiawan.A , & Aprisal (2026). Effects Of Increasing Soil Water Content On Liquidity Index And Slope Failure Potential Through laboratory Modelling (ID Paper:g 15395)

Pablis :

Nofrizal, Fauzan, Abdul Hakam. Bambang Istijono, Andriani Setiawan, Aprisal. Laboratory Study of Geotechnical Characteristics of Soil in LandslideProne Zone in Talamau District, West Pasaman Regency. Journal of Science Education Research *Journal of Research in* Science Education, http://jppipa.unram.ac.id/index.php/jppipa/index (Sinta 2)

DAFTAR ISI

DAFTAR TABEL

DAFTAR GAMBAR

DAFTAR NOTASI

I	= Intesitan hujan (mm/hari)
D	= Durasi hujan (hari)
Q	= Volume air dalam setiap kontainer (ml)
A	= Luas container model (cm2)
T	= Waktu (menit)
I	= Intensitas (mm/jam)
Kx	= Konduktivitas hidrolik dalam arah x dan y,
C (h)	= Kapasitas retensi air volumetric
Ky	= Volume kadar air tanah
y	= Tinggi tekanan
Hhy	= Tinggi hidrolik total
Fs	= Nilai faktor keamanan terhadap kekuatan tanah
τ_{f},	= Kekuatan geser rata – rata dari tanah
τ_{d}	= Tegangan geser rata – rata yang bekerja sepanjang bidang lonsor
c ‘	= Nilai kohesi lapisan tanah
β	= Jarak potongan lereng
R	= Radius sirkulasi aliran air
N	= Total gaya normal yang bekerja
W	= Berat potongan tanah terhadap b dan h
X	= Jarak horizontal terhadap senter line lereng
f	= Jarak tegak lurus rotasi momen
α	= Sudur kemiringan lereng
u_{w},	= Tekanan air pori tanah
C’	= Cohesi efektif
γ	= Berat jenis tanah
σ	= Tegangan geser

α	= Sudut kemiringan lereng
b	= Lebar bidang gelincir lereng
h	= Tinggi bidang gelincir lereng
FS	= Faktor kemanan lereng
FK	= Angka keamanan
W	= Berat sector bidang tanah
u	= Tekanan air *pori* tanah akibat hujan
C’	= Kohesi tanah efektif
Ø’	= Sudut geser dalam tanah
L	= Panjang lengan momen
P	= Gaya horizontal pada sisi bidang irisan
LI	= Likuid Indek
LL	= Likuid limit
SL	= Batas susut
PI	= Plastis indek
IC	= Indek kecairan tanah
e	= angka pori
Vv	= Volume pori
Vs	= Volume butiran padat
n	= porositas
Sr	= Derajat kejenuhan
W	= kadar air tanah
ɣd	= Berat volume kering
ɣs	= Berat volume padat

DAFTAR SINGKATAN

ID = intensity – duration

ED = event – duration

EI = event – intensity

USCS = Unified Soil Classification Sistem

BAB 1 PENDAHULUAN

1.1 Latar Belakang

Masalah kerusakan sarana prasarana bidang Teknik Sipil yang terus meningkat akibat longsor merupakan akibat dari perubahan iklim global, secara umum, faktor pemicu utama dari keruntuhan lereng dapat diklasifikasikan menjadi tiga jenis faktor pemicu yaitu peristiwa curah hujan, beban gempa, dan aktifitas manusia. Faktor aliran curah hujan bisa dalam bentuk aliran permukaan, infiltrasi,aliran debris, akan menjadi pemicu mengubah tekanan air pori tanah, perobahan kadar air tanah atau tekanan tanah di lereng dan secara langsung mengurangi kekuatan geser tanah. Meningkatnya tingkat curah hujan akan meningkatnya tingkat faktor infiltrasi, indek rembesan dan air pori tanah dan akan meninggi nilai kadar air tanah, sehingga akan mengakibatkan pada Kegagalan lereng, Duncan., dkk, (2014). Kegagalan lereng (slope failure), kebanyakan terjadinya dalam bentuk keruntuhan lereng, merupakan fenomena alam, dalam hal ini keruntuhan lereng di didefinisikan sebagai pergerakan tanah yang terjadi di karenakan adanya gangguan atau faktor yang mempengaruhi dan menyebabkan terjadinya pengurangan kuat geser serta peningkatan tegangan geser tanah. Keruntuhan lereng ini biasanya terjadi pada musim hujan, hal ini dikarenakan pada musim penghujan tingkat kadar air tanah akan meningkat sampai menuju tingkat kejenuhan kadar air tanah, dan secara fisikal banyak terjadi tahapan proses penimbunan tanah, dan pemotongan tebing yang terlalu curam. Berbagai penelitian telah difokuskan pada analisis kejadian tanah longsor, dan prilaku aliran selama hujan, melibatkan teknik seperti analisis teoritis, analisis numerik, percobaan model, dan pemantauan lapangan. Belakangan ini, beragam jenis percobaan model laboratorium telah dilakukan untuk menganalisis mekanisme longsor atau kegagalan lereng.

Dalam penelitian Park,J.Y., dkk.(2020), Universitas Nasional Gyeongsang, Jinju, Korea di Korea, penelitian tertentu dilakukan untuk menyelidiki mekanisme tanah longsor dengan penyebab kegagalan lereng yang ekstrim dirancang dengan kondisi curah hujan buatan untuk tanak dasar berpasir. Selain itu, Lee, K., dkk,(2013), dalam penelitiannya melakukan secara eksperimental studi untuk menyelidiki karakteristik infiltrasi dan drainase di lereng, model dirancang dengan kejadian keberulangan curah hujan pada durasi tertentu. Kim, D., dkk, (2016), melakukan serangkaian percobaan dengan flume longsor untuk mempelajari sensitivitas menanggapi berbagai sensor pemantauan aliran bawah permukaan. Dalam kasus lain, ada studi tentang mekanisme kejadian tanah longsor menurut bentuk lereng, Chien,W.N., dkk, (2012), kegagalan lereng lainnya dalam penelitian lain, tentang studi pada aliran permukaan dan erosi tanah sebagai dampak dari karakteristik curah hujan. Run,Q., dkk, (2012), dalam penelitian lain, banyak terjadinya longsoran lereng di bawah berbagai kondisi lereng selama hujan dilakukan secara eksperimental pada propil lereng dengan tanah dasarnya yang terdiri dari tanah bercampur berpasir, Acharya,dkk., (2009). Dalam penelitian lain, Gallage., dkk, (2012), dan Lourenco dkk, (2015), dan, Park,J.Y., dkk, (2020), dalam penelitianya dengan metode analisis gabungan antra percobaan labortorium dan pemodelan numerikal berkesimpulan bahwa, kegagalan lereng terjadi pada beberapa bagian bawah permukaan, dimana lapisan tanah dalam keadaan jenuh, tekanan air pori yang berlebihan, dan tekanan hidrostatik keadaan tekanan naik sehingga terjadi lonsor pada bidang gelincir lereng. Beberapa peneliti lainnya, telah melakukan penelitian tentang efek dari curah hujan ekstrim terhadap hal - hal keruntuhan lereng ini, diantaranya ,Mukhlisisn., dkk (2014), Malaysia adalah sebuah negara yang terletak berhampiran garisan khatulistiwa dengan iklim tropika yang menerima hujan yang banyak dan tinggi , dengan tingkat curah hujan sebesar 2.400 mm / tahun, menjadikan Malaysia terdampak kepada peristiwa-peristiwa keruntuhan lereng yang mana hujan adalah salah satu faktor utama yang penyebab kejadian keruntuhan lereng, maupun tanggul - tanggul timbunan. Muntohar,A.S., dkk, (2010), di antara model yang digunakan untuk menganalisis stabilitas lereng, model infiltrasi air hujan yang terintegrasi dengan model stabilitas lereng dapat menjadi cara yang efektif untuk mengevaluasi kegagalan lereng dan stabilitas lereng saat curah hujan tinggi. Beragam penelitian tentang longsoran lereng pada skala laboratorium telah melakukan penelitian dengan berbagai ukuran. Pada umumnya model berukuran lebar minimal 70 cm dan tinggi minimal 1 meter. Model-model analog tersebut digunakan untuk dapat lebih memahami proses kejadian longsoran, dengan tipe dan mekanisme longsoran yang berbeda-beda. Penelitian lain tentang efek peningkatan kadar air tanah dan peningkatan indek kecairan tanah pada lereng, diantaranya, Pratama, R. H.,dkk, (2022). Studi stabilitas lereng: Efek dari intensitas hujan terhadap peningkatan kadar air dan indek kecairan tanah dengan pemodelan laboratorium [Disertasi doktor, Institut Teknologi Bandung].

Dari sekian banyak pemodelan lonsoran dalam penelitian para peneliti, maka dalam penelitian disertasi ini penulis mengkaji tentang : **"Studi Stabilitas Lereng Efek Dari Intensitas Hujan Terhadap Peningkatan Kadar Air Dan Indek Kecairan Tanah Dengan Pemodelan Laboratorium ".**

1.2 Masalah Penelitian

Agar didapat parameter – parameter penyebab kekagagalan lereng yang terjadi pada sebuah lereng perlu dikaji sebagai berikut :

1. Bagaimana bentuk perilaku keruntuhan lereng efek dari peningkatan kadar air tanah terhadap perobahan zona tanah dari padat ke likuid limit
2. Seberapa besar pengaruh tingkat kadar air terhadap indek kecairan tanah dalam keruntuhan lereng pada kondisi batas zona Atterberg

3. Seberapa besar pengaruh tingkat intensitas hujan terhadap peningkatan kadar air dan indek kecairan tanah lereng pada pemodel laboratorium
4. Masih kurangnya kajian terpadu yang mengukur intensitas hujan, peningkatan kadar air, perobahan indek kecairan tanah, dan pemodelan laboratorium dalam saru kerangka komperehensif.

1.3 Tujuan Penelitian

Tujuan dari penelitian ini dalah :

1. Menganalisis pengaruh perubahan kadar air tanah dan peningkatan indek kecairan tanah pada kondisi sudut lereng 30^0, 45^0,60^0,dan 90^0 melalui simulasi laboratorium.
2. Mencari tingkat perobahan kadar air terhadap nilai indek kecairan tanah dan pengaruhnya terhadap keruntuhan lereng pada kondisi tanah Zona batas atterberg.
3. Untuk mendapatkan bentuk grafik dari peningkatan kadar air dan indek kecairan tanah dalam kegagalan lereng pada setiap besaran sudut lereng 30^0 45^0 .60^0,dan 90^0 melalui simulasi laboratorium.
4. Memberikan rekomendasi teknis berdasarkan hasil pemodelan terhadap mitigasi potensi longsor akibat curah hujan tinggi.

1.4 Kontribusi Bagi Ilmu Pengetahuan

kontribusi penelitian ini adalah sebagai berikut :

- ❖ Kontribusi utama dari penelitian ini adalah memberikan pemahaman baru tentang hubungan dinamis antara kadar air, geometri lereng, dan indek kecairan tanah serta pemanfaatannya sebagai alat prediksi keruntuhan lereng berbasis data laboratorium.

- Semakin kadar air tanah mendekati atau melebihi nilai likuit limid, maka tanah semakin cair, dan nilai indek kecairan tanah (Liquidity index), semakin besar dari 1, maka tanah akan menjadi cair, dan akan terjadi pergerakan tanah dalam bentu kelonsoran lereng
- Dapat menghasilkan bentuk grafik keruntuhan lereng pada sudut lereng 30^0, 45^0, 60^0, dan 90^0, efek dari meningkatnya kadar air terhadap peningkatan indek kecairan tanah

1.5 Manfaat Penelitian

Bidang Akademik :

1. Mendapatkan nilai standar besaran sudut lereng sesuai dengan kondisi tanah setempat
2. Mendapatkan besaran nilai kadar air tanah dan nilai likuit limit tanah, dan pengaruhnya terhadap indek kecairan tanah lereng untuk tanah dasar lempung kepasiran secara percobaan labortorium.
3. Mendapatkan bentuk grafik dari hasil percobaan berdasarkan fungsi geometri lereng dari peningkatan kadar air dan efeknya terhadap nilai likuid indek tanah pada zona zona batas aterberg.
4. Mendapatkan besaran sudut geometrik lereng kritis terhadap kegagalan lereng dengan simulasi laboratorium.
5. Penelitian dapat memberikan dasar ilmiah bagi strategi mitigasi bencana longsor dan pemantauan risiko lereng berbasis perubahan kadar air tanah dan parameter indeks kecairan tanah.

Bidang Profesi :

1 Dapat memberikan standar – standar dalam perencanaan dalam penangan lereng dalam perencanaan dan pelaksanaan struktur pada bangunan sipil.

2 Dapat sebagai pedoman mitigasi penanganan kegagalan lereng dalam hal pemetakan daerah rawan lonsor.

1.6 Batasan Masalah Penelitian

Dalam penelitian ini, penelitian dibatasi terhadap sebagai berikut:

1. Jenis tanah. Penelitian ini hanya difokuskan pada satu jenis tanah, yaitu pada tanah lempung berpasir yang diklasifikasikan berdasarkan metoda USCS. Karakteristik tanah lainnya tidak diteliti lebih lanjut.
2. **Skala pemodelan**. Studi dilakukan pada skala laboratorium, menggunakan model lereng kecil, dengan dimensi benda uji (80 cm x 40 x 34 cm x 40 cm)
3. **Variasi intensitas hujan** . buatan buatan dalam pemodelan laboratorium dibatasi pada tingkat intensitas 122 mm/jam, denga lama percobaan selama 30 menit.
4. **Parameter mekanik tanah**. Parameter mekanis yang diamati pada :
   - Kadar air tanah (%)
   - Indek kecairan tanah
   - Stabilitas lereng, dinyatakan melalui perobahan bentuk, retakan, dan keruntuhan
   - Pengujian kuat geser langsung dilakukan hanya pada kondisi tanah sebelum penghujanan
5. **Lingkup waktu**. Penelitian ini hanya mengamati respon lereng selama pengujian singkat selama 30 menit, dan tidak mencakup efek jangka panjang atau pengeringan ulang tanah setelah penghujanan

BAB 2. TINJAUAN KEPUSTAKAAN

2.1 Tinjauan Umum

Kegagalan lereng dalam bentuk keruntuhan lereng merupakan peristiwa pergerakan suatu massa tanah yang bergerak secara vertikal dari atas kebawah disepanjang lereng. Gerakan ini terjadi apabila gaya-gaya yang menahan massa tanah dilereng lebih kecil dari pada gaya yang mendorong atau meluncurkan tanah disepanjang lereng. Gaya yang menahan massa tanah disepanjang lereng dipengaruhi oleh besar kecilnya nilai kadar air tanah yang mempengaruhi masa tanah tersebut, sifat fisik/mekanisme tanah terutama daya ikat tanah dan sudut geser tanah yang bekerja disepanjang bidang luncuran. Gaya pendorong tersebut dipengaruhi diantaranya oleh kandungan kadar air tanah,air pori tanah akibat dari volume aliran infiltrasi pada saat curah hujan meningkat sampai nilai ekstrimnya beban, faktor tutupan lahan dan massa tanah, sebagaimana dijelaskan pada gambar berikut :

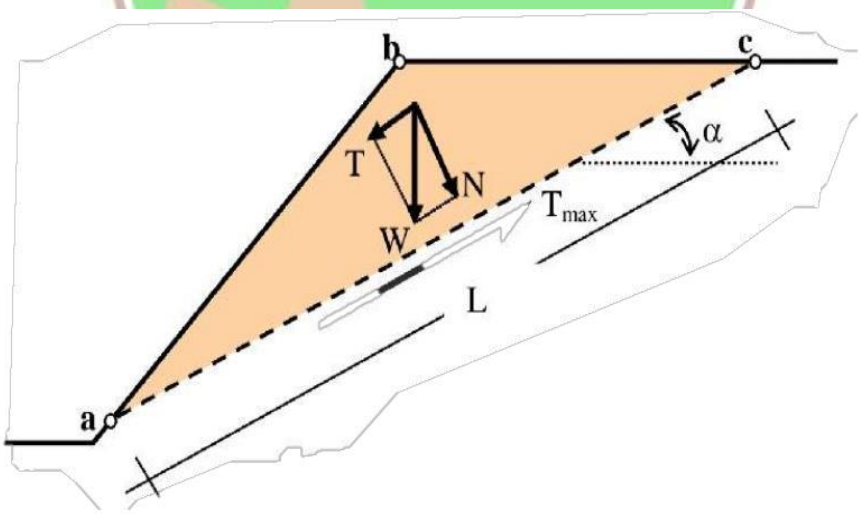

Gambar 2. 1 Gaya-gaya pada longsor bidang datar
(Sumber: Hakam, 2004)

Besaran gaya – gaya yang bekerja dapat dijelaskan menurut persamaan berikut :

$$W = \gamma \cdot A \tag{1}$$

$$N = W \cos \alpha \tag{2}$$

$$T = W \sin \alpha \tag{3}$$

$$T\ max = N\ tg\ \phi + c\ L \tag{4}$$

Maka besaran factor keamanan yang bekerja pada lereng dapat dicari dengan persamaan berikut :

SF = T max / T ; atau

$$SF = \frac{Ntg\varphi + cL}{W\ sin\alpha} \tag{5}$$

Dimana :

W = berat bidang runtuh (Ton)

A = luasan bidang runtuh (M^2)

ɣ = berat volume tanah (T/m^3)

T = Gaya yang bekerja bidang runtuh (T)

N = Gaya sejajar dengan bidang runtuh (T)

T max = Gaya perlawanan pada bidang runtuh (T/m)

SF = besaran factor kemana

2.2 Curah Hujan Pemicu Longsor

Hujan pemicu longsoran adalah hujan yang memiliki nilai intensitas hujan tinggi, sehingga air hujan mampu meresap ke lereng dan mendorong tanah untuk longsor. Secara umum terdapat dua tipe hujan pemicu longsoran di Indonesia, yaitu: tipe hujan tinggi, dan tipe hujan normal, tapi berlangsung lama. Tipe hujan tinggi misalnya adalah hujan yang dapat mencapai > 300 mm / bulan. Skala curah hujan tinggi ini berkisar antara 300 – 500 mm/bulan, atau lebih dari > 100 mm/hari, (BMKG 2020), Tipe hujan tinggi ini akan memberi efek memicu longsoran pada lereng-lereng yang tanahnya mudah menyerap air, Karnawati, D,. (1996;1997), seperti misalnya pada tanah lempung pasiran dan tanah pasir. Pada lereng demikian, longsoran dapat terjadi pada awal musim hujan. tipe hujan normal atau rendah adalah hujan yang kurang dari ≤ 100 mm per bulan. Hujan tipe ini apabila berlangsung selama beberapa minggu hingga beberapa bulan dapat efektif memicu longsoran pada lereng yang tersusun oleh tanah yang lebih kedap air, misalnya lereng dengan tanah lempung, Karnawati,D,. (2000). Pada lereng ini, longsoran umumnya terjadi mulai pada pertengahan musim hujan.

Kklasifikasi intensitas curah hujan ini dapat dibedakan atas beberapa tingkat sebagai mana yang dijelaskan pada table berikut : …………..

Tabel 2.1 Klasifikasi Intensitas curah hujan

No	Kriteria Intensitas Curah Hujan	Intensitas Curah Hujan (mm/jam)
1	Hujan ringan	0 – 5
2	Hujan Sedang	5 – 20
3	Hujan lebat	20 – 50
4	Hujan sanagat lebat	>50

Sumber : BMKG, WMO (World Meteorological Organization),dan SNI 03-1725-1989

Tabel 2.2 Klasifikasi Intensitas curah hujan /bulan /tahunan

No	Kriteria Intensitas Curah Hujan	Intensitas Curah Hujan (mm/bulan)	Intensitas Curah Hujan (mm/tahun)
1	Rendah	0 – 100	0 -1500
2	Sedang	100 – 300	1500 – 3000
3	Tinggi	300 - 500	3000 - 4500
4	Sangat tinggi	>500	4500 - 5000
5	Ekstrim	-	> 5000

Sumber : Standar BMKG 2020

Menurut Peta rata – rata curah hujan BMKG (2020), klasifikasi curah hujan dan tingkat kerentanan terhadap kerentanan longsor dapat dilihat sebagai mana dijelaskan menurut gambar berikut :

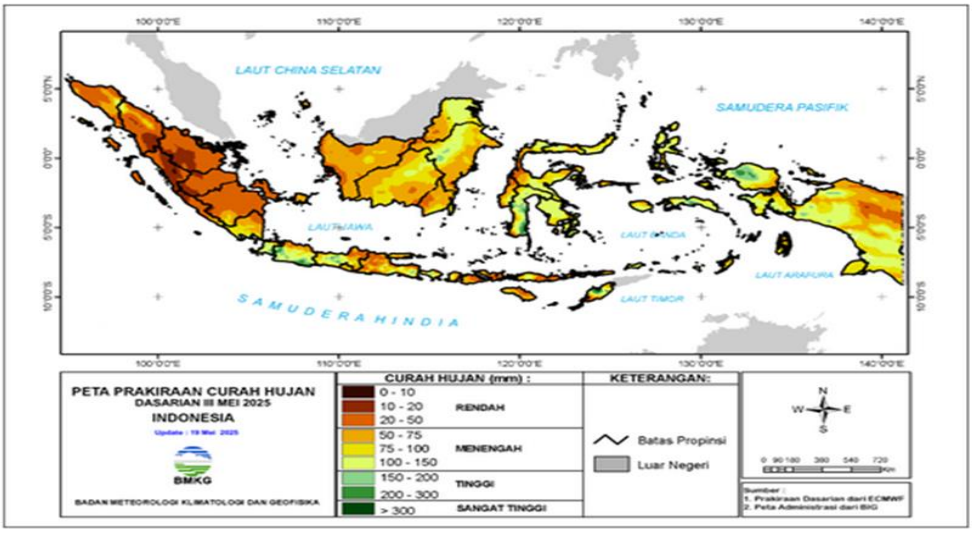

Gambar 2. 2 Peta standar besaran intensitas curah hujan
Sumber : BMKG 2021

Berdasarkan data kejadian curah hujan daerah Sumatera Barat pada umumnya, maka dapat disimpulkan curah hujan yang terjadi pada daerah rawan longsor berskala tinggi dengan intensitas diatas normal denga intensitas besar dari 50 mm/jam.

2.3 Ambang Batas Intensitas Hujan

Rainfall threshold atau ambang hujan ialah batas kritis (maksimum atau minimum) jumlah hujan yang turun hingga mencapai tanah, Reichenbach dkk., (1998). Hujan kritis adalah hujan yang diukur dari awal kejadian, yaitu pada saat intensitas hujan meningkat sangat drastis, hingga waktu kejadian tanah longsor, seperti yang dijelaskan pada gambar (Gambar 2.3). Peningkatan intensitas hujan yang sangat tajam ini menyebabkan lonjakan kurva hujan kumulatif yang tiba-tiba,dkk, Aleotti., dkk (2004).

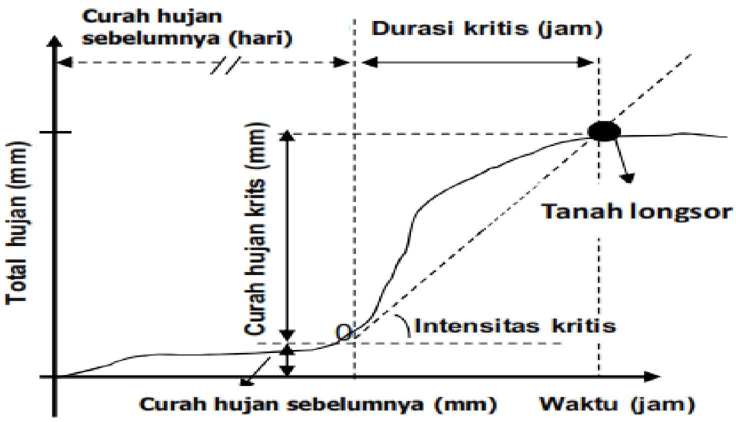

Gambar 2. 3 Ambang Batas Intensitas Curah hujan VS longsor Lereng
Sumber : Aleotti,. (2004)

Hujan dapat dikategorikan berdasarkan cakupan wilayah yaitu hujan global, regional dan lokal. Hujan global ditentukan dengan menggunakan data yang tersedia di seluruh belahan dunia. Hujan global merupakan hujan yang lebih umum tidak bergantung pada kondisi lokal, pola, dan riwayat hujan yang terjadi pada wilayah tertentu. Cara yang paling mudah untuk mendefinisikan hujan global ini adalah dengan mengetahui nilai batas bawah pada semua data rekaman hujan yang dihasilkan pada peristiwa tanah longsor. Hujan regional didefinisikan sebagai kumpulan data hujan pada wilayah - wilayah yang memiliki kesamaan karakteristik secara metereologi, geologi, dan fisiografis. Hujan lokal secara tegas dan implisit mempertimbangkan kondisi iklim dan geomorfologi suatu wilayah data hujan yang memicu terjadinya tanah longsor dari berbagai jenis hujan di atas dipisahkan dengan data hujan yang tidak memicu terjadinya tanah longsor. Hujan dapat ditentukan dengan menggunakan dua pendekatan yaitu permodelan empirik (*empirical based model*) dan permodelan proses fisik (*physical-process model*), Guzzetti, dkk, (2005). Gambar 2.2 di atas. Gambar ini menjelaskan secara sederhana proses terjadinya tanah longsor di mana curah hujan kritis menunjukkan jumlah curah hujan dari waktu ("titik nol") akan meningkat tajam dalam intensitas curah hujan yang diamati memicu tanah longsor, sebagaimana dijelaskan pada grafik

2.2 diatas. Intensitas hujan buatan mengacu pada Standar kondisi hujan jaman, dimana hujan lebat antara 20 - 50 mm/jam, dan kondisi hujan sangat lebat yaitu >50 mm/jam. Dalam penelitian ini dengan menggunakan alat rainfall simulator sederhana, intensitas hujan dihitung dengan rumus persamaan emperis sebagai berikut :

$$I = \frac{Q}{Axt} x\ 600 \quad (1)$$

Sumber : Anonim, (2011). Instruction Manual Rainfall Simulator.

Dimana :

Q = volume air dalam setiap kontainer (ml)

A = Luas container model (cm^2)

T = waktu (menit)

I = intensitas (mm/jam)

2.4 Struktur Tanah

Dalam pengertian teknik secara umum, tanah didefinisikan sebagai material yang terdiri dari agregat (butiran) mineral–mineral padat yang tidak tersementasikan (terikat secara kimia) satu sama lain dari bahan–bahan organik yang telah melapuk (yang berpartikel padat) disertai dengan zat cair dan gas mengisi ruang-ruang kosong di antara partikel-partikel padat tersebut. Tanah berguna sebagai bahan bangunan pada berbagai macam pekerjaan teknik sipil, disamping itu tanah berfungsi juga sebagai pendukung pondasi dari bangunan (Das, 1994). Sifat mekanis tanah merupakan sifat perilaku dari struktur massa tanah bila dikenai suatu gaya atau tekanan yang dijelaskan secara teknis mekanis (Kusuma, dkk, 2016). Untuk mengetahui sifat fisik tanah dapat dilakukan dengan cara pengamatan secara langsung, sedangkan untuk mengetahui mekanika tanah harus melalui uji laboratorium.

Klasifikasi tanah adalah ilmu yang mempelajari cara-cara membedakan sifat-sifat tanah satu sama lain dan mengelompokkan tanah kedalam kelas-kelas tertentu berdasarkan atas kesamaan sifat yang dimiliki (Hardjowigeno, 2003). Tujuan umum dari klasifikasi tanah adalah menyediakan suatu susunan yang teratur (sistematik) bagi pengetahuan mengenai tanah dan hubungannya dengan tanaman, baik mengenai produksi maupun perlindungan kesuburan tanah, Darmawijaya,. (1997). Terdapat dua sistem klasifikasi yang sering digunakan, yaitu USCS (*Unified Soil Classification* System), dan AASHTO (*American Association of State Highway and Transportation Officials*). Sistem-sistem ini menggunakan sifat-sifat indeks tanah yang sederhana seperti distribusi ukuran butiran, batas cair dan indeks plastisitas. Klasifikasi tanah dari Sistem *Unified* mula pertama diusulkan oleh Casagrande,. (1942), kemudian direvisi oleh kelompok teknisi dari USBR (*United State Bureau of Reclamation*). Dalam bentuk yang sekarang, sistem ini banyak digunakan oleh berbagai organisasi konsultan geoteknik , Hardiyatmo,. (2002).

Dari lokasi pengambilan sampel tanah yang diambil yakni pada daerah dataran talamau Kabupaten Pasaman, struktur tanahnya dapat di perlihatkan pada gambar berikut :

Gambar 2. 4 Struktur tanah dan kondisi lereng Gunung Talamau di Kabupaten Pasaman

Tabel 2. 3 Interpretasi gambar dan kondisi tanah

Faktor	Kondisi lapisan tanah
Jenis tanah	Tanah terdiri dari jenis tanah andosol (struktur remah, retensi air tinggi, resiko erosi
Kemiringan lereng	Kemiringan lereng dari $\geq 15\,\%$, hingga $> 40\,\%$; rentan longsor atau erosi
Lapisan Aluvial	Rentan likuefaksi; sering material lumpur/pasir masuk sungai
Patahan Aktif	Talamau Fault meningkatkan risiko gempa dan tanah longsor

Sumber : Dinas ESDM Propinsi Sumatera Barat,. (2022)

2.4.1 Sistem Klasifikasi USCS (*Unified Soil Classification System*)

Sistem klasifikasi tanah ini diusulkan oleh Prof. Arthur Cassagrande, system ini didasarkan pada sifat tekstur tanah system ini menempatkan tanah dalam tiga kelompok yaitu tanah berbutir kasar, tanah berbutir halus (*fine grained soil*), dan tanah organis. yaitu tanah dimana lebih dari 50 % (>50%) dari berat total sampel lolos saringan No 200, dan tanah berbutir kasar (*coarse grained soil*) adalah tanah yang mempunyai presentase lolos saringan No. 200 < 50 % dari berat total sampel sedangkan tanah berbutir halus adalah tanah dengan persentase lolos saringan No. 200, besar dari 50 % (> 50 %). Tanah ini dibagi dengan symbol-simbol tertentu sebanyak 15 buah, yaitu:

a. **Simbol Komponen:**
   1) Kerikil : G (*gravel*)
   2) Pasir : S (*sand*)
   3) Lempung: C (*clay*)
   4) Lanau : M (*silt*)
   5) Organis : O *(organic)*
   6) Humus : Pt *(peat)*

b. **Simbol Gradasi:**
   1) Bergradasi Baik : W (*well-graded*)

2) Bergradasi Buruk : P (*poorly-graded*)

c. **Simbol Batas Cair:**

1) Plastisitas Tinggi : H (*high-plasticity*)

2) Plastisitas Rendah : L (*low-plasticity*)

Sistem klasifikasi USCS terbagi atas 3 kelompok, sebagaimana diterangkan berikut ini :

a. **Tanah Berbutir Kasar**

Yang termasuk dalam kerikil adalah tanah yang mempunyai presentase lolos saringan No. 4 > 50 % termasuk kelompok pasir. Baik pasir maupun kerikil dibagi lagi dalam 4 kelompok, yaitu:

1) Kelompok GW dan SW adalah tanah kerikilan dan kepasiran bergradasi baik dengan butiran halus yang sedikit atau tanpa butiran halus yang non plastis (lolos saringan No.200 < 5%).
2) Kelompok GP dan SP adalah tanah kerikilan dan kepasiran bergradasi buruk dengan butiran halus sedikit yang non plastis.
3) Kelompok GM dan SM adalah mencakup tanah kerikil atau pasir kelanauan (lolos saringan No.200 > 12%) dengan plastisitas rendah atau non plastis. Batas cair dan indeks plastis terletak di bawah garis A. Dalam kelompok ini bisa termasuk baik yang bergradasi baik maupun yang bergradasi buruk.
4) Kelompok GC dan SC adalah mencakup tanah kerikil atau kepasiran dengan butiran halus (lolos saringan No.200 < 12%) lebih bersifat lempung dengan plastisitas rendah sampai tinggi, batas cair dan indeks plastisitas tanah ini terletak di atas garis A dengan grafik plastisitas.

b. **Tanah Berbutir Halus**

Tanah berbutir halus dibagi dalam lanau (M) yang berasal dari bahasa Swedia dan lempung (C) yang di dasarkan pada batas cair dan indeks plastis juga tanah organis (O) termasuk dalam fraksi ini. Lanau adalah tanah berbutir halus yang mempunyai batas cair dan indeks plastis terletak di bawah garis A dan lempung berada di atas garis A. Lempung organis adalah kekecualian dari peraturan di atas karena batas cair dan indeks plastisnya berada di bawah garis A. Lanau, Lempung dan tanah organis dibagi lagi menjadi batas cair yang rendah (L) dan tinggi (H), garis pembagi antara batas cair yang rendah dan tinggi ditentukan pada angka 50.

1) Kelompok ML dan MH adalah tanah yang diklasifikasikan sebagai lanau pasiran, lanau lempung atau lanau anorganis dengan plastisitas relatif rendah. Juga termasuk tanah jenis butiran lepas, bubur batu, tanah yang mengandung mika juga beberapa jenis lempung.
2) Kelompok CH dan CL terutama adalah lempung anorganis.

   Kelompok CH adalah lempung dengan plastisitas sedang sampai tinggi mencakup lempung gemuk, lempung gumbo. Lempung dengan plastisitas rendah yang diklasifikasikan CL biasanya adalah lempung kurus, lempung pasir atau lempung lanau.
3) Kelompok OL dan OH adalah tanah yang ditunjukan sifat- sifatnya dengan adanya bahan organik, lempung dan lanau organis termasuk kedalam kelompok ini dan mereka mempunyai plastisitas berkisar pada kelompok ML dan MH.

c. Tanah Organik

Tanah ini tidak dibagi lagi tapi diklasifikasikan dalam satu kelompok. Biasanya mereka sangat mudah ditekan dan tidak mempunyai sifat sebagai bahan bangunan yang di inginkan, tanah khusus dari kelompok ini adalah humus,tanah lumpur dengan tekstrur organis yang tinggi. Sistem klasifikasi Unified berdasarkan tanah yang lolos dan tertahan sebagai berikut:

Tabel 2.4 Sistem klasifikasi tanah unified

Divisi utama			Simbol Kelompok	Nama umum
Tanah berbutir kasar Lebih dari 50% butiran tertahan pada ayakan No.200	Pasir Lebih dari 50% fraksi kasar lolos ayakan No.40	Kerikil bersih (hanya kerikil)	GW	Kerikil bergradasi-baik dan campuran kerikil-pasir, sedikit atau sama sekali tidak mengandung butiran halus
			GP	Kerikil bergradasi-buruk dan campuran kerikil-pasir, sedikit atau sama sekali tidak mengandung butiran halus
		Kerikil dengan butiran halus	GM	Kerikil berlanau, campuran kerikil-pasir-lanau
			GC	Kerikil berlempung, campuran kerikil-pasir-lempung
	Kerikil 50% atau lebih dari fraksi kasar tertahan pada ayakan No.40	Pasir bersih (hanya pasir)	SW	Pasir bergradasi-baik, pasir berkerikil, sedikit atau sama sekali tidak mengandung butiran halus
			SP	Pasir bergradasi-buruk, pasir berkerikil, sedikit atau sama sekali tidak mengandung butiran halus
		Pasir dengan butiran halus	SM	Pasir berlanau, campuran pasir-lanau
			SC	Pasir berlempung, campuran pasir-lempung
Tanah berbutir halus 50% atau lebih Lolos ayakan No.200		Lanau dan Lempung Batas cair 50% atau kurang	ML	Lanau anorganik, pasir halus sekali, serbuk batuan, pasir halus berlanau atau berlempung
			CL	Lempung anorganik dengan plastisitas rendah sampai dengan sedang lempung berkerikil, lempung berpasir, lempung berlanau, lempung "Kurus" (lean clays)

Divisi utama		Simbol Kelompok	Nama umum
		OL	Lanau-organik dan lempung berlanau organik dengan plastisitas rendah
	Lanau dan Lempung Batar cair lebih dari 50%	MH	Lanau anorganik atau pasir halus diatomae, atau lanau diatomae, lanau elastis
		CH	Lempung anorganik dengan plastisitas tinggi, lempung “gemuk” (fat clays)
		OH	Lempung organic dengan plastisitas sedang sampai dengan tinggi
Tanah-tanah dengan kandungan organic sangat tinggi		PT	Peat (gambut), muck, dan tanah-tanah lain dengan kandungan organik tinggi

Sumber : Mekanika tanah,. Das.Braja. M,. (1995), dan SNI 6371 ;2015

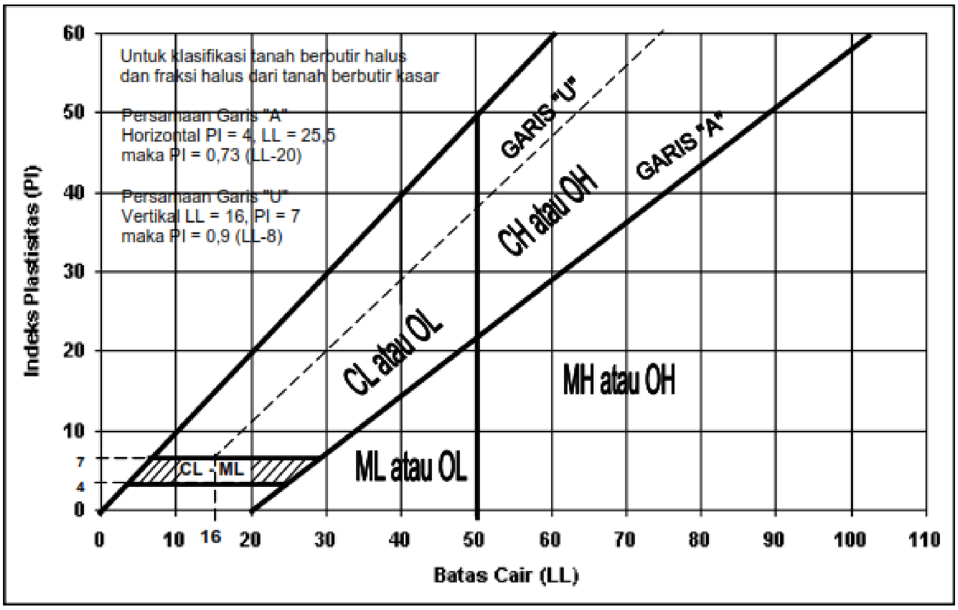

Gambar 2. 5 Grafik plastisitas jenis tanah

2.4.2 Pengujian Laboratorium

2.4.2.1 Sifat Fisik Tanah

Sifat fisik tanah yaitu sifat suatu elemen tanah yang berhubungan dengan elemen penyusunan masa tanah yang ada, misalnya volume tanah, kadar air, dan berat tanah. Dalam keadaan tidak jenuh, tanah terdiri dari tiga bagian yaitu butitan padat, air, dan udara. Ilustrasi untuk memahami susunan elemen pada massa tanah dapat diasumsikan seperti Gambar 2.3 dibawah ini (Das, 1998).

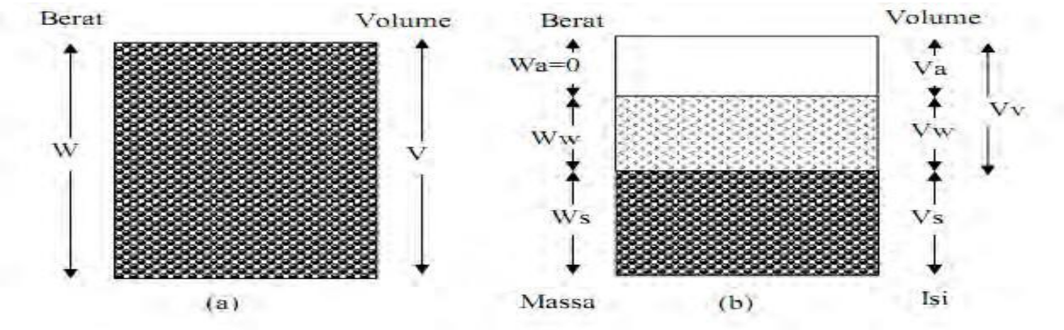

(a) Elemen tanah dalam keadaan asli ; (b) tiga fase elemen tanah.

Gambar 2. 6 Diagram komposisi dan elemen tanah
Sumber : Braja M. Das, 1988

Pada gambar 2.2 (a) menunjukkan suatu elemen tanah yang mempunyai volume V dan berat W, sedangkan gambar 2.2 (b) menunjukkan hubungan volume dan berat dalam tiga fase yang dipisahkan (butiran padat, air, dan udara). Hubungan volume yang umum dipakai untuk suatu elemen tanah adalah:

1. Angka Pori (e) adalah perbandingan antara volume pori (Vv) dengan volume butiran padat (Vs) yang dinyatakan dalam desimal, dapat dirumuskan :

$$e = \frac{V_v}{V_s} \quad (2)$$

2. Porositas (n) adalah perbandingan antara volume pori (Vv) dengan volume tanah total (V) yang dinyatakan dalam persen atau desimal, dapat dirumuskan:

$$n = \frac{V_v}{V} \qquad (3)$$

3. Derajat Kejenuhan (Sr) adalah perbandingan antara volume air (Vw) dengan volume pori (Vv) yang dinyatakan dalam persen, dapat dirumuskan :

$$S_r = \frac{V_w}{V_v} \times 100\%$$

(4)

4. Kadar Air (w) adalah perbandingan antara berat air (Ww) dengan berat butiran padat (Ws) dalam tanah yang dinyatakan dalam persen, dapat dirumuskan :

$$w = \frac{w_w}{w_s} \times 100\% \qquad (5)$$

5. Berat jenis (*Specific Gravity*) adalah perbandingan antara berat volume butiran padat (γs) dengan berat volume air (Vw) pada temperatur 4^0C. Berat dari berbagai jenis tanah berkisar antara 2,65 sampai 2,75 (Hardiyatmo, H.C 2001). Nilai-nilai berat jenis dari berbagai tanah dijelaskan dalam Tabel 2.5 dibawah ini.

Tabel 2.5 Berat Jenis Tanah

Macam Tanah	Berat Jenis
Kerikil	2,65 - 2,68
Pasir	2,65 - 2,68
Lanau tak organik	2,62 - 2,68
Lempung organik	2,58 - 2,65
Lempung tak organik	2,68 - 2,75
Humus	1,37
Gambut	1,25 - 1,8

Sumber : Hardiyatmo, C.H,. (2001)

6. Berat Volume Kering (γd) adalah perbandingan antara berat butiran padat (Ws) dengan volume tanah total (V), dapat dirumuskan :

$$\gamma_d = \frac{w_s}{V} \quad (6)$$

7. Berat Volume Butiran Padat (γ_s) adalah perbandingan antara berat butiran padat (W_s) dengan volume butiran padat (V_s), dapat dirumuskan:

$$\gamma_s = \frac{w_s}{V_s} \quad (7)$$

Kadar air, dinyatakan dalam persen, di mana terjadi transisi dari keadaan padat ke keadaan semi-padat didefinisikan sebagai batas-susut (*shrinkage limit*). Kadar air di mana transisi dari keadaan semi-padat ke keadaan plastis terjadi dinamakan batas plastis (*plastic limit*), dan dari keadaan plastis ke keadaan cair dinamakan batas cair (*liquid limit*). Batas-batas ini dikenal sebagai batas-batas Atterberg (*Atterberg Limits*). Kedudukan batas-batas konsistensi untuk tanah disajikan dalam gambar 2.4 berikut.

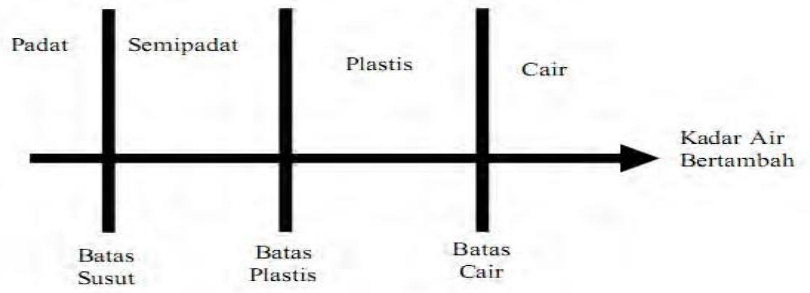

Gambar 2. 7 Batas-batas Atterberg
Sumber :Das. Braja.M,.(1988)

Dari diagram atterberg diatas dapat diuraikan atas beberapa hal dibawah ini diantaranya adalah sebagai berikut :

1. Batas Cair *(Liquid Limit)* LL, didefenisikan sebagai kadar air tanah pada batas antara keadaan cair dan keadaan plastis, yaitu batas atas dari daerah plastis.
2. Batas Plastis (*Plastic Limit*) PL, didefenisikan sebagai kadar air pada kedudukan antara plastis dan semi padat, yaitu persentase kadar air

dimana tanah dengan diameter 3,2 mm mulai retak-retak ketika digulung.

3. Batas Susut (*Shrinkage Limit*) SL, didefinisikan sebagai kadar air pada kedudukan semi-padat dan padat, yaitu persentase kadar air dimana pengurangan kadar air selanjutnya tidak mengakibatkan perubahan volume tanah selanjutnya.
4. Indeks Plastisitas (*Plasticity Index*) PI, adalah perbedaan antara batas cair dan batas plastis suatu tanah dari dasar lereng .

Dimana persamaan – persamaan dalam Atterberg dapat dijelaskan dalam persamaan berikut :

$$PI = LL - PL \quad (8)$$

$$SL = wi\ (\%) - \Delta w\ (\%) \quad (9)$$

$$LL = Wn\left(\frac{N}{25}\right)^2 \quad (10)$$

Dimana :

PI = Plastis indek

SL = Batas susut

LL = Likuid limit

N = Jumlah pukulan

Wn = Kadar air penutup dasar goresan dari contoh tanah

Δw = Perubahan kadar air awal degan kadar air pada batas susut

2.4.2.2 Sifat Mekanik Tanah

Sifat mekanis tanah merupakan sifat perilaku dari struktur massa tanah pada suatu gaya atau tekanan yang dijelaskan secara teknis mekanis. Pengujian untuk mengetahui sifat mekanik tanah salah satunya yaitu :

1. Pengujian Pemadatan

Pemadatan adalah suatu proses memadatnya partikel tanah sehingga terjadi pengurangan volume udara dan volume air dengan memakai cara mekanis. Kepadatan tanah tergantung banyaknya kadar air, jika kadar air tanah sedikit maka tanah akan keras begitu pula sebaliknya bila kadar air banyak maka tanah akan menjadi lunak atau cair. Pemadatan yang dilakukan pada saat kadar air lebih tinggi dari pada kadar air optimumnya akan memberikan pengaruh terhadap sifat tanah. Tujuan pemadatan tanah adalah memadatkan tanah pada kadar air optimum dan memperbaiki karakteristik mekanisme tanah, yang akan memberikan keuntungan yaitu :

a. Memperkecil pengaruh air terhadap tanah.
b. Bertambahnya kekuatan tanah.
c. Memperkecilkan pemampatannya dan daya rembes airnya.
d. Mengurangi perubahan volume sebagai akibat perubahan kadar air.

Sumber : Mekanika tanah ,Hardiyatmo, C.H,. (2001)

Pemadatan tanah dapat dilaksanakan di lapangan maupun di laboratorium. Di lapangan biasanya tanah akan digilas dengan mesin penggilas yang didalamnya terdapat alat penggetar, getaran akan menggetarkan tanah sehingga terjadi pemadatan. Sedangkan di laboratorium menggunakan pengujian standar yang disebut dengan uji proktor, dengan cara suatu palu dijatuhkan dari ketinggian tertentu beberapa lapisan tanah di dalam sebuah mold. Dengan dilakukannya pengujian pemadatan tanah ini, maka akan terdapat hubungan antara kadar air dengan berat volume.

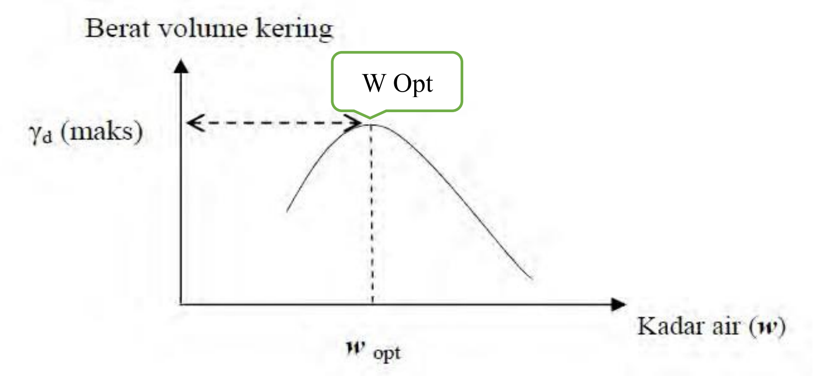

Gambar 2. 8 Hubungan antara kadar air dan berat volume tanah

Dari gambar 2.8 diatas dapat dijelaskan bahwa untuk mencari kepadatan optimum lapisan tanah dengan melakukan percobaan labortorium dengan metoda proctor tes melakukan berapa sampel dengan penambahan kadar air sehingga didapat kadar air optimum dari beberapa sampel yang diuji, setelah didapat kadar air omc dari sampek, maka hubungan dari kadar air dengan kepadatan maka didapti kepadatan tanah kering optimumnya.Untuk mencari kepadatan laboratorium dari sampel tanah ini dengan memakai metoda proctor tes.

2.4.2.3 Hubungan kadar air, liquid limit, dan sifat mekanis tanah

Ketika kadar air meningkat mendekati atau melebihi *liquid limit*, kohesi tanah (c) dan sudut geser dalam (ϕ\phiϕ) mengalami penurunan. Hubungan ini dapat dimodelkan secara empiris, pada bersamaan berikut:

1. Indek kecairan tanah

Indeks Kecairan Tanah (Liquidity Index, LI) adalah parameter geoteknik yang digunakan untuk menilai konsistensi atau kekuatan tanah lempung berdasarkan kadar airnya. Indeks ini membantu dalam menentukan apakah suatu tanah berada dalam kondisi kaku (stiff), plastis, atau mendekati keadaan cair.

$$LI = \frac{W-PL}{LL-PL} \quad (13)$$

Di mana,

w adalah kadar air tanah (%),

LL adalah batas cair tanah (Liquid Limit) (%),

PL adalah Batas plastis tanah (Plastic Limit) (%).

Besaran nilai Indeks kecairan tanah digunakan dalam analisis stabilitas pergerakan tanah pada lereng, terutama dalam perencanaan struktur pengaman lereng, serta mitigasi atas risiko longsor. Batasan – batasan nilai indek kecairan tanah (likuid indek) dapat dilihat pada gambar dibawah ini :

Tabel 2.6 Indek Likuit tanah

Nilai Indek Likuit	Deskripsi
Li< 1	Tanah semi padat, kekuatan tinggi
0< LI > 1	Tanah kondisi Plastis,Kekuatan sedang,tanah seperti material plastis
LI > 1	Tanah mulai kehilangan konsistensi, mendekati kondisi cair, tanah bersifat liquid / cair
LI > 1.5	Tanah pada kondisi sangat lunak / cair , berarti kadar air tanah lebih tinggi dari batas likuiditasnya, sehingga tanah berperilaku seperti cairan dan kehilangan kohesinya.

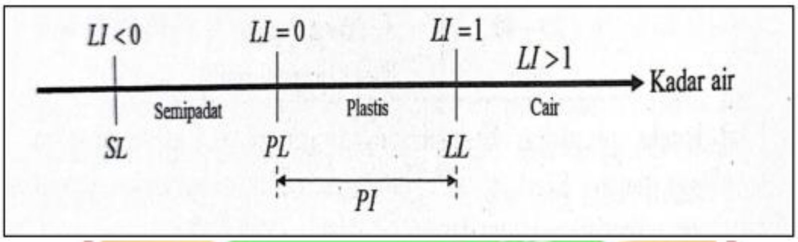

Gambar 2. 9 Grafik Indeks Kecairan Tanah

Sumber : ASTM D4318 – Standard Test Methods for Atterberg Limits, dan IS 2720 (Indian Standard), bagian konsistensi pada Tanah

2. Hubungan kadar air tanah dengan likuid limit

Kadar air tanah adalah persentase berat air yang terkandung dalam tanah dibandingkan dengan berat tanah padatnya. Sedangkan **liquid limit** adalah kadar air di mana tanah berubah dari keadaan plastik menjadi cair (bergelincir atau mengalir).Liquid limit menunjukkan batas kelembaban maksimum di mana tanah masih dapat menahan bentuk dan tidak berubah menjadi cair. Ini merupakan parameter penting dalam mekanika tanah untuk mengklasifikasikan tanah dan memahami sifat plastisitas serta kekuatan tanah, hubungan antara kadar air tanah dan sifat likuid limit dapat dijelaskan sebagai berikut:

- Kadar air tanah yang aktual dapat dibandingkan dengan liquid limit untuk menentukan kondisi konsistensi tanah saat itu, apakah tanah berada pada kondisi padat, plastis, atau cair.
- Jika kadar air tanah lebih rendah dari liquid limit, tanah berada dalam keadaan plastis atau padat.

- Jika kadar air tanah mendekati atau melebihi liquid limit, tanah cenderung menjadi lunak, kehilangan kekuatan dan lebih mudah berubah bentuk (cair).
- Dengan mengetahui liquid limit dan kadar air tanah, secara ilmu geoteknik dapat memprediksi perilaku tanah di lapangan, seperti daya dukung dan kemungkinan likuifaksi. Kadar air tanah yang sebenarnya dapat dibandingkan dengan liquid limit untuk menentukan kondisi konsistensi tanah sebagai berikut:
  - Jika **w < LL**, tanah berada dalam kondisi **plastis** atau **semi-padat**.
  - Jika **w ≈ LL**, tanah berada di batas antara kondisi plastis dan cair.
  - Jika **w > LL**, tanah cenderung dalam kondisi **cair** dan kehilangan kekuatan gesernya.

Das, B.M,. (2010). Dalam *Principles of Geotechnical Engineering*, 7th Edition, Cengage Learning.Disini dapat disimpulkan bahwa, liquid limit adalah batas di mana tanah mulai berperilaku seperti cairan, sehingga menjadi indikator penting untuk memprediksi stabilitas dan kekuatan tanah.

Hubungan persamaan Regresi sederhana antara kadar air dengan Liquid Limit dapat diuraikan sebagai berikut : Liquid limit biasanya didapat dari pengujian laboratorium (uji Casagrande atau uji cone). Namun, secara empiris liquid limit dapat diperkirakan dari kadar air dan parameter tanah lain.

$$LL = a \times w + b \quad (14)$$

Dimana:

LL = liquid limit (variabel dependen)

w = kadar air tanah (variabel independen)

a, b = konstanta regresi yang akan dicari

Kondisi nilai likuit limit dapat berubah, dengan efek dari perobahan nilai kadar air tanah (w), maka dapat mempengaruhi perobahan nilai kohesi dan sudut geser dari lapisan tanah, sebagai mana yang diuraikan menurut persamaan berikut dibawah ini :

$$C' = a.(LL - w)^b \quad (15)$$

$$\phi' = c.e^{-d(w-LL)} \quad (16)$$

Dimana, LL adalah nilai likuit limit (%), w adalah nilai perobahan kadar air, e adalah nilai bilangan ekponen a, b, c, d adalah parameter tanah.

3. Hubungan dengan indeks plastisitas dengan konsistensi tanah

Salah satu parameter tanah dalam batas – batas atterberg tanah, yakni, Indeks

Tabel 2.7 Nilai Indek Konsistensi tanah

Nilai Indek Konsistensi	Deskripsi
IC < 1	Tanah dalam kedaan solit
1< IC < 1	Tanah dalam keadaan plastis
IC ~ 0	Tanah mulai kehilangan konsistensinya, mendekati keadaan cair, tanah menjadi cair/cair.

Sumber : BS 1377-2:1990, Classification tests, standar pengujian kadar air dan liquid limit

Plastisitas (PI - Plasticity Index) adalah parameter dalam ilmu mekanika tanah yang menunjukkan rentang nilai kadar air di mana tanah berada dalam keadaan plastis.dimana nilai indek plastisitas tanah (PI) dihitung sebagai selisih antara batas cair dan batas plastis dari tanah.

2.5 Struktur Tanah Pada Lereng

Bentuk kelonsoran pada lereng merupakan suatu massa tanah yang bergerak secara vertikal dari atas kebawah disepanjang lereng. Gerakan ini terjadi apabila gaya-gaya yang menahan (resisting force) massa tanah dilereng lebih kecil dari pada gaya yang mendorong atau meluncurkan tanah disepanjang lereng. Gaya yang menahan massa tanah disepanjang lereng dipengaruhi oleh kedudukan muka air tanah, sifat fisik/mekanisme tanah terutama daya ikat tanah dan sudut geser tanah yang bekerja disepanjang bidang luncuran. Gaya pendorong tersebut dipengaruhi diantaranya oleh kandungan kadar air tanah,air pori tanah akibat dari volume aliran infiltrasi pada saat curah hujan meningkat sampai nilai ekstrinya beban ,faktor tutupan lahan dan massa tanah.Tanah yang cenderung terjadi longsor adalah tanah yang memiliki gaya tarik menarik antar partikel (kohesi) kecil akibat tidak ada ikatan antar tanah. Komposisi tanah itu sendiri terdiri dari air, tanah, dan udara seperti **Gambar. 2.10** dibawah ini.

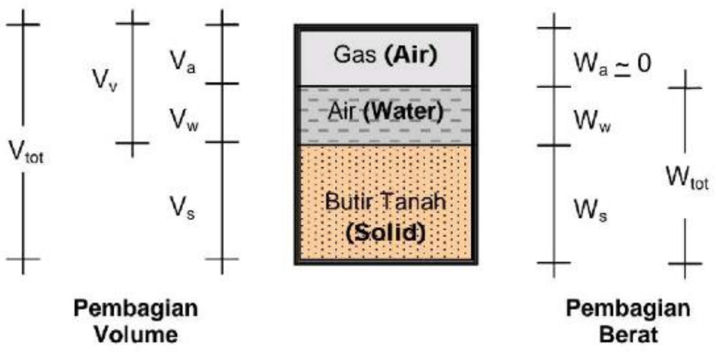

Gambar 2. 10 Susunan butir material sampel tanah

Menurut Hakam.A,. (2020), Lempung adalah material terkecil dan mempunyai fraksi terkecil dari tanah. Ukuran butiran lempung antara 0.002 hingga 0.001 mm. Berbeda dengan sifat butiran tanah sebelummnya, lempung mempunyai sifat kohesif yang tinggi. Sifat kohesif (]engket) lempung ini disebabkan mineral yang membentuk lempung tersebut sedemikian rupa sehingga terjadi dua kutub listrik statis pada perrnukaannya. Mineral lempung berbentuk seperti lempengan-lempengan kecil (seperti lembaran-lembaran keras tebal) yang bermuatan listrik negatif pada bidang pernukaan dan bermuatan positif pada sisi• sisinya. Dari bentuk dan muatan listrik negatifnya inilah maka lempung bersifat kohesif dan menarik molekul air, sampai pada kondisi jenuh maka akan perpotensi lereng akan lonsor,

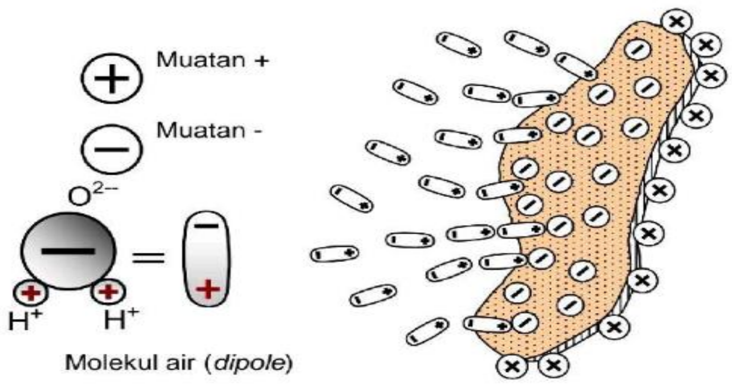

Gambar 2. 11 Partikel lempung dan molekul air

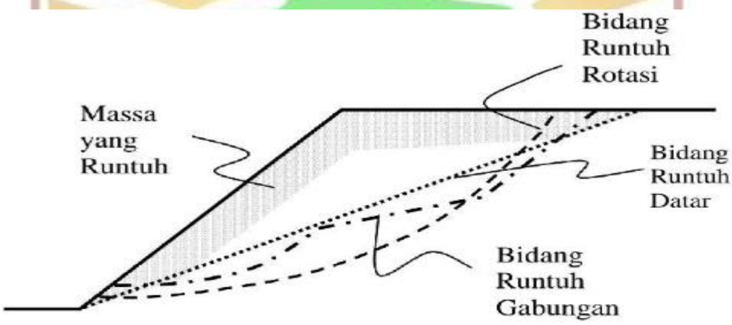

Gambar 2. 12 Gambar bidang runtuh lereng
Sumber :Hakam,A,. (2010)

Partikel penyusun tanah terdiri dari tanah, air dan udara, hal ini yang menyebabkan tanah yang tidak padat masih memiliki rongga udara yang suatu ketika apabila terjadi goncangan atau kelebihan volume air, tanah yang semula memiliki gaya tarik menarik akan kehilangan kuat gesernya. Kehilangan kuat geser tanah ini yang menyebabkan terjadinya longsor baik itu pada saat musim hujan dengan intensitas air berlebih pada tanah, saat terjadinya gempa yang membuat tanah kehilangan gaya gesernya, seperti yang dijelaskan pada gambar berikut.

2.5.1 Stabilan lereng

Dari beberapa bentuk lereng dan beberapa pola keruntuhan lereng yang ada, kita harus periksa dan mengadakan penilaian terhadap lereng tersebut, dengan demikian stabilitas lereng jadi terjaga. Stabilitas lereng dalam arti yang luas merupakan kemantapan dan kekokohan sebuah lereng berdiri, dengan gaya yang terjadi padanya, baik gaya vertikal maupun gaya horizontal, secara formula dikatakan faktor keamanan. Sebuah lereng dikatakan stabil apa bila terjadi keseimbangan antara gaya yang menyebabkan lereng tergeser dengan gaya yang melawan gaya geser tersebut. Besaran faktor aman ini harus besar atau sama dari 1.5, sebaliknya apabila nilai keamanan lereng ini kecil dari 1.5, maka kondisi lereng dalam keadaan labil. Lereng dapat dikatakan stabil apabila Secara teoritis massa yang bergerak dapat dihentikan dengan menaikkan faktor keamanannya. Faktor penyebab yang mempengaruhi terjadinya longsoran ditentukan oleh menurunnya faktor keamanan kemantapan lereng sehingga menjadi kurang dari batas keseimbangan. Dalam analisis harus dipertimbangkan kondisi beban yang menyangkut pengaruh intensitashujan dan perobahan air pori tanah yang akan merobah tegangan izin tanah lateral dan horizontal dan bebean luar lainnya.

Kestabilan dari sebuah lereng secara umum dapat dicari dengan persamaan berikut:

$$F_s = \frac{\tau_f}{\tau_d}$$

(22)

Dimana :

Fs, adalah nilai faktor keamanan terhadap kekuatan tanah

τ_f, adalah kekuatan geser rata – rata dari tanah

τ_d, adalah tegangan geser rata – rata yang bekerja sepanjang bidang lonsor

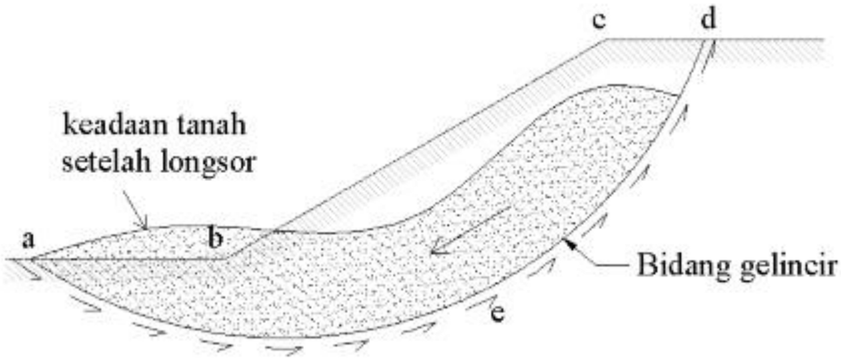

Gambar 2. 13 Sketsa keruntuhan lereng dan gaya yang bekerja

Dari gambar 2.13 diatas merupakan ilustrasi dari kejadian lonsor pada suatu potongan lereng, sebagaimana dijelaskan berikut ini :

1. **Garis a-b-c-d:**
   - Merupakan bentuk **permukaan tanah sebelum terjadi longsor**.
   - Lereng ini terlihat cukup curam, yang menunjukkan potensi ketidakstabilan tanah.
2. **Garis b-e-d (Bidang Gelincir):**
   - Merupakan **bidang gelincir (slip surface)**, yaitu jalur tempat tanah bergerak saat terjadi longsor.
   - Biasanya berupa permukaan melengkung atau cekung yang menjadi tempat terjadinya pergeseran massa tanah akibat gaya gravitasi.
3. **Area yang diarsir di antara a-b-e-d:**
   - Menunjukkan **massa tanah yang mengalami pergeseran**.
   - Ini adalah bagian tanah yang tergelincir dari posisi semula ke arah bawah lereng mengikuti bidang gelincir.
4. **Garis b-e-d ke arah a-b (keadaan tanah setelah longsor):**
   - Menunjukkan **bentuk lereng setelah longsor**.
   - Terjadi pengurangan volume tanah di bagian atas (a-b) dan penumpukan tanah di bagian bawah (b-e).
5. **Anak panah di sepanjang bidang gelincir:**

- ❖ Menandakan arah pergerakan massa tanah selama longsor terjadi pada suatu potongan lereng

Dari ilustrasi gambar 2.13 diatas, gambar ini menggambarkan mekanisme terjadinya longsor akibat ketidakstabilan lereng. Longsor terjadi ketika gaya penggerak (gaya berat tanah, air, aktivitas manusia, dan lain - lainnya.) melebihi gaya penahan tanah. Apabila tanah telah mengalami kecairan, dimana nilai likuid limit tanah besar dari 1, tanah kemudian bergerak menuruni bidang lereng melalui bidang gelincir yang umumnya berbentuk melengkung seperti yang terlihat dari titik **b → e → d**.

BAB 3 METODOLOGI PENELITIAN

3.1 Rancangan Penelitian

Dalam analisis bentuk kegagalan lereng akibat pengaruh dari kenaikan kadar air tanah, dan pengaruhnya terhadap perilaku keruntuhan lereng, maka diperlukan data-data parameter – parameter tanah dan data percobaan yang cukup lengkap. Data tersebut diperoleh dari hasil survey dan investigasi labortorium. Kelengkapan dan keakuratan data sangat menunjang terhadap hasil analisis tujuan penelitian dari topik penelitian.

3.2 Lokasi Pengambilan Sampel

Untuk lokasi pengambilan sampel, sampel Penelitian diambil dari contoh tanah lempung berpasir dilakukan dari satu, dan dua titik daerah rawan lonsor, diambil darilokasi bencana lonsor Talamu Kabupaten Pasaman, dan dilakukan pengujian nilai propertis tanah dilaboratorium. Untuk pengujian labortorium dilakukan di laboratorium tanah Teknik Sipil Unand dan Institut Teknologi Padang.

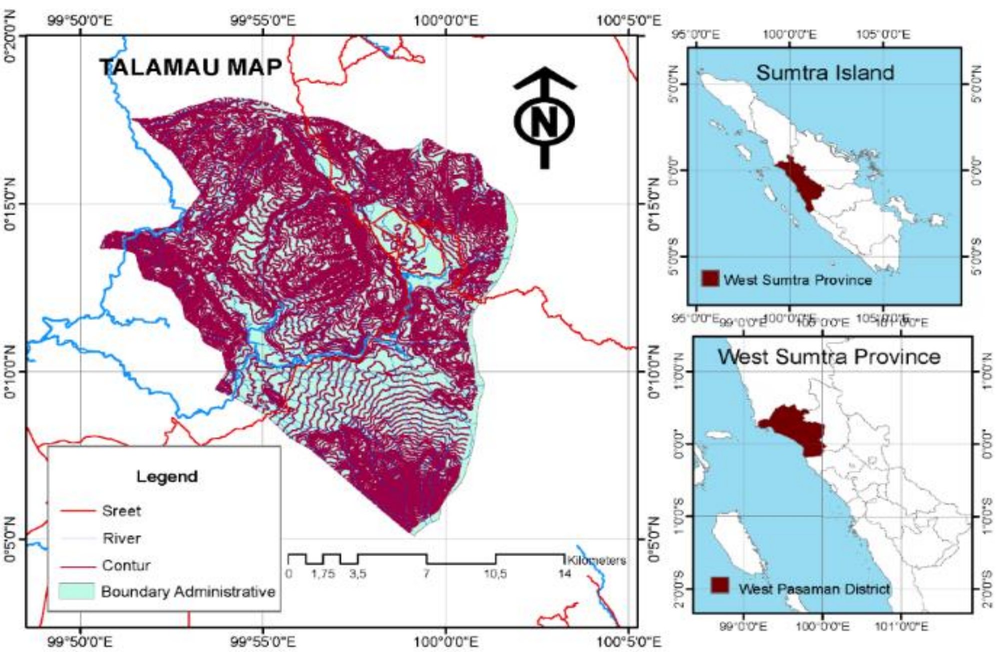

Gambar 3.1 Lokasi Daerah Longsor Dataran Tinggi Talamau di Sumatera Barat

3.3 Pengumpulan Data

Proses data sifat fisik dan mekanik material tanah dasar lereng yang diambil sebagai sampelnya dari daerah studi, dan dilakukan pengujiannya uji propertis tanah di labor geoteknik jurusan teknik sipil Universitas Andalas dan labor teknik sipil Institut Teknologi Padang, sebagaimana diuraikan pada sub bab berikut.

3.3.1 Data Primer

Data yang yang peroleh dari lapangan dengan melakukan pengamatan langsung titik longsor pada daerah studi dan pengambilan sampel tanah dengan melakukan pengeboran lapisan tanah pada zona solit – semi solit – Plastic (Zona SL – PL –LL) sebagai berikut :

- ❖ Densitas
- ❖ Porositas
- ❖ Sebaran Besar Butir
- ❖ Plastisitas tanah
- ❖ Klasifikasi nama tanah
- ❖ Koefisien Permeabilitas
- ❖ Kohesi
- ❖ Sudut Geser Dalam
- ❖ Kadar air tanah awal dan sesudah penjenuhan
- ❖ Kepadatan tanah
- ❖ Simulasi intensitas curah hujan melalui alat simulator pada model yang dibuat
- ❖ Percobaan keruntuhan lereng dengan model alat model lereng untuk besaran sudut kemiringan lereng yang berbeda.

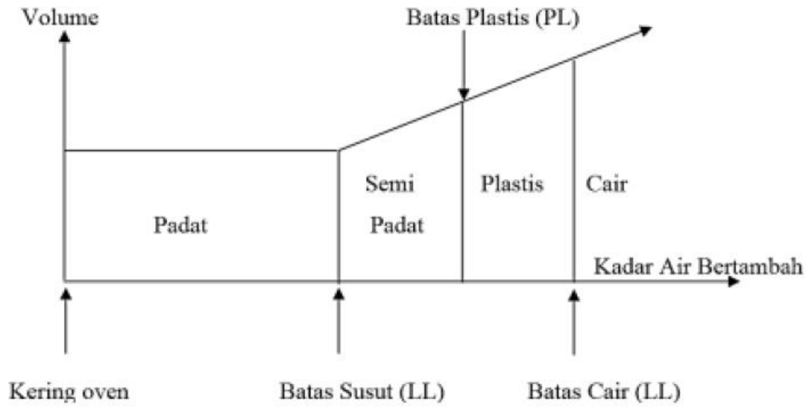

Jarak pengamatan keruntuhan lereng

Gambar 3.2 Diagram Batas Atterberg

3.4 Rencana Percobaan

Prosedur penelitian adalah urut–urutan atau tahap–tahap yang harus dilakukan dalam penelitian ini adalah sebagai berikut :

1. Tahap Persiapan, yang meliputi kegiatan studi merancang model percobaan
2. Penyusunan instrument Percobaan
3. Pelaksanaan percobaan penelitian

Instrumen penelitian yang akan dilakukan membuat model lereng yang dibuat sedemikian rupa berdasarkan bentuk lereng dialam dengan skala tertentu dengan membuat hujan buatan sebagaimana seperti gambar berikut :

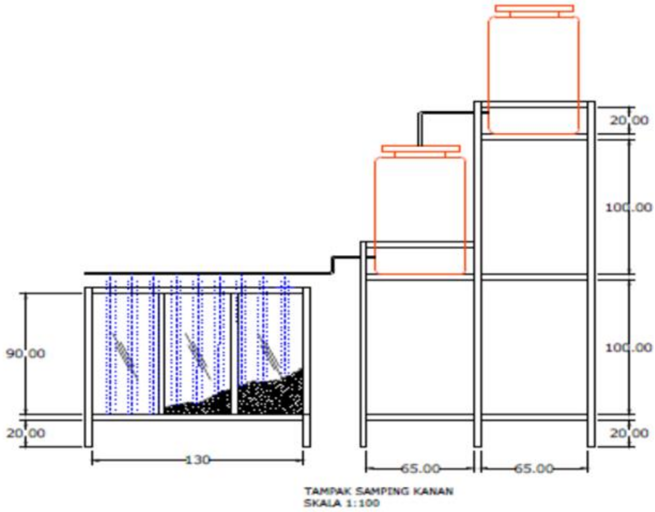

Gambar 3. 3 Sketsa Model Untuk Pengujian Keruntuhan Lereng

3.4.1 Pembuatan Model Lereng

Lereng tersebut dibuat dalam model semi 3-dimensi di laboratorium dengan skala fisik 1 : 10. Berdasarkan pengamatan dilapangan dari berbagai macam besaran sudut lereng dilapangan. Model lereng dibuat dalam sudut 30^0, 45^0, 60^0 dan 90^0. Tinggi model lereng adalah 34 cm. Lebar bagian bawah model lereng adalah 34 cm, sedangkan lebar bagian atas lereng bervariasi bergantung pada sudut kemiringan lerengnya. Lebar lereng yang ditinjau adalah 34 cm. Model lereng dibuat dari lapisan tanah sampel dari lapangan degan paramter tanah hasil pengujian labortorium yang dipadatkan pada kondisi 90 % dari nilai berat volume keringnya (γd g/cm^3) dan kadar air nya (%). Kemudian dimasukan dalam model pengujian hingga membentuk lereng dengan kemiringan yang diinginkan, seperti terlihat pada Gambar 3.4 berikut ini :

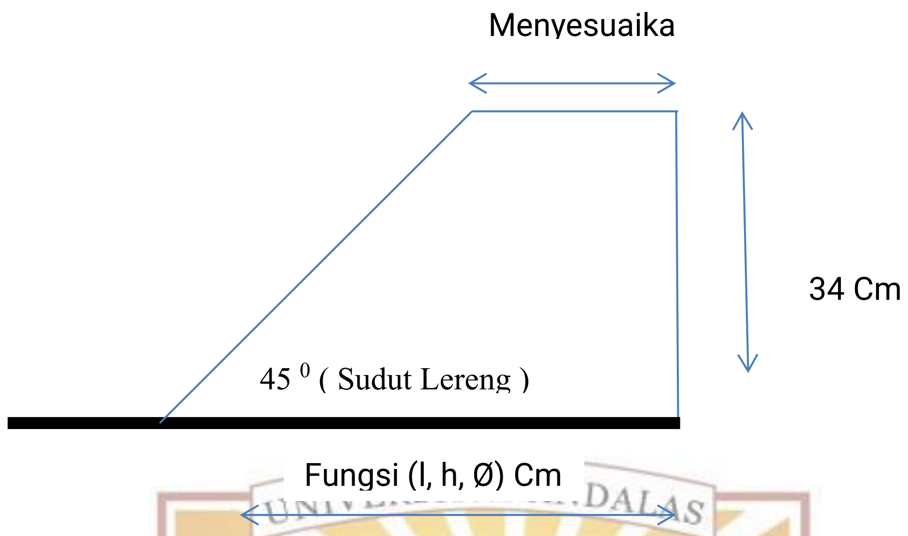

Gambar 3. 4 Ukuran Model Lereng Yang digunakan

3.5 Metodologi

Dalam penelitian ini metode yang dipakai adalah metode ekperimen labortorium dengan mengambil sampel dari lapangan, yaitu dari daerah rawan lonsor, diambil dari daerah talamau dengan skenario atau tahapan – tahapan sebagai berikut:

Penelitian ini difokuskan untuk mengkaji nilai – nilai propertis tanah dasar, mekanisme keruntuhan lereng untuk tanah dasar akibat perobahan kadar air tanah pengaruh intensitas hujan pada skala tetap. Dalam skenario penelitiannya dirancang menjadi beberapa tahapan yaitu, pengujian propertis tanah dasar, tingkat intensitas dan durasi curah hujan kritis, dan rembesan air pada lapisan tanah pada alat percobaan lereng.

Dalam penelitian disertasi ini, mengkaji respon tingkat kadar air tanah, dan pengaruhnya terhadap indek kecairan tanah yang akan menjadi penyebab keruntuhan lereng untuk tanah dasar lempung berpasir. Model ini dibuat dengan Sketsa 3 D untuk pengujian terhadap keruntuhan lereng, dan peningkatan kadar air tanah, dan perobahan nilai likuit limit dari lapisan tanah, seperti gambar berbentuk rangka dengan ukuran seperti gambar dibawah

Gambar 3. 5 Dekomentasi pengujian besaran sudut lereng

3.6 Langkah – Langkah Pengujian

Penelitian ini difokuskan untuk mengkaji mekanisme keruntuhan lereng untuk tanah dasar lempung akibat pengaruh perobahan kadar air .Dalam skenario penelitiannya dirancang menjadi beberapa tahapan yaitu :

1. Pengujian tingkat aliran curah hujan kritis, dan rembesan air pada lapisan tanah pada alat percobaan lereng
2. Pengujian pengujian keruntuhan lereng dengan tahapan – tahapan berikut :

Tahap I :

Merupakan tahapan pengujian awal sampel yang digunakan yaitu meliputi uji sifat-sifat fisik dan nilai parameter tanah,dan erobilitas tanah (seperti berat jenis, berat volume, dan ukuran partikel tanah,dan nilai kadar air tanah ,nilai batas – batas aterberg dari tanah).

Tahap II :

Tahapan ini untuk melakukan pengujian prilaku keruntuhan lereng akibat dari aliran intensitas dan durasi hujan pada skala tetap, dan Pada tahapan ini diuji perobahan kadar air mulai dari waktu tertentu sampai keadaan keruntuhan pada bagian lereng guna mengetahui derajat pembasahan akibat rembesan air akibat dari kejadian intensitas hujan yang terjadi selama percobaan.

Tahap III :

Verifikasi hasil percobaan dengan kondisi lapisan tanah lereng dengan mempergunakan aplikasi program perangkat lunak geoslope atau aplikasi lainnya.

Tahap V :

Pembahasan untuk mencari pengaruh perobahan nilai kadar air tanah dan besaran nilai likuit limit, dan nilai indek kecairan tanah (likuid Indek), dan pengaruh terhadap prilaku keruntuhan lereng untuk lapisan tanah dasar pada kondisi sudut kemiringan lereng tertentu.

3.7 Pengolahan Data

Sebanyak satu sampai dua sampel dengan nilai propertis tanah model lereng yang teertentu dari hasil percobaan labortorium, menghasilkan data yang kemudian diolah secara analisis, dan perangkat lunak computer. Program tersebut memproses data dasar menjadi bentuk penampang lereng. Dari penampang tersebut diolah dalam suatu perangkat lunak untuk mendapatkan tampilan prilaku bentuk keruntuhan lereng sebagai pengaruh dari perobahan tingkat kadar air tanah yang terjadi untuk menghasilkan nilai indek kecairan tanah dan laju keruntuhan dan kedalaman keruntuhan dari lereng berdasarkan, dan parameter – parameter tanah dasar dari lereng dan efek terhadap penyebab prilaku keruntuhan lereng. Sebagai luaran dari penelitian ini penulis mencari "Hubungan antara perobahan dari tingkat kadar air tanah dan nilai likuid limit terhadap nilai indek kecairan tanah, dan untuk mendapatkan bentuk dari sebuah grafik prilaku keruntuhan lereng secara percobaan laboratorium”. Sebagai langkah – langkah dari penelitian dan hasil yang akan didapat dapat dilihat pada table berikut :

Adapun tahapan – tahapan alur penelitian mulai dari awal penelitian sampai tahapan pengumpulan data, Pengujian, pengolahan data, verifikasi data, sampai tahapan proses hasil dapat dilihat pada flow chart berikut ini :

Tabel 3.1 Langkah – Langkah Percobaan

No	Tahap Pengujian	Jenis Percobaan	Hasil Yang Akan Didapat
1	Tahap I	Uji sifat-sifat fisik dan nilai parameter tanah	Nilai propertis tanah;diantaranya Porositas, Sebaran butiran, Densitas, Platisitas, Klasifikasi tanah, Koef. permeabilitas, Kohesi, Sudut geser dalam, Kadarair tanah awal, dan sesudah penjenuhan,dan Erobilitas lapisan tanah (Data primer)
2	Tahap II	Percobaan prilaku kegagalan lereng dengan alat model lereng dengan pemberian besaran intensitas hujan dari waktu awal sampai terjadi lonsor lereng	• Pemberian intensitas hujan dari interval waktu awal sampai saat terjadi keruntuhan dari model lereng berdasarkan geometric lereng • Pengukuran kadar air tanah setiap interval waktu tertentu sampai terjadi keruntuhan pada model lereng,dengan alat sensor alat pengujian kadar air (WC) • Nilai kohesi, sudut geser dalam, dan berat jenis dari tanah lereng • Pengamatan bentuk prilaku keruntuhan pada lereng dari percobaan yang dilakukan • (Data Primer)
4	Tahap III	Analisis Data	Verifikasi hasil percobaan

No	Tahap Pengujian	Jenis Percobaan	Hasil Yang Akan Didapat
			dengan berbagai kondisi perobahan tingkat kadar air tanah dari lereng dengan mempergunakan hasil analisis.
5	Tahap IV	Hasil Analisis Data	Analisis Formula laju tingkat keruntuhan lereng, sebagai efek dari tingkat perobahan kadar air tanah terhadap perobahan indek kecairan tanah dengan berbagai sudut geometri lereng 30, 45, 60, 90^0 yang ditemukan dalam model penelitian.

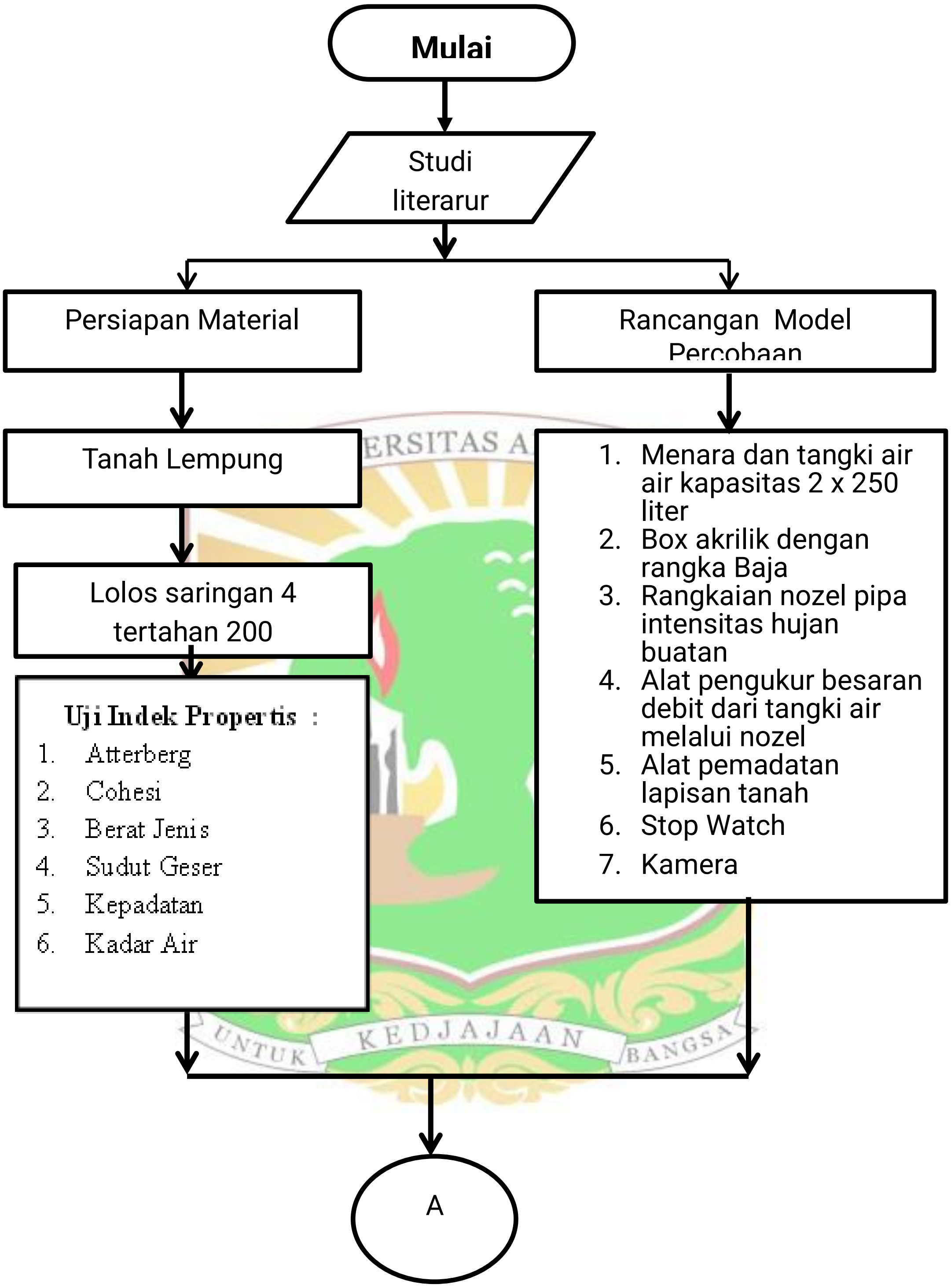
Mulai
Studi literarur
Persiapan Material
Rancangan Model Percobaan
Tanah Lempung
Lolos saringan 4 tertahan 200
Uji Indek Propertis :
1. Atterberg
2. Cohesi
3. Berat Jenis
4. Sudut Geser
5. Kepadatan
6. Kadar Air
1. Menara dan tangki air air kapasitas 2 x 250 liter
2. Box akrilik dengan rangka Baja
3. Rangkaian nozel pipa intensitas hujan buatan
4. Alat pengukur besaran debit dari tangki air melalui nozel
5. Alat pemadatan lapisan tanah
6. Stop Watch
7. Kamera
A

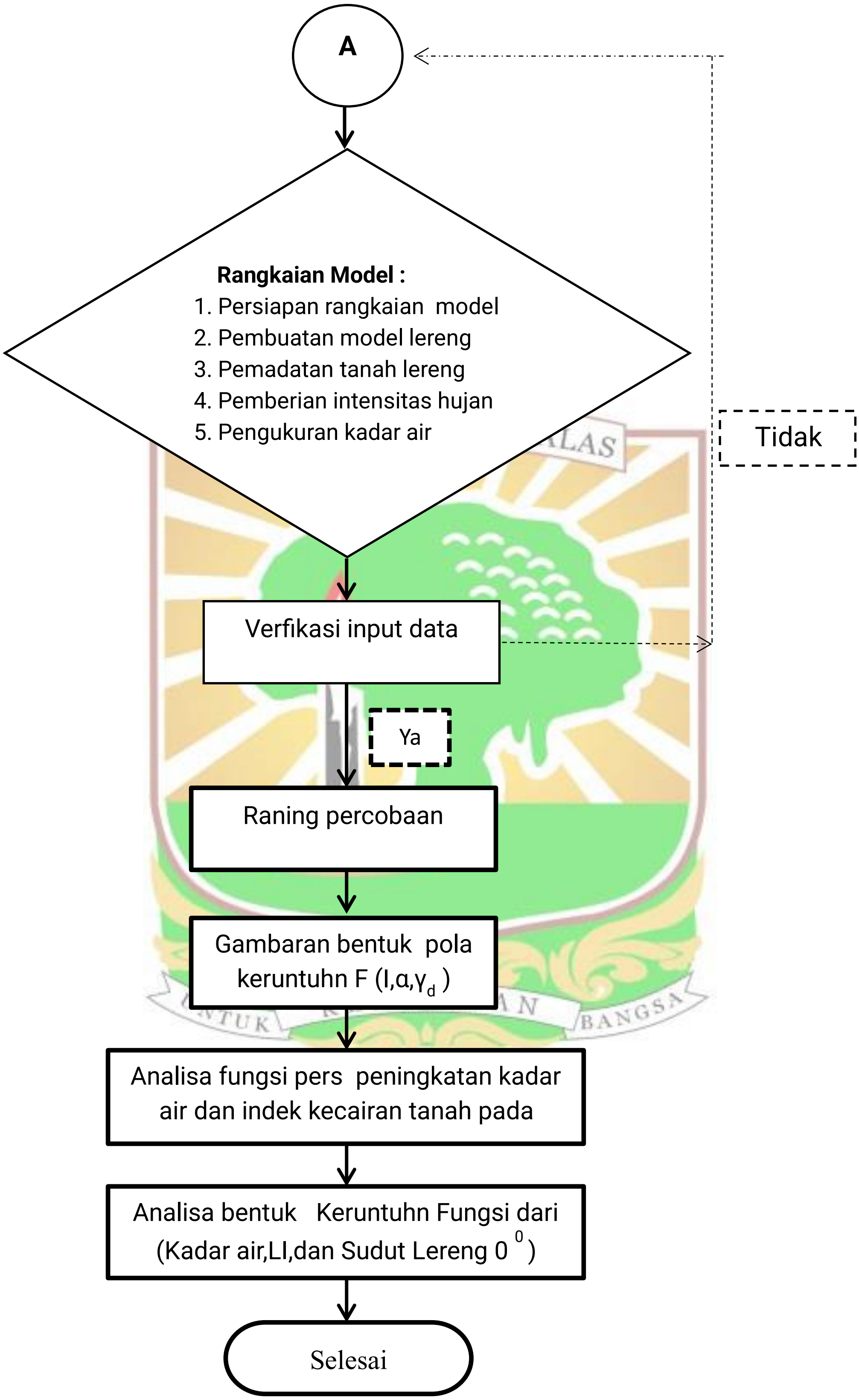

Gambar 3. 6 Diagram aliran penelitian

BAB 4 HASIL DAN PEMBAHASAN

4.1 Tinjauan Umum

Gerakan tanah dalam bentuk lonsor lereng merupakan suatu massa tanah yang bergerak secara vertikal dari atas kebawah disepanjang lereng. Gerakan ini terjadi apabila gaya-gaya yang menahan (resisting force) massa tanah dilereng lebih kecil dari pada gaya yang mendorong atau meluncurkan tanah disepanjang lereng. Gaya yang menahan massa tanah disepanjang lereng dipengaruhi oleh kedudukan muka air tanah, sifat fisik/mekanisme tanah terutama daya ikat tanah dan sudut geser tanah yang bekerja disepanjang bidang luncuran. Gaya pendorong tersebut dipengaruhi diantaranya oleh kandungan kadar air tanah,air pori tanah akibat dari volume aliran infiltrasi pada saat curah hujan meningkat sampai nilai ekstrinya beban ,faktor tutupan lahan dan massa tanah.Tanah yang cenderung terjadi longsor adalah tanah yang memiliki gaya tarik menarik antar partikel (kohesi) kecil akibat tidak ada ikatan antar tanah. Komposisi tanah itu sendiri terdiri dari air, tanah, dan udara seperti Gambar. 4.1 dibawah ini.

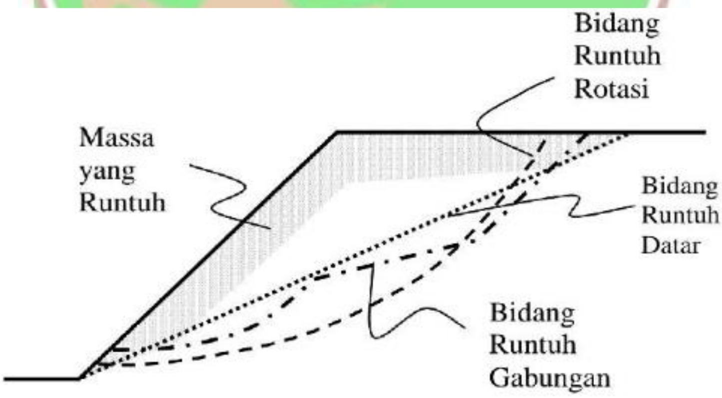

Gambar 4. 1 Gambar bidang runtuh lereng
Sumber ; Abdul Hakam,. (2010)

4.2 Data Hasil Penelitian

4.2.1 Hasil percobaan

1. Data parameter tanah

Data Parameter tanah adalah ukuran atau acuan untuk mengetahui atau menilai hasil suatu proses perubahan yang terjadi dalam tanah baik dari sifat fisik dan jenis tanah. Dengan mengenal dan mempelajari sifat-sifat tersebut, keputusan yang diambil dalam perancangan penelitian akan lebih ekonomis. Karena sifat-sifat tersebut maka penting dilakukan penyelidikan tanah (soil investigation). Dari percobaan yang dilakukan erhadap sampel tanah yang dijadikan dasar lereng dapat ditampilkan pada tabel dibawah ini.

Tabel 4.1 Data nilai parameter tanah

Pengujian	Parameters	Nilai	Unit
Kadar Air	w	60.594	%
Berat Volume	γ	1.558	gram/cm3
Specific gravity	Gs	2.627	
Analisa saringan	Gravel	0.000	%
	Sand	34.067	%
	Clay	65.933	%
Atterberg limit	LL	47,853	%
	PL	38,455	%
	PI	9,395	%
Direct shear	c	0.218	kg/cm2
	φ	22.835	º
Pemadatan	w opt	48.455	gram/cm3
	γ dry max	1.235	gram/cm3

2. Data sebaran butiran

Tujuan dari pemeriksaan sebaran butiran ini adalah untuk menentukan distribusi butir (gradasi) dari suatu sampel tanah dengan menggunakan saringan ukuran paling kecil tertahan di saringan no. 200 dan menentukan klasifikasi tanah (USCS) Unified Soil Classification System, sesuai dengan hasil pemeriksaan sebaran gradasi butir tanah, sebagaimana yang ditampilkan pada tabel berikut.

3. Klasifikasi tanah metoda USCS

Berdasarkan dari data percobaan sebaran butiran dalam mencari klasifikasi tanah dasar lereng dari data sebaran butiran, maka klasifikasi tanah dicari dengan metoda USCS (*Unified Soil Clasification System*) :

Dari data diatas dapat disimpulkan struktur tanah dasar percobaan lereng dapat disimpulkan sebagai berikut :

Tabel 4.2 Data sebaran butiran

No. Saringan	Berat tertahan	Jlh Berat tertahan	Tertahan (%)	Lolos (%)	Diamater Butiran
4	0,0	0,000	0,00	100,00	4,75
10	4,3	4,300	1,43	98,57	2
20	22,2	26,500	8,83	91,17	0,84
40	32,3	58,800	19,60	80,40	0,42
100	38,1	96,900	32,30	67,70	0,15
200	5,3	102,200	34,07	65,93	0,075
PAN	197,8	300	100,00	0,00	

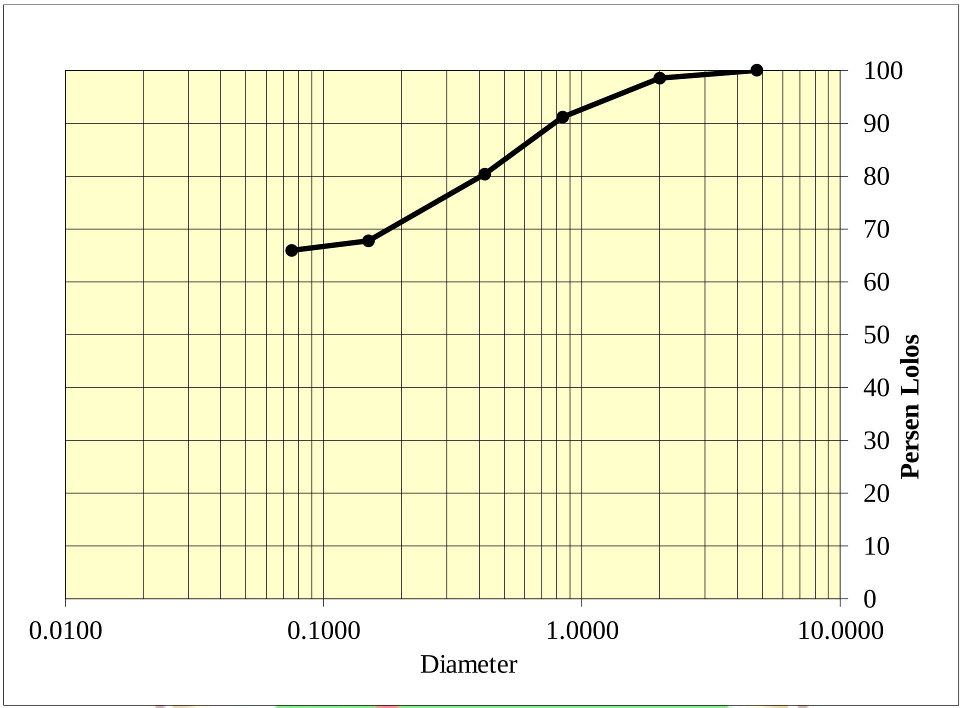

Gambar 4. 2 Grafik sebaran butiran

Tabel 4.3 Jenis lapisan tanah dasar pemodelan lereng lereng

No	Jenis tanah dasar	Persentase (%)	Keterangan
1	Kerikil	0,00	% tertahan saringan 4
2	Pasir	34,047	% Tertahan saringan 200
3	Lempung	65,93	% Lolos saringan 200

Gambar 4. 3 Pengujian Analisa saringan di labortorium

4. Pengujian batas – batas Atterberg (SNI 03 1966,1967,4143:1990)

Atterberg menggambarkan batas-batas konsistensi dari tanah berbutir halus dengan mempertimbangkan kandungan kadar airnya. Batas-batas tersebut terbagi atas 3 pengujian, yaitu:

- Pengujan batas susut, (perubahan kondisi padat ke semi padat)
- Pengujian batas plastis, (perobahan kondisi semi padat ke plastis)
- Pengujian batas cair, (perobahan kondisi tanah dari plastis ke cair),dari percobaan propertis tanah sebagai mana yang ditampilkan pada table berikut.

Tabel 4.4 Pemeriksaan Batas - Batas Konsistensi

Jenis Pemeriksaan		Batas Cair				Batas Plastis	
No	**Banyaknya Pukulan**	20	24	29	32	A	B
1	Berat Cawan + Tanah Basah	8,55	7,54	8,05	10,23	6,94	7,07
2	Berat Cawan + Tanah Kering	7,13	6,45	6,79	8,31	6,21	6,52
3	Berat Air (1-2)	1,42	1,09	1,26	1,92	0,73	0,55
4	Berat Cawan	4,25	4,2	4,15	4,13	4,24	5,14
5	Berat Tanah Kering (2-4)	2,88	2,25	2,64	4,18	1,97	1,38
6	Kadar Air (3 : 5) x 100 (%)	49,306	48,444	47,727	45,933	37,056	39,855
7	Rata - rata	47,853				38,455	

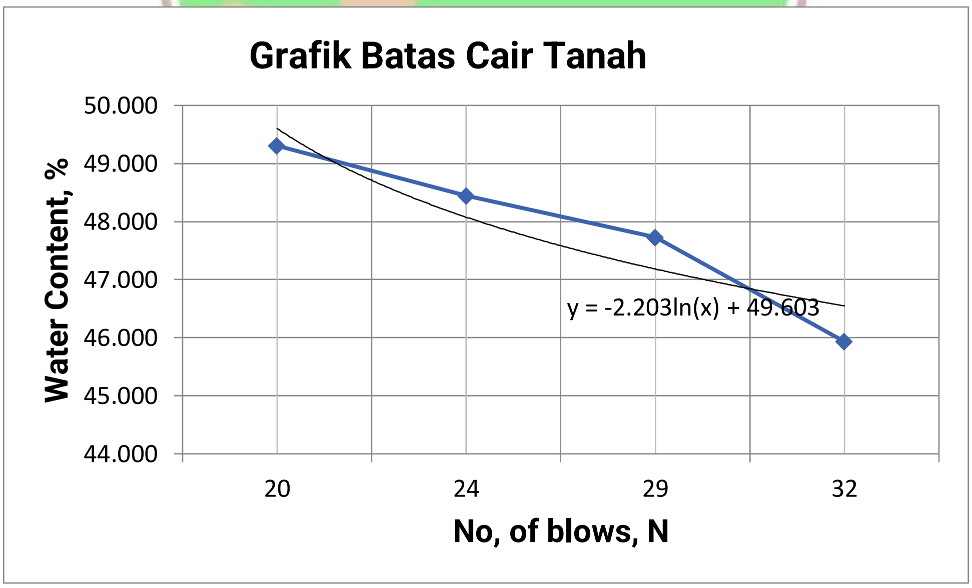

Gambar 4. 4 Grafik Batas Cair Tanah

Tabel 4. 5 Batas Susut Tanah

Nomor Cawan Susut		I (gram)	II (gram)
Berat Cawan Susut W_1		19,010	19,190
Berat Cawan + tanah basah	W_2	29,780	29,450
Berat Cawan + Tanah Kering W_3		25,740	25,700
Berat tanah Kering	$W_0 = W_3 - W_1$	6,730	6,510
Berat Mangkok Sampel Susut W_4		28,990	28,990
Berat Mangkok Sampel Susut + Hg W_5		114,840	100,160
Berat Air Raksa (Hg)	$W_6 = W_5 - W_4$	85,850	71,170
Volume Tanah Kering (cm3)	$V_0 = W_6 / 13,6$	6,313	5,233
Batas Susut Tanah	$SL = \{(V_0/W_0) - (1/Gs)\} \times 100\%$	33,410	19,999

Tabel 4. 6 Nilai batas – batas Atterberg

Uraian	**Simbol**	**Nilai**	**Satuan**
BATAS CAIR (LIQUID LIMIT)	LL	47,853	%
BATAS PLASTIS (PLASTIC LIMIT)	PL	38,455	%
INDEKS PLASTISITAS (PLASTICITY INDEX)	PI	9,395	
Batas Susut	SL	26,704	%

Berdasaarkan nilai batas Atterberg diatas maka jenis tanah didapat sebagai berikut:

Lolos saringan 200 = 65,93 %

LL (Liquid Limit) = 47,853 %

PL (Plastic Limit) = 38,455 %

PI (Plasticity Index) = 9,395 %

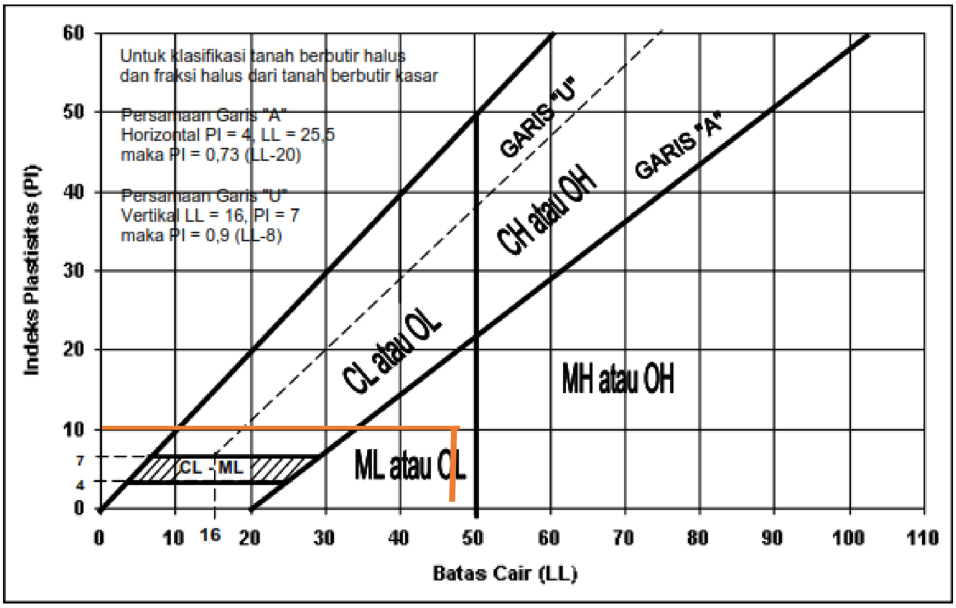

Gambar 4. 5 Grafik plastisitas jenis tanah

Maka tanah dikategorikan pada tanah lanau organik plastis tinggi, dengan symbol ML atau OL (Lanau anorganik, pasir halus sekali, serbuk batuan, pasir halus berlanau atau berlempung, atau Lanau-organik dan lempung berlanau organik dengan plastisitas)

Gambar 4. 6 Dokumentasi Pengujian Liquid Limit

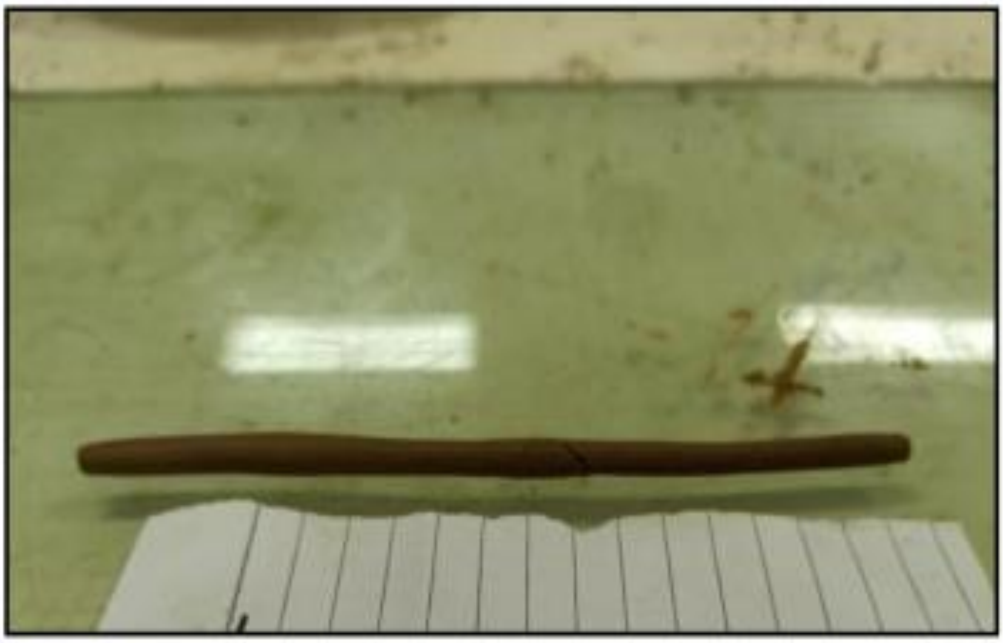

Gambar 4. 7 Dokumentasi pengujian plastis Limit

5. Kepadatan tanah dasar lereng

Kepadatan tanah dasar pada pemodelan percobaan lereng berdasarkan besaran sudut lereng yang ditentukan berdasarkan berat volume dan kadar air awal, dapat ditampilkan pada tabel berikut :

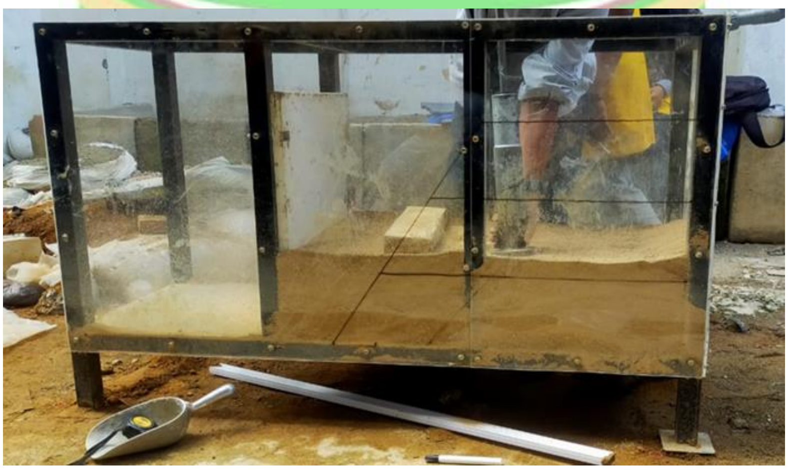

Gambar 4. 8 Pemadatan lapisan tanah dasar lereng

Kepadatan tanah dasar dari model lereng dalam penelitian ini berdasarkan fungsi dimensi lereng dan kadar air awal dari lereng sebelum dilakukan penghujan pada percobaan dalam model dari lereng ini berdasarkan skala pemodelaan labortorium dengan derajat sudut lereng berfariasi dengan besaran sudut 30,45,60, dan 90 ^{0} (derjat), sebagaimana yang dijelaskan pada sub bab berikut ini.

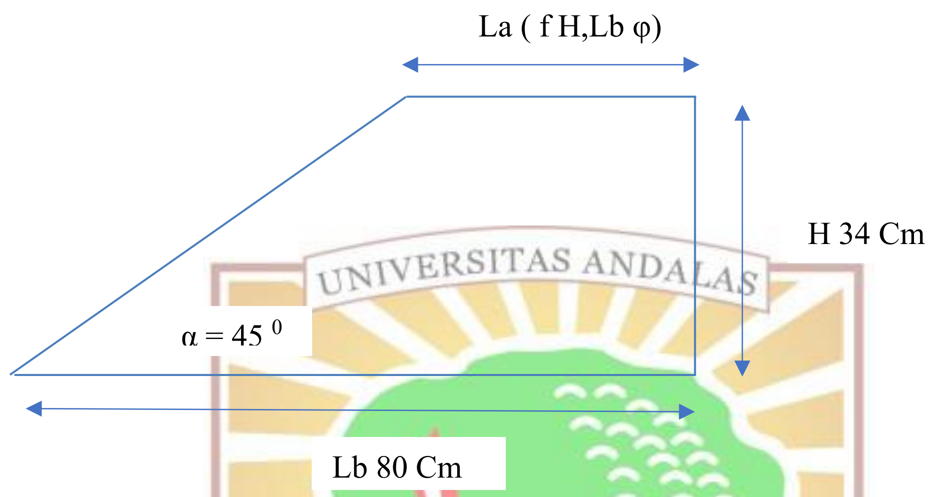

Gambar 4. 9 Dimensi benda uji

Tabel 4. 7 Nilai kepadatan lereng dan kadar air awal

Sudut lereng (0^{0})	Kadar air awal (%)	Kepadatan tanah γd (gr/cm3)
30	17,67	1,75
45	25,00	1,06
60	7,41	1,05
90	9,64	1,13

Tabel 4. 8 Gambar potongan dan kepadatan lereng

No	Gambar Potongan	Sudut Lereng	Kepadatan (γ_d) (Gr/cm^3)

No	Gambar Potongan	Sudut Lereng	Kepadatan (γ_d) (Gr/cm^3)
1		30	1.75
2		45	1.06
3		60	1.05
4		90	1.13

4.2.2 Kondisi Geometrik Benda Uji

Dimensi dan kemiringan dasar dari benda uji yang digunakan untuk analisis percobaan terdiri dari satu lapis tanah dasar yang mempunyai kepadatan tertentu untuk setiap benda uji seperti yang diilustrasikan pada tabel 3.6 diatas. Dimensi benda uji dari lereng memiliki panjang total 80 meter,dan lebar 34 cm, dan tinggi benda uji setinggi 34 cm, dan kemiringan lereng nya terdiri dari 30, 45,60,dan 90 ^{0} (derajat). Ketebalan kumulatif lapisan tanah adalah 34 sentimeter, dengan kedalaman lapisan permukaan dan bawah permukaan diasumsikan sama. Ketebalan spesifik ini mencerminkan kondisi yang umum terjadi di banyak wilayah kaya tanah liat atau lembung. dimana aktivitas tanah longsor sering terjadi. Daerah seperti ini, yang memiliki kedalaman tanah berkisar antara 50 hingga 100 sentimeter yang memberikan wawasan penting mengenai faktor geoteknik yang mempengaruhi stabilitas lereng di wilayah tersebut.Dalam percobaan ini bentuk besaran benda uji sebagaimana yang dijelaskan pada gambar berikut sesuai besaran geometric dari masing – masing benda uji.

(a) Lereng 30 ^{0}

(b) Lereng 45 ^{0}

(c) Lereng 60 ^{0}

(d) Lereng 90 ^{0}

Gambar 4. 10 Dimensi benda uji untuk sudut geometri

Dari percobaan simulasi Keruntuhan lereng sangat ditentukan oleh seberapa besar intensitas hujan (Rainfall intensitas), dan memberi efek terhadap perobahan besaran tingkat kadar air tanah, nilai batas cair tanah(likuid limit),dan batas plastis tanah, dan nilai plastis indek tanah yang akan memberi efek terhadap tingkat kecairan tanah yang terjadi yang akan mempengaruhi tingkat kepadatan tanah dari lereng yang dibentuk dengan sudut geometik lereng tertentu. Dari percobaan simulasi hujan ini pada percobaan ini dapat disajikan pada sub bab berikut yang tertera pada gambar geometri prilaku pergerakan tanah pada bidang lereng benda uji, sebagai mana disajikan pada gambar berikut :

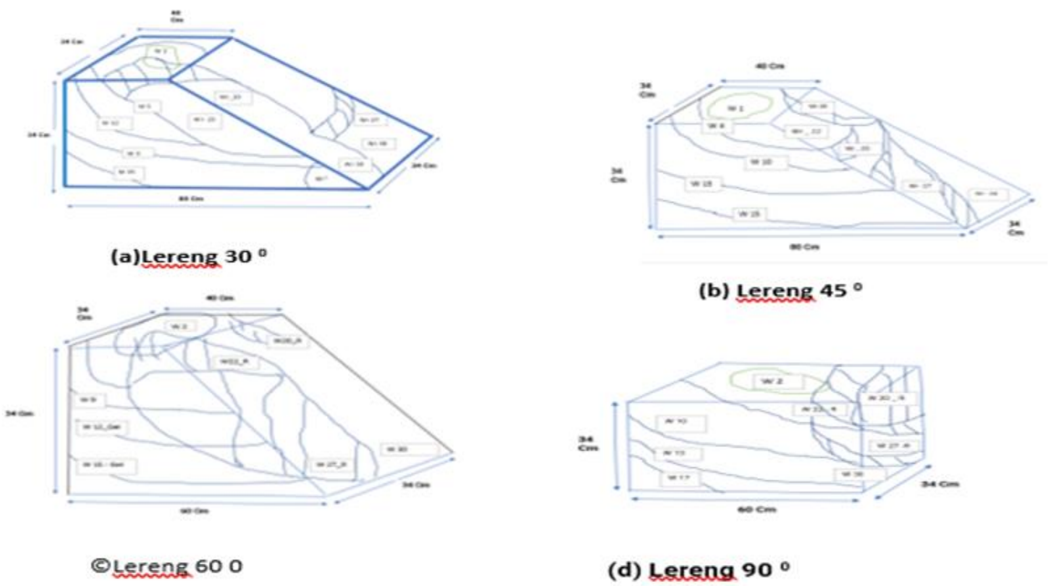

Gambar 4. 11 Profil kontur pergerakan tanah pada lereng

4.2.3 Percobaan tren simulasi hujan

Keruntuhan lereng sangat ditentukan oleh seberapa besar intensitas (*Rainfall intensitas*), dan memberi efek terhadap perobahan besaran tingkat kadar air tanah yang akan memberi efek terhadap tingkat indek kecairan tanah akan terjadi yang akan merobah jenis kepadatan tanah dari lereng yang dibentuk dengan sudut geometik lereng tertentu. Dari percobaan simulasi hujan ini pada percobaan dapat disajikan pada sub bab berikut yang tertera pada tabel berikut:

Tabel 4. 9 Data percobaan tren intensitas hujan

No	Waktu T (Menit)	Tinggi Intensitas hujan (mm/menit)	Tinggi Intensitas hujan Rata-rata (mm/menit)
1	0	17	121
2	1	105	121
3	2	122	121
4	3	117	121
5	4	120	121
6	5	122	121
7	6	121	121
8	7	122	121
9	8	121	121
10	9	122	121
11	10	120	121
12	11	119	121
13	12	122	121
14	13	122	121
15	14	120	121
16	15	122	121
17	16	120	121
18	17	122	121
19	18	122	121
20	19	124	121
21	20	120	121
22	21	122	121
23	22	120	121
24	23	122	121
25	24	121	121
26	25	122	121
27	26	120	121
28	27	122	121
29	28	121	121
30	29	118	121
31	30	122	121
Hujan Rata 2		121	

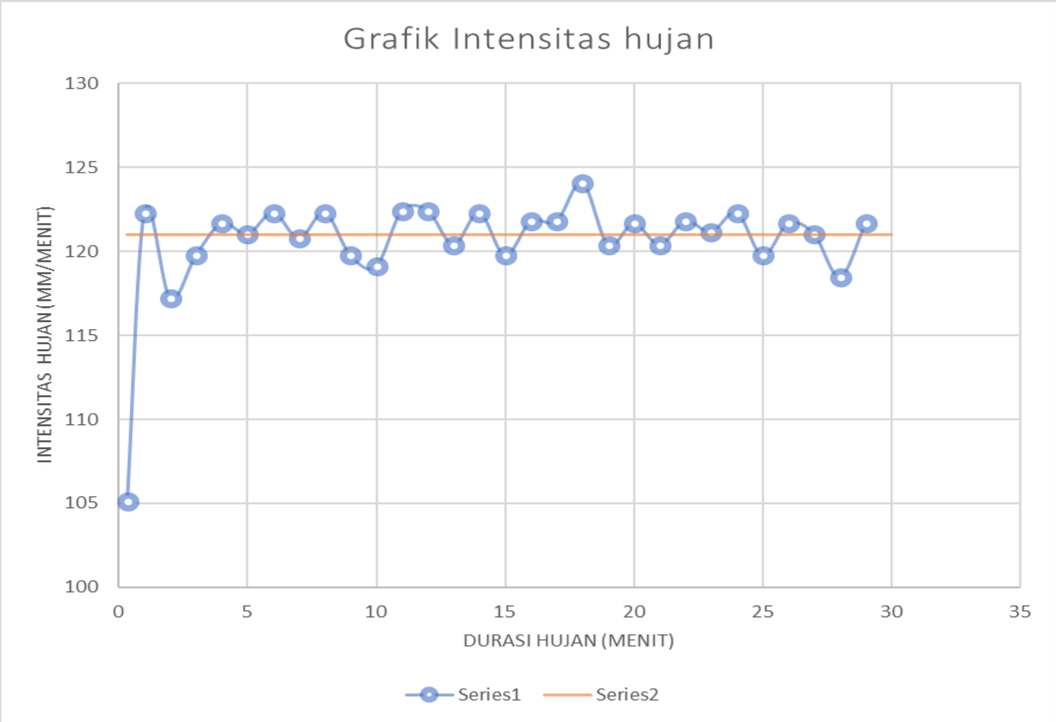

Gambar 4. 12 Grafik percobaan tren intensitas hujan

4.2.4 Percobaan simulasi hujan pada lereng

Percobaan ini bertujuan untuk memahami dampak curah hujan terhadap kestabilan lereng dan proses erosi dan pergerakan tanah pada lereng dengan kemiringan 30, 45, 60, dan 90^0 (derajat). Simulasi ini dilakukan di laboratorium dengan menggunakan model lereng buatan yang terbuat dari kotak akrilik atau bahan transparan lainnya, yang diisi dengan tanah lapisan atas (top soil) dengan kelembapan awal yang terukur.

Langkah-langkah percobaan :

1. **Persiapan Lereng:**

Lereng buatan disiapkan dengan sudut kemiringan tetap sebesar 30, 45, 60, dan 90^0 (derajat). Tanah dimasukkan secara merata dan dipadatkan sesuai standar tertentu sebagai analogi derajat kondisi lapangan.

2. **Instalasi Alat:**

Sistem simulasi hujan dipasang di atas model lereng. Alat ini mampu menyemprotkan air secara merata menyerupai intensitas hujan alami.

Sensor kelembapan dan pengukur limpasan (runoff collector) juga dipasang di bagian bawah lereng.

3. **Pelaksanaan Simulasi Hujan:**

Simulasi hujan dijalankan dengan intensitas dan durasi tertentu, besaran rata – rata intensitas hujan sebesar 121 mm/jam selama 30 menit. Selama proses, pengamatan dilakukan terhadap:

- Waktu munculnya limpasan (runoff)
- Volume limpasan
- Jumlah tanah yang tererosi
- Perubahan struktur permukaan lereng
- Perobahan nilai kadar air tanah

4. **Pengamatan dan Dokumentasi:**

Hasil pengamatan didokumentasikan melalui video dan pencatatan data. Fenomena yang dicatat meliputi aliran permukaan, pengendapan partikel, alur-alur erosi (*rill erosion*), probahan nilai kadar air tanah dan kemungkinan terjadinya longsoran kecil.

4.2.5 Data Percobaan Intensitas Hujan

Data yang terkumpul untuk melihat hubungan antara intensitas hujan, kemiringan lereng, dan laju erosi atau stabilitas lereng. Biasanya juga dilakukan perbandingan dengan model lereng yang diberi perlakuan.

4.2.5.1 Percobaan Simulasi Hujan pada Lereng 30 ^{0}

Tabel 4. 10 Percobaan simulasi hujan pada lereng 300

No	Waktu T (Menit)	Tinggi curah hujan (mm/menit)	Tinggi curah hujan Kumulatif (mm/menit)	Tinggi curah hujan Rata-rata (mm/menit)	Kadar Air Setelah Penghujan (%)	Kondisi Lereng Selama penghujanan
1	0	17	17	121	-	Mulai

No	Waktu T (Menit)	Tinggi curah hujan (mm/menit)	Tinggi curah hujan Kumulatif (mm/menit)	Tinggi curah hujan Rata-rata (mm/menit)	Kadar Air Setelah Penghujan (%)	Kondisi Lereng Selama penghujanan
						Percobaan
2	1	105	122	121	-	
3	2	122	245	121	-	Aliran Masuk lapisan lereng
4	3	117	362	121	-	
5	4	120	482	121	-	
6	5	122	603	121	30	Terjadi depormasi pada bidang lereng
7	6	121	724	121	30	
8	7	122	846	121	30	
9	8	121	967	121	30	
10	9	122	1090	121	30	Bidang gelincir mulai terjadi
11	10	120	1209	121	46,96	
12	11	119	1328	121	46,96	
13	12	122	1451	121	46,96	Bidang gelincir mulai membesar
14	13	122	1573	121	46,96	
15	14	120	1694	121	46,96	
16	15	122	1816	121	50,63	Aliran rembesan mulai kedasar
17	16	120	1936	121	50,63	
18	17	122	2057	121	50,63	
19	18	122	2179	121	50,63	
20	19	124	2303	121	50,63	
21	**20**	120	2424	121	55,51	Mulai terjadi runtuh pada kepala lereng
22	21	122	2545	121	55,51	
23	22	120	2666	121	55,51	Keruntuhan makin bertambah
24	23	122	2788	121	55,51	
25	24	121	2909	121	55,51	
26	25	122	3031	121	59,92	Tumit lereng semakin labil terhadap runtuh
27	26	120	3151	121	59,92	
28	27	122	3272	121	59,92	Kaki dan kepala
29	28	121	3393	121	59,92	

No	Waktu T (Menit)	Tinggi curah hujan (mm/menit)	Tinggi curah hujan Kumulatif (mm/menit)	Tinggi curah hujan Rata-rata (mm/menit)	Kadar Air Setelah Penghujan (%)	Kondisi Lereng Selama penghujanan
30	29	118	3512	121	59,92	lereng lonsor total
31	**30**	122	3634	121	**63**	Lonsor sudah berhenti
Hujan Rata 2		121				

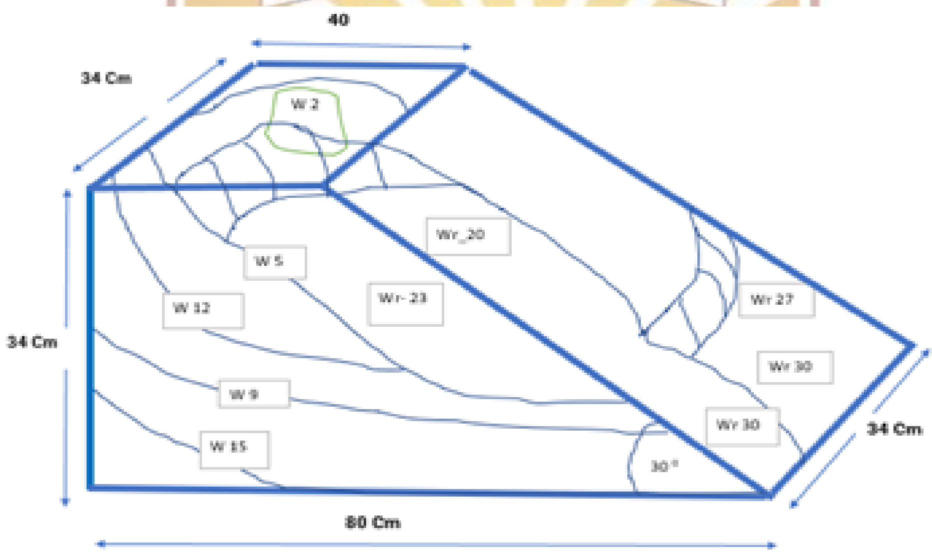

Gambar 4. 13 Bidang gelincir lereng sudut 30^0

Tabel 4. 11 Prilaku keruntuhan dan nilai kadar air tanah pada lereng 300

No	T (menit)	Bid Gelincir @ Runtuh	Kadar air (%)	Berat Volume ɣ (gr/cm 3)	Ket
1	2'	Bidang rembes	-	-	Rembesan
2	5'	Bidang gelincir	30,0		Gelincir
3	9'	bidang gelincir	30,0		Gelincir
4	15'	Bidang gelincir ke dasar	47,0		Gelincir
5	20'	Runtuh di kepala lereng	55,5		Runtuh

6	23'	Runtuh bertambah	55,5		Runtuh
7	27'	Kepala dan kaki lereng runtuh	59,9		Runtuh
8	30'	Keruntuhan max berhenti	63,0	1,581	Runtuh berakhir

1. Analisis Data Intensitas Hujan Lereng 0 ^{0}

Data tersebut menggambarkan pengaruh curah hujan terhadap stabilitas lereng selama periode waktu tertentu. Berikut adalah analisis detailnya:

❖ Hubungan Curah Hujan dengan Kondisi Lereng

- **Curah Hujan Awal (T = 0–4 menit)**

  Pada awal percobaan, curah hujan dimulai dengan intensitas 17 mm/menit, kemudian meningkat secara signifikan hingga mencapai 122 mm/menit. Lereng masih dalam kondisi stabil pada fase ini, meskipun aliran mulai masuk ke lapisan lereng setelah 2 menit.

- **Periode Deformasi (T = 5–9 menit)**

  Setelah 5 menit curah hujan dengan rata-rata intensitas 121 mm/menit, deformasi mulai terjadi pada bidang lereng, diikuti dengan bidang gelincir yang mulai muncul pada menit ke-9. Hal ini menunjukkan bahwa curah hujan tinggi mulai mempengaruhi kestabilan internal lereng.

- **Periode Gelincir Membesar (T = 10–15 menit)**

  Ketika curah hujan terus berlanjut dengan intensitas konstan (sekitar 121 mm/menit), kadar air tanah meningkat menjadi 46,96% (T = 10 menit) dan terus naik hingga 50,63% (T = 15 menit). Pada fase ini, bidang gelincir semakin membesar, dan aliran rembesan mulai mencapai dasar lereng.

- **Periode Keruntuhan (T = 20–30 menit)**

  Pada menit ke-20, keruntuhan mulai terjadi di kepala lereng dengan kadar air mencapai 55,51%. Keruntuhan semakin parah hingga kaki dan kepala lereng mengalami longsor total pada menit ke-27. Kadar air pada fase akhir mencapai 63%, yang menjadi salah satu penyebab utama keruntuhan total lereng.

❖ Kadar Air Tanah

- Kadar air mulai signifikan setelah curah hujan berlanjut selama lebih dari 10 menit.
- Peningkatan kadar air tanah menyebabkan lereng kehilangan kohesi, sehingga kekuatan lereng menurun drastis.

❖ **Kronologi Keruntuhan**

- **T = 5 menit:** Deformasi awal pada bidang lereng.
- **T = 9 menit:** Bidang gelincir mulai terlihat.
- **T = 12 menit:** Bidang gelincir semakin besar.
- **T = 20 menit:** Keruntuhan dimulai dari kepala lereng.
- **T = 27 menit:** Lereng mengalami longsor total, terutama di kaki dan kepala.
- **T = 30 menit:** Longsor berhenti.

4.2.5.2 Percobaan Simulasi Hujan pada Lereng 45 ^{0}

Tabel 4.12 Percobaan simulasi hujan pada lereng 45^0

No	Waktu T (Menit)	Tinggi curah hujan (mm/menit)	Tinggi curah hujan Kumulatif (mm/menit)	Tinggi curah hujan Rata-rata (mm/menit)	Kadar Air Setelah Penghujan (%)	Kondisi Lereng Selama penghujanan
1	0	0	0	121	-	Mulai Percobaan
2	1	105	105	121	-	
3	2	122	227	121	-	Aliran Masuk lapisan lereng
4	3	117	345	121	-	
5	4	120	464	121	13,74	
6	5	122	586	121	13,74	Terjadi depormasi pada bidang lereng
7	6	121	707	121	13,74	
8	7	122	829	121	13,74	
9	8	121	950	121	13,74	

No	Waktu T (Menit)	Tinggi curah hujan (mm/menit)	Tinggi curah hujan Kumulatif (mm/menit)	Tinggi curah hujan Rata-rata (mm/menit)	Kadar Air Setelah Penghujan (%)	Kondisi Lereng Selama penghujanan
10	9	122	1072	121	13,74	Bidang gelincir mulai terjadi
11	10	120	1192	121	**43,75**	
12	11	119	1311	121	**43,75**	
13	12	122	1434	121	**43,75**	Bidang gelincir mulai membesar
14	13	122	1556	121	**43,75**	
15	14	120	1676	121	**43,75**	
16	15	122	1799	121	**46,15**	Aliran rembesan mulai kedasar
17	16	120	1918	121	**46,15**	
18	17	122	2040	121	**46,15**	
19	18	122	2162	121	**46,15**	
20	19	124	2286	121	**46,15**	
21	**20**	120	2406	121	50,00	Mulai terjadi runtuh pada kepala lereng
22	21	122	2528	121	50,00	
23	22	120	2649	121	50,00	Keruntuhan makin bertambah
24	23	122	2770	121	50,00	
25	24	121	2891	121	50,00	
26	25	122	3014	121	52,17	Tumit lereng semakin labil terhadap runtuh
27	26	120	3134	121	52,17	
28	27	122	3255	121	52,17	Kaki dan kepala lereng lonsor total
29	28	121	3376	121	52,17	
30	29	118	3495	121	52,17	
31	**30**	122	3616	121	68,75	Lonsor sudah berhenti
Hujan Rata 2		121				

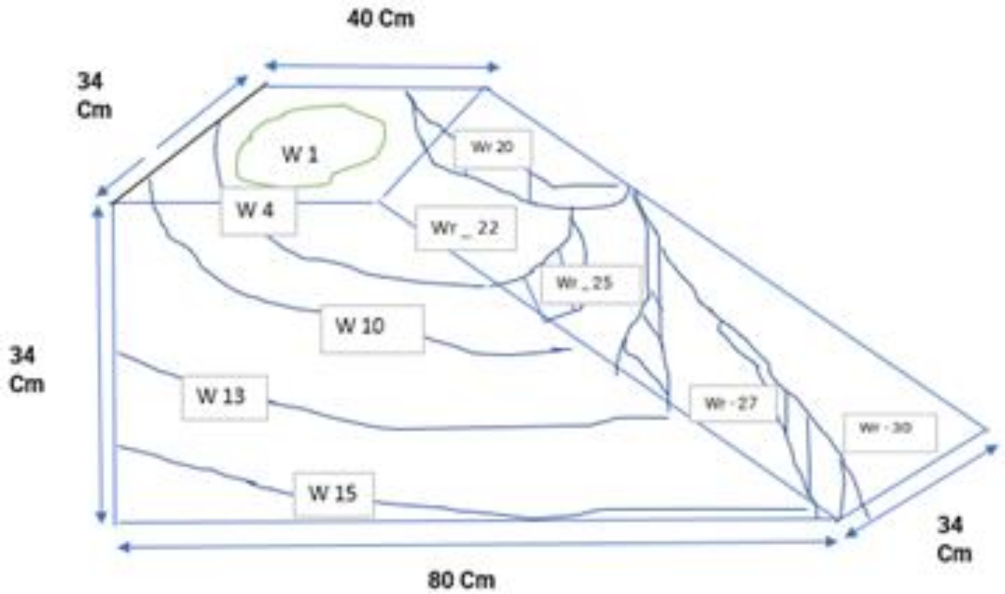

Gambar 4. 14 Kontur bidang gelincir dan pergerakan tanah sudut lereng 450

Tabel 4. 12 Prilaku keruntuhan dan nilai kadar air tanah pada lereng 450

No	T (menit)	Bid Gelincir @ Runtuh	Kadar air (%)	Berat Volume ɣ (gr/cm 3)	Ket
1	2'	Bidang rembes terbentuk	-	-	Rembesan
2	4'	Bidang aliran merembes kebawah	-		Rembesan
3	10'	bidang gelincir Mulai terjadi	43,8		Gelincir
4	13'	Bidang gelincir membesar	43,8		Gelincir
5	15'	Bidang gelincir mergerak kebawah lereng	46,2		Gelincir
6	20'	Runtuh dikepala lereng	50,0		Runtuh
7	22'	Runtuh dikepala lereng	50,0		Runtuh
8	25'	Keruntuhan membesar kearah bawah kaki lereng	52,2		Runtuh
9	27	Keruntuhan membesar ke kaki lereng	52,2		Runtuh
10	30'	Runtuh sudah	68.17	1,778	Runtuh

No	T (menit)	Bid Gelincir @ Runtuh	Kadar air (%)	Berat Volume ɣ (gr/cm 3)	Ket
		berhenti			berakhir

6. Analisis Data Intensitas Hujan Lereng 45^0

Untuk melakukan analisis perilaku keruntuhan lereng dari tabel tersebut, kita dapat mengamati korelasi antara curah hujan, kadar air setelah penghujanan, serta kondisi lereng pada berbagai tahapan waktu. Analisis ini akan mencakup:

❖ **Pengaruh Tinggi Curah Hujan Kumulatif terhadap Kadar Air**

Tinggi curah hujan kumulatif meningkat seiring waktu, menyebabkan kadar air dalam lereng meningkat. Misalnya, kadar air berubah dari **13,74%** pada menit ke-4 menjadi **68,75%** pada menit ke-30.

❖ **Kondisi Lereng dan Tahapan Keruntuhan**

- Pada awal percobaan, lereng stabil.
- **Menit ke-5**: Deformasi pada bidang lereng mulai terjadi.
- **Menit ke-9**: Bidang gelincir mulai terbentuk, menunjukkan ketidakstabilan awal.
- **Menit ke-12**: Bidang gelincir membesar, menandakan kerusakan lebih lanjut.
- **Menit ke-16**: Aliran rembesan mencapai dasar lereng, mempercepat proses pelunakan tanah.
- **Menit ke-20**: Keruntuhan awal pada kepala lereng mulai terjadi.
- **Menit ke-27**: Lereng mengalami longsor total pada kaki dan kepala.
- **Menit ke-30**: Longsor berhenti dengan kadar air mencapai **68,75%**, menunjukkan saturasi penuh.

4.2.5.3 Percobaan Simulasi Hujan pada Lereng 60^0

Tabel 4. 13 Percobaan simulasi hujan pada lereng 600

No	Waktu T (Menit)	Tinggi curah	Tinggi curah hujan	Tinggi curah hujan	Kadar Air Setelah	Kondisi Lereng

		hujan (mm/menit)	Kumulatif (mm/menit)	Rata-rata (mm/menit)	Penghujan (%)	Selama penghujanan
1	0	17	17	121	-	Mulai Percobaan
2	1	105	122	121	-	
3	2	122	245	121	-	Aliran Masuk lapisan lereng
4	3	117	362	121	-	
5	4	120	482	121	-	
6	5	122	603	121	28,00	Terjadi depormasi pada bidang lereng
7	6	121	724	121	28,00	
8	7	122	846	121	28,00	
11	10	120	966	121	38,46	
12	11	119	1085	121	38,46	
13	12	122	1208	121	38,46	Bidang gelincir mulai membesar
14	13	122	1330	121	38,46	
15	14	120	1451	121	38,46	
16	15	122	1573	121	45,00	Aliran rembesan mulai kedasar
17	16	120	1693	121	45,00	
18	17	122	1814	121	45,00	
19	18	122	1936	121	45,00	
20	19	124	2060	121	45,00	
21	**20**	120	2181	121	50,00	Mulai terjadi runtuh pada kepala lereng
22	21	122	2302	121	50,00	
23	22	120	2423	121	50,00	Keruntuhan makin bertambah
24	23	122	2544	121	50,00	
25	24	121	2666	121	50,00	
26	25	122	2788	121	57,14	Tumit lereng semakin labil terhadap runtuh
27	26	120	2908	121	57,14	
28	27	122	3029	121	57,14	Kaki dan kepala lereng lonsor total
29	28	121	3150	121	57,14	
30	29	118	3269	121	57,14	
31	**30**	122	3390	121	67,62	Lonsor sudah berhenti
Hujan Rata 2		121				

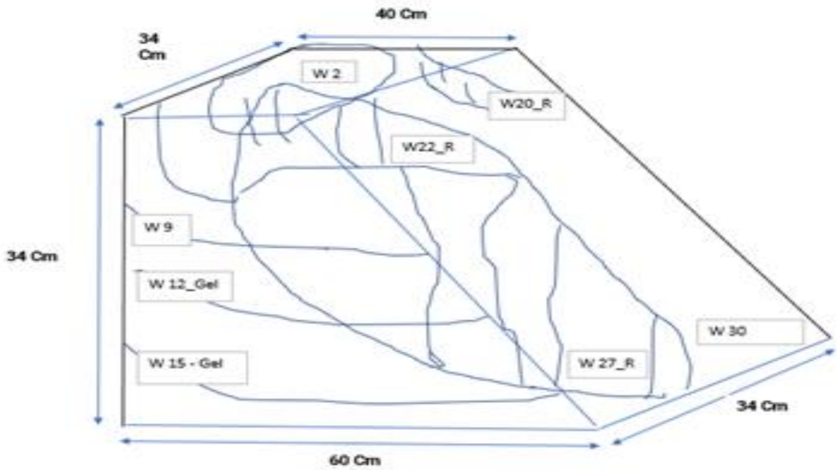

Gambar 4. 15 Kontur bidang gelincir dan pergerakan tanah sudut lereng 60^0

Tabel 4. 14 Prilaku keruntuhan dan nilai kadar air tanah pada lereng 600

No	Wktu T (menit)	Bid Gelincir @ Runtuh	Kadar air (%)	Berat Volume ɣ (gr/cm 3)	Ket
1	2'	Bidang rembes terbentuk	-	-	Rembesan
2	9'	Bidang gelincir terjadi	28		Gelincir
3	12'	bidang gelincir Mulai membesar	38,46		Gelincir
4	15'	Bidang gelincir membesar kearah bawah lereng	38,46		Gelincir
5	20'	Runtuh dikepala lereng	50		Runtuh
6	22'	Runtuh dibagian badan lereng	50,00		Runtuh
7	27'	Runtuh membesar dari kepala hingga kaki lereng	57,14		Runtuh
8	30'	Runtuh sudah berhenti	67,62	1,616	Runtuh

1. Analisis Data Intensitas Hujan Lereng 60^0

❖ Hubungan Tinggi Curah Hujan dan Waktu

Curah hujan rata-rata adalah **121 mm/menit**, dengan variasi kecil antara 117 hingga 124 mm/menit. Curah hujan kumulatif terus meningkat seiring waktu, menunjukkan bahwa hujan terjadi secara kontinu tanpa henti selama 30 menit. Kondisi curah hujan yang stabil namun tinggi ini memberikan beban air yang signifikan pada lereng, mempengaruhi kestabilan lereng.

❖ **Perubahan Kadar Air dan Pengaruhnya pada Lereng**

- **Awal percobaan (0–4 menit):** Tidak ada informasi kadar air yang tercatat. Namun, dalam waktu ini, air hujan mulai mengalir masuk ke lapisan lereng.
- **5–9 menit:** Kadar air meningkat hingga **28%**. Pada menit ke-5, deformasi awal pada bidang lereng teramati. Hal ini menunjukkan bahwa air hujan telah cukup meresap, melemahkan kekuatan geser material lereng.
- **10–15 menit:** Kadar air bertambah hingga **38,46%**, memicu pembesaran bidang gelincir. Air hujan meresap semakin dalam, menambah tekanan air pori dan mengurangi kohesi antar partikel lereng.
- **16–20 menit:** Kadar air naik ke **45%**, menyebabkan aliran rembesan mencapai dasar lereng. Kondisi ini menunjukkan saturasi tanah di bagian bawah, yang menjadi pemicu ketidakstabilan pada kepala lereng.
- **21–27 menit:** Kadar air mencapai **50–57,14%**. Runtuh parsial pada kepala dan tumit lereng terjadi, menandakan hilangnya daya dukung lereng secara keseluruhan.
- **28–30 menit:** Kadar air mencapai puncaknya di **67,62%**, di mana seluruh lereng mengalami longsor total. Setelah itu, proses longsor berhenti.

❖ **Kronologi Keruntuhan Lereng**

- **0–4 menit:** Hujan mulai masuk ke lapisan tanah tanpa deformasi berarti.

- **5–9 menit:** Deformasi awal teramati, dan bidang gelincir mulai terbentuk pada menit ke-9.
- **10–15 menit:** Bidang gelincir membesar, menandai awal keruntuhan.
- **16–20 menit:** Aliran rembesan mencapai dasar, dan kepala lereng mulai runtuh.
- **21–27 menit:** Kepala dan tumit lereng menjadi semakin labil, hingga seluruh bagian lereng mulai mengalami longsor.
- **28–30 menit:** Longsor total terjadi, dan proses berhenti pada kadar air maksimum.

4.2.5.4 Percobaan Simulasi Hujan pada Lereng 90 ^{0}

Tabel 4. 15 Percobaan simulasi hujan pada lereng 90^{0}

No	Waktu T (Menit)	Tinggi curah hujan (mm/menit)	Tinggi curah hujan Kumulatif (mm/menit)	Tinggi curah hujan Rata-rata (mm/menit)	Kadar Air Setelah Penghujan (%)	Kondisi Lereng Selama penghujanan
1	0	17	17	121	-	Mulai Percobaan
2	1	105	122	121	-	
3	2	122	245	121	-	Aliran Masuk lapisan lereng
4	3	117	362	121	-	
5	4	120	482	121	-	
6	5	122	603	121	28,00	Terjadi depormasi pada bidang lereng
7	6	121	724	121	28,00	
8	7	122	846	121	28,00	
9	8	121	967	121	28,00	
10	9	122	1090	121	28,00	Bidang gelincir mulai terjadi
11	10	120	1209	121	38,46	
12	11	119	1328	121	38,46	
13	12	122	1451	121	38,46	Bidang gelincir mulai membesar
14	13	122	1573	121	38,46	
15	14	120	1694	121	45,00	
16	15	122	1816	121	45,00	Aliran rembesan mulai kedasar
17	16	120	1936	121	45,00	
18	17	122	2057	121	45,00	

No	Waktu T (Menit)	Tinggi curah hujan (mm/menit)	Tinggi curah hujan Kumulatif (mm/menit)	Tinggi curah hujan Rata-rata (mm/menit)	Kadar Air Setelah Penghujan (%)	Kondisi Lereng Selama penghujanan
19	18	122	2179	121	45,00	
20	19	124	2303	121	45,00	
21	**20**	120	2424	121	50,00	Mulai terjadi runtuh pada kepala lereng
22	21	122	2545	121	50,00	
23	22	120	2666	121	50,00	Keruntuhan makin bertambah
24	23	122	2788	121	50,00	
25	24	121	2909	121	50,00	
26	25	122	3031	121	57,14	Tumit lereng semakin labil terhadap runtuh
27	26	120	3151	121	57,14	
28	27	122	3272	121	57,14	Kaki dan kepala lereng lonsor total
29	28	121	3393	121	57,14	
30	29	118	3512	121	57,14	
31	**30**	122	3634	121	67,62	Lonsor sudah berhenti
Hujan Rata 2		121				

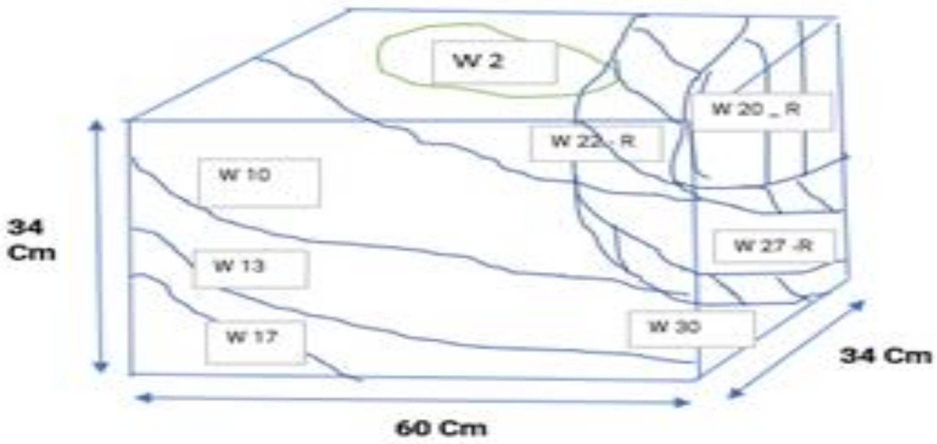

Gambar 4. 16 Kontur bidang gelincir dan pergerakan tanah sudut lereng 90^0

Tabel 4. 16 Prilaku keruntuhan dan nilai kadar air tanah pada lereng 90^0

No	T (menit)	Bid gelincir @ Runtuh	Kadar air tanah (%)	Berat Volume ɣ (gr/cm 3)	Ket
1	2'	Bidang rembes terbentuk	-	-	Rembesan
2	10'	Bidang gelincir terjadi	28		Rembesan
3	13'	bidang gelincir Mulai membesar	38,46		Gelincir
4	17'	Bidang gelincir membesar kearah bawah lereng	45		Gelincir
5	20'	Runtuh dikepala lereng	50		Runtuh
6	22'	Runtuh dibagian badan lereng	50,00		Runtuh
7	27'	Runtuh membesar dari kepala hingga kaki lereng	57,14		Runtuh
8	30'	Runtuh sudah berhenti	67,62	1,618	Runtuh

1. **Analisis Data Intensitas Hujan Lereng 90^0**

❖ **Hubungan Curah Hujan dan Kondisi Lereng**

Curah hujan rata-rata sebesar **121 mm/menit** memengaruhi kondisi lereng secara bertahap:

- **Awal Hujan (0-5 menit)**:
    - Pada awal percobaan, curah hujan mencapai **105–122 mm/menit**, namun belum memengaruhi kadar air lereng secara signifikan.
    - Mulai terjadi aliran air yang masuk ke lapisan lereng pada menit ke-2.
    - Pada menit ke-5, deformasi pada bidang lereng terdeteksi, yang menunjukkan awal dari tekanan air pori meningkat.

- **Tahap Deformasi (5-10 menit)**:
    - Deformasi berlanjut dengan kadar air mencapai **28%** pada menit ke-5 hingga menit ke-10.
    - Pada menit ke-9, mulai terjadi bidang gelincir akibat melemahnya kekuatan tanah di dalam lereng.
- **Tahap Perkembangan Bidang Gelincir (10-16 menit)**:
    - Kadar air meningkat hingga **38,46%** pada menit ke-10. Bidang gelincir mulai membesar pada menit ke-12.
    - Pada menit ke-15, aliran rembesan mulai mencapai dasar lereng, mengindikasikan saturasi penuh di beberapa lapisan tanah.
- **Tahap Runtuh Parsial (16-20 menit)**:
    - Dengan kadar air mencapai **45%**, kepala lereng mulai runtuh pada menit ke-20.
    - Keruntuhan ini diikuti oleh keruntuhan yang semakin bertambah pada menit ke-22.
- **Tahap Keruntuhan Total (25-30 menit)**:
    - Pada menit ke-25, kadar air mencapai **57,14%**, dan tumit lereng menjadi sangat labil.
    - Pada menit ke-27, kaki dan kepala lereng mengalami longsor total.
    - Keruntuhan berhenti pada menit ke-30 setelah kadar air meningkat menjadi **67,62%**, menunjukkan sistem lereng telah mencapai kondisi runtuh sepenuhnya.

❖ **Pengaruh Kadar Air**

- Kadar air adalah faktor kunci dalam melemahkan kekuatan geser tanah. Peningkatan kadar air menyebabkan tekanan air pori meningkat, mengurangi kohesi tanah dan mempercepat deformasi.

- Kadar air meningkat dari 28% (awal deformasi) hingga 67,62% (keruntuhan total), menunjukkan hubungan linear antara kadar air dan tingkat keruntuhan

4.2.6 Pengaruh peningkatan kadar air terhadap indek kecairan tanah

Simulasi ini bertujuan untuk memahami dampak peningkatan kadar air tanah terhadap kestabilan lereng dengan berbagai sudut kemiringan. Kadar air tanah yang meningkat, akibat hujan atau infiltrasi, berpotensi menurunkan kekuatan geser tanah, meningkatkan tekanan pori, serta memicu terjadinya longsor, terutama pada lereng yang curam. Empat sudut kemiringan lereng yang disimulasikan adalah 30°, 45°, 60°, dan 90°, mewakili kondisi dari lereng landai hingga tegak. Peningkatan kadar air tanah memiliki dampak signifikan terhadap kestabilan lereng, terutama pada kemiringan diatas 45°. Lereng curam seperti 60° dan 90° sangat rentan terhadap kedalaman bidang gelincir yang terjadi akibat naiknya tekananair pori tanah. Oleh karena itu, pengelolaan air permukaan dan rembesan air bawah permukaan sangat krusial untuk mencegah kegagalan lereng, terutama di daerah dengan curah hujan tinggi. Hasil percobaan pada simulasi ini dapat dijajikan pada tabel dan grafik dibawah ini sesuai besaran sudut model percobaan :

Tabel 4.17 Efek kadar air terhadap indek kecairan tanah pada lereng 30 ^{0}

Parameter	Satuan	Nilai	Waktu (menit)	Kadar air (%)	Indek Kecairan Tanah	Ket
Kepadatan lereng (ɣb)	gr/cm3	-	2'	0	-4,092	Rembesan
Berat jenid (Gs)	gr/cm3	2,63	5	30	-0,900	Gelincir
Batas Plastis (PL)	%	38,455	9	30	-0,900	Gelincir
Indek Plastis (PI)	%	9,395	15'	47	0,909	Gelincir
Batas Susut (SL)	%	26,704	20'	55,5	1,814	Mulai Runtuh

Batas cair (LL)	%	47,853	23 '	55,5	1,814	Runtuh
-	%	-	27'	59,9	2,282	Runtuh
-	-	-	30'	63	2,612	Runtuh

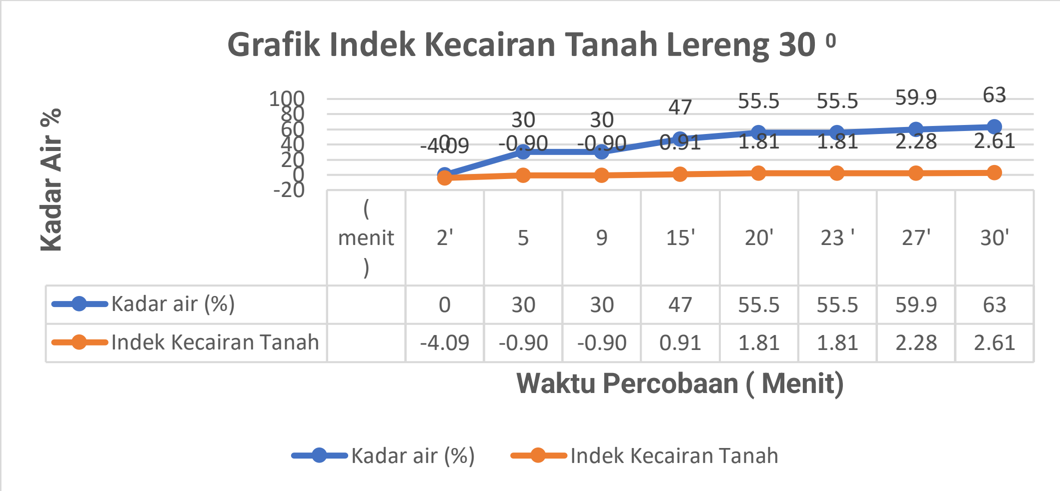

Gambar 4. 17 Grafik indek kecairan tanah lereng 30^0

Tabel 4. 18 Efek kadar air terhadap indek kecairan tanah pada lereng 45^0

No	Parameter	Satuan	Nilai	Waktu (menit)	Kadar air (%)	Indek Kecaira Tanah	Ket
1	Kepadatan lereng (ɣb)	gr/cm3	1,06	2'	0,0	-39,3	Rembesan
2	Berat jenid (Gs)	gr/cm4	2,63	4'	0,0	-39,3	Rembesan
3	Batas Plastis (PL)	%	38,45	10'	43,8	4,5	Gelincir
4	Indek Plastis (PI)	%	9,7	13'	43,8	4,5	Gelincir
5	Batas Susut(SL)	%	26,7	15'	46,2	6,9	Gelincir
6	**Batas cair (LL)**	%	47,5	20'	40,0	0,7	Mulai runtuh
7	Kadar Air Runtuh Rerata	%	-	22'	50,0	10,7	Runtuh
8	Indek Kecairan Tanah (LI)	-	-	25'	52,2	12,9	Runtuh
	-			27	52,2	12,9	Runtuh
	-			30'	68,2	28,9	Runtuh berakhir

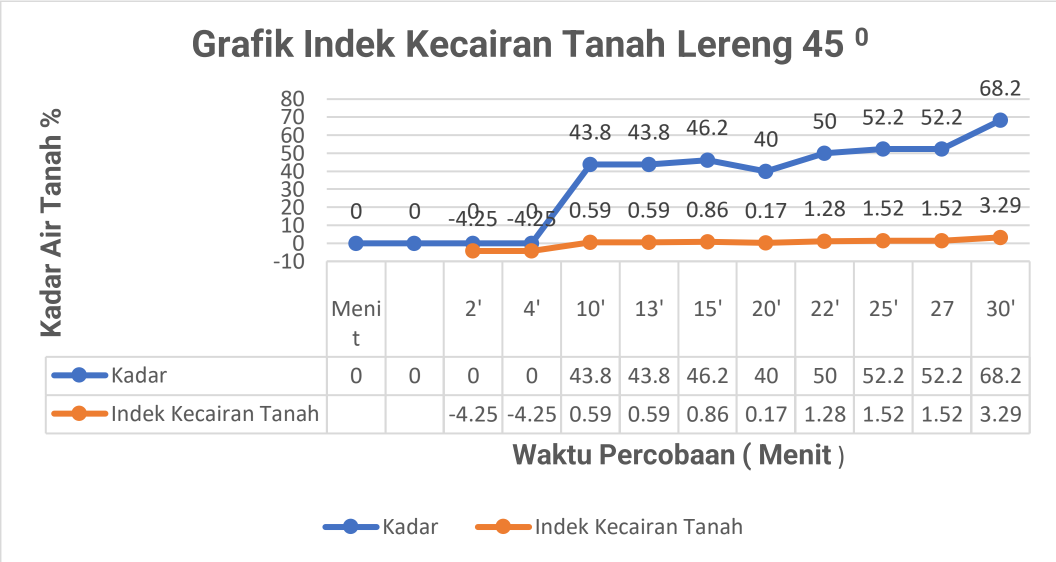

Gambar 4. 18 Grafik indek kecairan tanah lereng 45^0

Tabel 4. 19 Efek kadar air terhadap indek kecairan tanah pada lereng 60^0

Parameter	Satuan	Nilai	Waktu (menit)	Kadar air (%)	Indek Kecairan Tanah	Ket
Kepadatan lereng (ɣb)	gr/cm3	-	2'	0,0	-39,3	Rembesan
Berat jenid (Gs)	gr/cm4	2,63	9'	0,0	-39,3	Rembesan
Batas Plastis (PL)	%	38,45	12'	43,8	4,5	Gelincir
Indek Plastis (PI)	%	9,7	15'	43,8	4,5	Gelincir
Batas Susut(SL)	%	26,7	20'	46,2	6,9	Gelincir
Batas cair (LL)	%	47,5	22'	40,0	0,7	Mulai runtuh
Kadar Air Runtuh Rerata	%	-	27'	50,0	10,7	Runtuh
Indek Kecairan Tanah (LI)	-	-	30'	52,2	12,9	Runtu

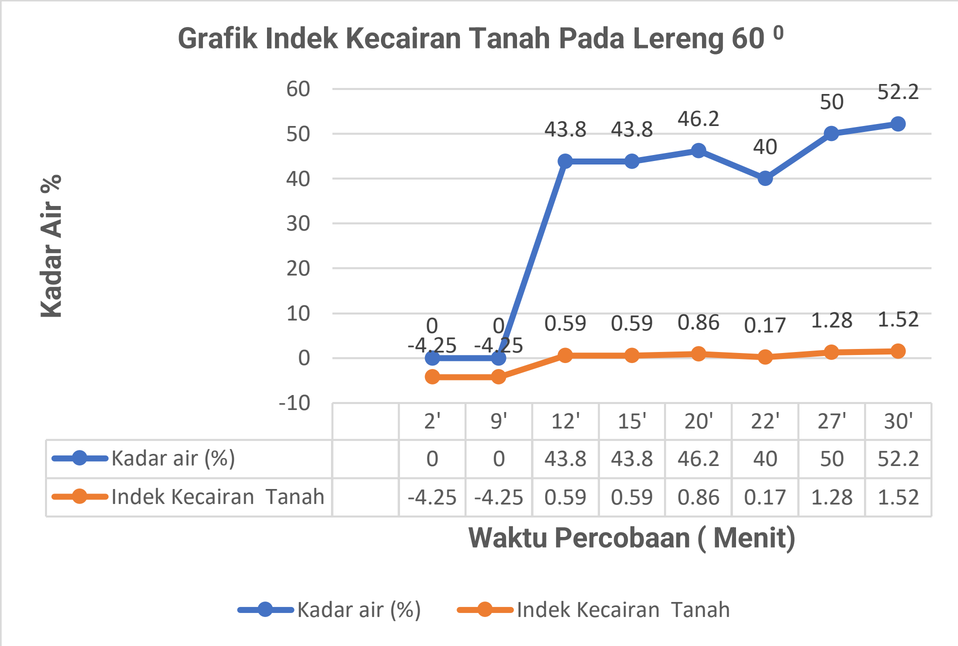

Gambar 4. 19 Grafik indek kecairan tanah lereng 60^0

Tabel 4. 20 Perobahan kadar air terhadap indek kecairan tanah pada lereng 90^0

Parameter	Satuan	Nilai	Waktu (menit)	Kadar air (%)	Indek Kecairan Tanah	Ket
Kepadatan lereng (ɣb)	gr/cm3	1,13	2'	0	-39,3	Rembesan
Berat jenid (Gs)	gr/cm4	2,63	10'	28	-11,3	Rembesan
Batas Plastis (PL)	%	38,45	13'	38,46	-0,8	Gelincir
Indek Plastis (PI)	%	9,7	17'	45	5,7	Gelincir
Batas Susut(SL)	%	26,7	20'	50	10,7	Mulai Runtuh
Batas cair (LL)	%	47,5	22'	50,00	10,7	Runtuh
Kadar Air Runtuh Rerata	%	-	27'	57,14	17,9	Runtuh
Indek Kecairan Tanah (LI)	-	-	30'	67,62	28,4	Runtuh

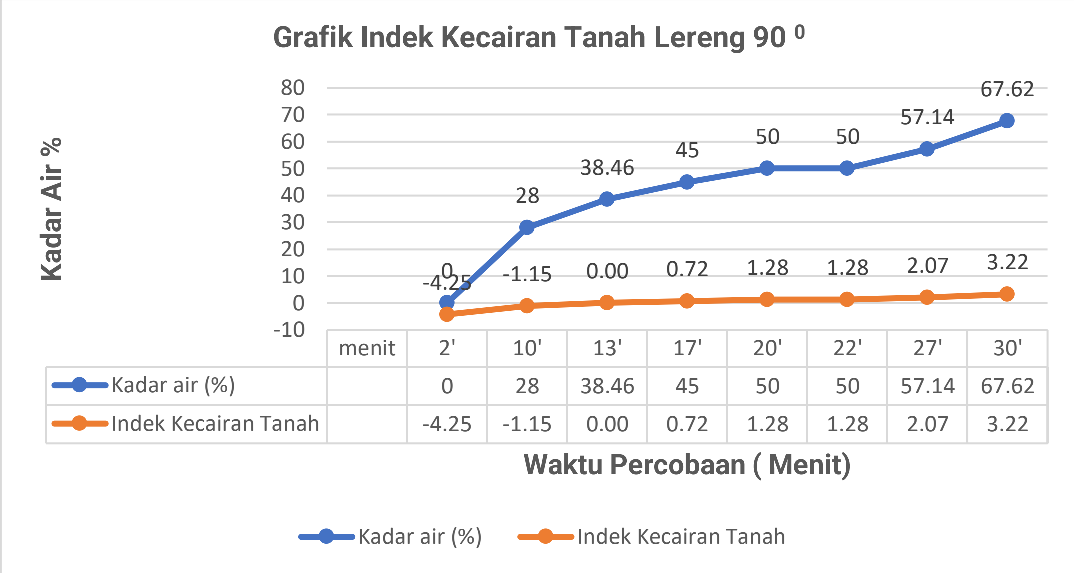

Gambar 4. 20 Grafik indek kecairan tanah lereng 90^0

Tabel 4. 21 Kadar air gabungan pada setiap besaran sudut lereng

No	Waktu	Kadar air lereng 30^0	Waktu	Kadar air lereng 45^0	Waktu	Kadar air lereng 60^0	Waktu	Kadar air lereng 90^0
1	2'	0	2'	0	2'	0	2'	0
2	5	30	4'	0	9'	0	10'	28
3	9	30	10'	43,8	12'	43,8	13'	38,46
4	15'	47	13'	43,8	15'	43,8	17'	45
5	20'	55,5	15'	46,2	20'	46,2	20'	50
6	23 '	55,5	20'	40	22'	40	22'	50
7	27'	59,9	22'	50	27'	50	27'	57,14
8	30'	63	25'	52,2	30'	52,2	30'	67,62
9			27	52,2				
10			30'	68,2				

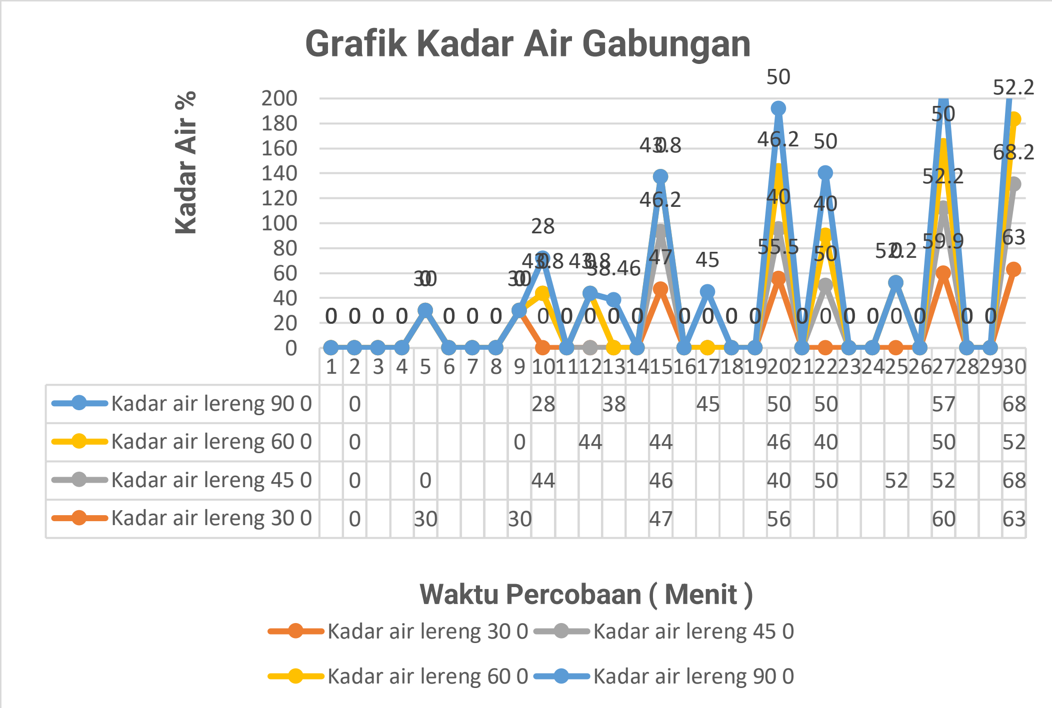

Gambar 4. 21 Grafik kadar air gabungan berdasarkan besaran sudut lereng

Tabel 4. 22 Data Indek Kecairan tanah gabungan

Waktu (Menit)	Indek Kecairan Tanah lereng 30⁰	Indek Kecairan Tanah lereng 45⁰	Indek Kecairan Tanah lereng 60⁰	Indek Kecairan Tanah lereng 90⁰
1				
2	- 4,09	-4,25	-4,25	-4,25
3				
4		-4,25		
5	- 0,90			
6				
7				
8				
9	- 0,90		-4,25	
10		0,59		-1,15
11				
13		0,59		0,00
14				
15	0,91	0,86	0,59	
16				
17				0,72

Waktu (Menit)	Indek Kecairan Tanah lereng 30^0	Indek Kecairan Tanah lereng 45^0	Indek Kecairan Tanah lereng 60^0	Indek Kecairan Tanah lereng 90^0
18				
19				
20	1,81	0,17	0,86	1,28
21				
22		1,28	0,17	1,28
23	1,81			
24				
25		1,52		
26				
27	2,28	1,52	1,28	2,07
28				
29				
30	2,61	3,29	1,52	3,22

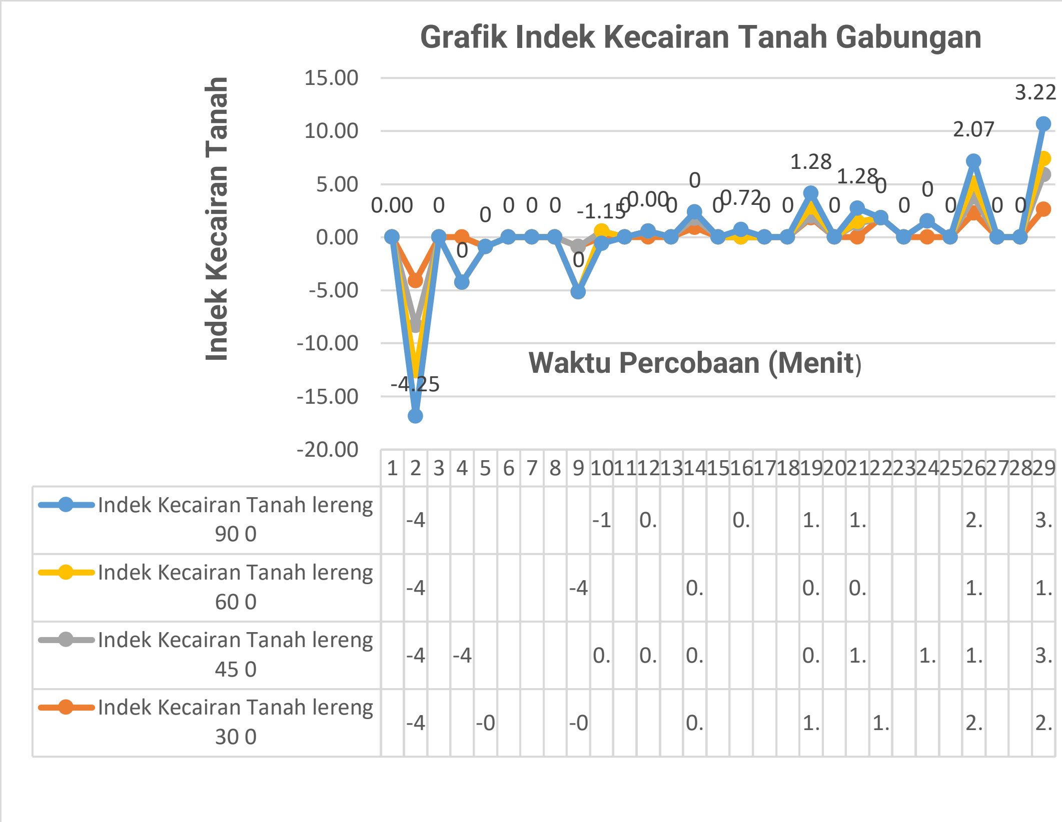

Gambar 4. 22 Grafik indek kecairan tanah gabungan

Berdasarkan analisis grafik dan data data diatas, maka tanah pada sudut lereng diatas, setelah mengalami percobaan penghujanan selama 30 menit dengan kadar air tersebut pada tabel diatas, maka tanah mengalami perobahan konsistensinya dan pada kondisi cair, dengan indek kecairan (Likuid Indek) lebih besar dari 1 (> 1), maka tanah lereng tersebut pada kondisi cair akan mengakami pergerakan . terutama pada lereng – lereng yang mempunyai sudut geometrinya diatas 45 derjat. Pada penelitian ini lereng yang bersudut 60, dan 90^0 sangat rentan mengalami kegagalan lereng dengan prilaku lonsor terutama pada kaki lereng.

4.3 Pembahasan

Stabilitas lereng sangat dipengaruhi oleh sifat - sifat fisik dan mekanik tanah, terutama kadar air, batas-batas Atterberg (LL, PL, PI, SL), serta kepadatan dan sudut geometri lereng. Salah satu parameter penting dalam menilai potensi kelongsoran adalah Indeks Kecairan (Liquidity Index/LI) yang menunjukkan seberapa dekat kondisi tanah terhadap batas cairnya (LL). Semakin tinggi LI, semakin besar potensi tanah menjadi tidak stabil atau mengalami kelongsoran. Dari analisis data yang diperdapat dari percobaan yang dilakukan pada model lereng yang dilakukan terhadap beberapa kondisi lereng, akibat dari peningkatan kadar air tanah pada lereng sangat penting untuk memahami mekanisme pergerakan tanah dalam bentuk kegagalan lereng dan merancang strategi mitigasi. Dengan menggunakan metode analisis yang tepat, kita dapat memprediksi potensi ketidakstabilan lereng dan mengambil langkah pencegahan sebelum terjadi bencana, sebagai mana dijelaskan berikut ini :4.3.1 Jenis tanah dan indek kecairan tanah

Berdasarkan hasil analisis klasifikasi tanah menurut metoda USCS pada sub bab diatas, dengan data analisis saringan Lolos saringan 200, sebesar 65,93 % berjenis lempung, dan nilai Liquid Limit (LL), sebesar 47,853 %, dan nilai Plastis Limit (PL), sebesar 38,455 %, dan nilai indeks plastis (PI), sebesar 9,395 % . Dengan memakai grafik Grafik plastisitas jenis tanah pada sub bab diatas, Maka tanah dikategorikan pada tanah lanau organik plastis tinggi, dengan symbol ML atau OL . Nilai *Liquid Indeks (LI)* untuk berbagai sudut lereng menunjukkan bahwa tanah berada dalam kondisi cair *(LI > 1).* Ini berarti tanah kehilangan kohesi dan mengalami pelemahan signifikan. Untuk besaran sudut geometri lereng 30,60,60, dan 90 ^{0} , nilai kadar air runtuh akhirnya sebesar 63 %, 68,2 %, 52,2 %, dan 67,62 % yang kategori tinggi menunjukkan bahwa lereng berada dalam kondisi jenuh air, sehingga daya dukung tanah menurun drastis, maka tanah akan mengalami pergerakan dalam bentuk kegagalan lereng. Dengan nilai indek kecairan tanah (LI > 1) menunjukkan bahwa kadar air tanah melebihi batas cair, menandakan bahwa tanah dalam kondisi sangat lunak atau cair, kondisi ini menunjukan pada kondisi yang tidak stabil untuk lereng. Semakin tinggi sudut lereng, meskipun kepadatan tanah relative tinggi, dengan kadar air tinggi menyebabkan indek kecairan tanahnya (LI) tetap tinggi, maka lereng mengalami risiko longsor sangat tinggi.

4.3.2 Pengaruh Sudut Geometri Lereng

Pada sudut lereng yang lebih tinggi (60° dan 90°), memiliki liquid indek (LI) lebih besar, menunjukkan bahwa kestabilan lereng semakin buruk seiring meningkatnya kemiringan lereng, sangat berpotensi terjadi pergerakan tanah untuk lereng 60 ^{0} degan kadar air tanah pada akhir keruntuhan sebesar 52,62 %, dengan indek kecairan tanah 1,52, dan untuk lereng 90 ^{0} dengan nilai kadar air tanah pada saat akhir keruntuhan sebesar 67,62 %, dengan indek kecairan tanah sebesar 3,22. Pada sudut lereng 30°, meskipun tanah masih jenuh dengan nilai indek kecairan tanah sebesar 2,61 (*LI* > 1), dengan faktor kelandaaian lerengnya kategori kecil, maka gaya gelincirnya kecil , maka kegagalan lereng dalam bentuk pergerakan tanah dapat dikategorikan tidak secepat pada sudut 60° dan 90°. Pada lereng bergeometri Sudut 90° adalah kondisi yang paling berisiko karena tanah hampir tidak memiliki daya dukung.

4.3.3 Mekanisme Kegagalan Lereng

Dengan kondisi tanah yang jenuh dan berada dalam keadaan cair dengan nilai indek kecairan tanahnya kategori tinggi, maka kegagalan lereng kemungkinan besar dalam bentuk keruntuhan *flow slide* (longsoran aliran).Tekanan pori yang tinggi dalam tanah berkontribusi terhadap hilangnya gesekan antar partikel, menyebabkan tanah mengalir seperti aliran lumpur. Mekanisme kegagalan lereng lonsor aliran atau flow failure merupakan salah satu jenis gerakan massa tanah atau batuan di mana material bergerak menyerupai cairan. Proses ini umumnya terjadi secara cepat dan melibatkan volume material yang besar. Beban tambahan atau getaran (misalnya dari hujan deras atau gempa) dapat memicu pergerakan tanah lebih lanjut. Bentuk dari lonsor aliran dapat dilihat seperti gambar berikut :

Gambar 4. 23 Dokumentasi bentuk lonsor aliran pada model percobaan

BAB 5 KESIMPULAN DAN SARAN

5.1 Kesimpulan

Penelitian ini dilakukan untuk mengevaluasi studi kegagalan lereng sebagai efek dari tingkat intensitas hujan terhadap perobahan kadar air tanah dan dampaknya terhadap perobahan indek kecairan tanah pada sebuah lereng dengan pemodelan laboratorium. Berdasarkan pada Analisa pembahasan dari percobaan yang dilakukan diatas, maka pada laporan disertasi ini dapat disimpulkan atas beberapa hal sebagai brkut :

1. Lereng dengan sudut lebih curam lebih berisiko mengalami longsor karena kondisi tanah yang jenuh dan kehilangan kohesi, maka lereng dapat dikategorikan dalam rawan kondisi labil.
2. Kegagalan lereng lebih cenderung berbentuk longsoran aliran (*flow slide*), karena nilai indek kecairan tanahnya melebihi nilai indek kecairan kritis (LI > dari 1)
3. Besaran kadar air tanah apabila melebihi nilai likuit limit tanah , maka tanah berpotensi cair dan akan terjadi pergerakan tanah sampai menuju kegagalan lereng dalam bentuk lonsoran aliran .
4. Peningkatan kadar air tanah yang melebihi batas cair secara signifikan meningkatkan nilai Liquid Indek, sehingga memperbesar potensi kelongsoran lereng, terlebih pada geometri lereng yang lebih besar.
5. Pada lereng yang mempunya sudut geometri lebih besar dari sudut > 45° dalam kondisi tanah jenuh air (LI > 1) sangat rawan mengalami longsor, meskipun memiliki kepadatan yng baik .
6. Liquid Limit dan Kadar Air adalah sebagai parameter atau indikator kunci dalam menilai risiko kelongsoran lereng secara laboratorium, maupun terhadap konsisi dilapangan

5.2 Saran

Berdasarkan analisis yang diperoleh dari penelitian ini terdapat beberapa saran yang perlu diberikan untuk penelitian lebih lanjut guna meningkatkan pemahaman untuk memperkecil aspek - aspek dalam kegagalan lereng dalam studi kestabilan lereng ini diantaranya sebagai berikut :

1. Pada permukaan lereng diperlukan perbaikan drainase, yang bertujuan untuk mengurangi kadar air tanah dengan pemasangan drainase horizontal dan vertikal pada badan lereng tersebut.
2. Penguatan Lereng Menggunakan dinding penahan tanah atau perkuatan geotekstil untuk memperbaiki stabilitas lereng.
3. Vegetasi dan erosi control, dengan menanami vegetasi untuk meningkatkan kohesi tanah dan mengurangi infiltrasi aliran air hujan.
4. Pemasangan alat pemantau bencana lonsor dengan menggunakan inclinometer atau piezometer untuk memantau pergerakan lereng dan tekanan pori.
5. Jika kegagalan sudah terjadi, diperlukan tindakan darurat seperti relokasi material atau dengan Tindakan stabilisasi yang berguna terjadinya keberulangan bencana dengan semen/kapur
6. Peningkatan kadar air tanah yang melebihi batas cair secara signifikan meningkatkan nilai LI, sehingga memperbesar potensi kelongsoran lereng, terlebih pada lereng yang curam, maka diperlukan upaya mitigasi penangan bencana.

DAFTAR PUSTAKA

Agus Setyo Muntohar dkk, (2010), Rainfall infiltration: infinite slope model for landslides triggering by rainstorm, Nat Hazards (2010) 54:967–984 DOI 10.1007/s11069-010-9518-5

Agus Setyo dkk, (2014), Rainfall infiltration infinite slope model for landslides triggering by rainstorm, Nat Hazards (2010) 54:967–984 DOI 10.1007/s11069-010-9518-5

Alejandro R.(2014) Green-Ampt model of a rain garden and comparison to Richards equation model, Journal Of Hydrologig Engineering © ASCE / May / June 2004

Hakam.A, dkk, (2015), West Sumatra Landslide During in 2012 to 2015, International Journal of Earth Sciences and Engineering ISSN 0974-5904, Vol. 09, No. 03, June, 2016, pp. 289-293.

Anusron Chueasamat dkk, (2018), Soils and Foundations Volume 58, Issue 2, April 2018, Pages 290-305,Sciencedirect journal.

Istijono,B,dkk, (2016), Development Of Stability Criteria For Risk Reduction In The Sianok Canyon In Bukittinggi Indonesia, International Journal of Earth Sciences and Engineering ISSN 0974-5904, Vol. 09, No. 01, February, 2016, pp. 02.

CHO, S.E. and LEE, S.R. (2001) Instability of unsaturated soil slopes due to infiltration. Computers and Geotechnics, v.28, pp.185– 208.

CHIGIRA, M. (2001) Micro-sheeting of granite and its relationship with landsliding specifically after the heavy rainstorm in June 1999, Hiroshima prefecture, Japan. Engg. Geol. v.59, pp.219231.

Duncan, J.M., Wright, S.G., Brandon, T.L, (2014). Soil strength and slope stability.Wiley

Dinas ESDM Propinsi Sumatera Barat (2020), data dan peta kejadian lonsor pada titik rawan lonsor Sumatera Barat

E.Pinom dkk, (2020), Characterization of Critical Rainfall for Slopes Prone To Rainfall-Induced Land slides, ASCE Journal,NH.1527-6996.0000385. © 2020 American Society of Insinyur Sipil.

Geo-Slope (1998b). *Slope/w Version 4.21,V, Users Manual*, GEO-SLOPE International Ltd., Calgary, Alberta, Canada.

Gasmo, J.M., Rahardjo, H. and Leong, E.C. (2000) Infiltration effects on stability of a residual soil slope. Computers and Geotechnics, v.26, pp.145–165.

Hugo A. Loáiciga dkk, (2018) , Infiltration on sloping terrain and its role on runoff generation and slope, Journal of Hydrology 561 (2018) 584–597, Sciencedirect journal.

Iverson, R. M. (2000). Landslide triggering by rain infiltration. *Water Resources Research*, *36*, 1897 –1910.

Iverson, R. M., dan Major, J. J. (1986). Groundwater seepage vectors and the potential for hillslope failure and debris flow mobilization. *Water ResourcesResearch*, *22*(11), 1543–1548.

Iverson, R. M., Reid, M. E., dan LaHusen, R. G. (1997). Debris-flow Mobilization from Landslides. *Annv. Rev. Earth Planet*, *25*, 85–138. Kartiko, R. D. (2009). *Evaluation of Landslide Susceptibility in The Tropical.*

Jayawardena AW, Rezaur RB. (2000). Measuring drop size distribution and kinetic energy of rainfall using a force transducer. *Hydrological Processes* **14**(1): 37–49.

Jayawardena AW, Rezaur RB. (2000b). Drop size distribution and kinetic energy load of rainfall in Hong Kong. *Hydrological Processes* **14**(6): 1069– 1082.

Kabir, M.H., and Taha, M.R. (2004), Assessment of physical properties of granite residual soil as an isolation barrier, Electronics Journal of Geotechnical Engineering, Vol. 9– Bundle B.

Liu, Q. Q., dan Li, J. C. (2015). Effects of Water Seepage on the Stability of Soil slopes.*IUTAM Symposiumon the Dynamics of Extreme Events Influenced.*

Lysandros Pantelidis dkk, (2012), Stability Assessment of Slopes Using Different Factoring Strategies, Journal of Geotechnical and Geoenvironmental Engineering.2012,ASCE Journal

Mukhlisin.M, dkk, (2015), Analysis of Rainfall Effect to Slope Stability in Ulu Klang, Malaysia, 72:3 (2015) 15–21 | www.jurnalteknologi.utm.my | ISSN 2180–3722 |

Mukhilisin, M., Kosugi, K., Satofuka, Y. and Mizuyama, T. (2006). Effects of Soil Porosity on Slope Stability and Debris Flow Runout at a Weathered Granitic Hillslope. Vadoze Zone Jour.,v.5, pp.283-295

Mukhilisin, M., Taha, M.R. and Kosugi, K, (2008) Numerical analysis of effective soil porosity and soil thickness effects on slope stability at a hillslope of weathered granitic soil formation. Geosciences Jour., v.12(4), pp.401-410

Mukhilisin, M., Kosugi, K., Satofuka, Y. and Mizuyama, T. (2006). Effects of Soil Porosity on Slope Stability and Debris Flow Runout at a Weathered Granitic Hillslope. Vadoze Zone Jour.,v.5, pp.283-295

Mukhlisin, M., Taha, M.R. and Kosugi, K. (2008). Numerical analysis of effective soil porosity and soil thickness effects on slope stability at a hillslope of weathered granitic soil formation. Geosciences Jour., v.12(4), pp.401-410

Mukhlisin,M, dkk, (2015), Analysis of Rainfall Effect to Slope Stability in Ulu Klang, Malaysia , Jurnal Teknologi Sciences & Engineering) 72:3 (2015) 15–21

Ohta, T., Tsukamoto, Y. and Hiruma, M. (1985), The behavior of rainwater on a forested hillslope, I, The properties of vertical infiltration and the nfluence of bedrock on it (in Japanese, with English summary.) Jour. Jpn. For. Soc., v.67, pp.311–321.

Okri Asfino Putra,(2020), Evaluation of Shear Strength Characteristics of Unsaturated Undisturbed Volcanic Ash Soil Subjected to Static and Cyclid Loading for Slope Stability Analysis,Disertasy ,Graduate Scollo of Engineering Kyushu University Fukuoka,Japan.2020

Rahardjo, H. (2000). Rainfall-Induced Slope Failures. NSTB 17/6/16 Main Report. Nanyang Technological University,Singapore.

Rahardjo, H., Leong, E.C. Deutscher, M.S. Gasmo, J.M. Tang,S.K. (2000). Rainfall-Induced Slope failures. Geotechnical Engineering Monograph 3. NTU-PWD Geotechnical Research Centre,Nanyang Technological University, Singapore.

Rahardjo, H., Leong, E.C. and Rezaur, R.B. (2008), Effect of antecedent rainfall on pore-water pressure distribution characteristics in residual soil slopes under tropical rainfall.Hydrol. Process, v.22, pp.506–523.

Rezaur RB, Rahardjo H, Leong EC, Lee TT. (2000). Hydrology of three slopes in Singapore. *Hydrological Processes*. (Submitted for possible review and publication. Ref: 695)

Rahardjo, H., LI, X.W., Toll, D.G. and Leong, E.C. (2001), The effect of antecedent rainfall on slope stability. Geotechnical and Geological Engineering, v.19, pp.371–399.

Rahardjo, H., Leong, E.C. and Rezaur, R.B. (2008), Effect of antecedent rainfall on pore-water pressure distribution characteristics in residual soil slopes under tropical rainfall.Hydrol. Process, v.22, pp.506–523.

Saparas, I., Rahardjo, H., Toll, D.G. and Leong, E.C. (2002), Controlling parameters for rainfall-induced landslides.Computers and Geotechnics. v.29, pp.1–27.

Shimizu, Y., Tokashiki, N. and Okado, F. (2002), The September 2000 torrential rain disaster in the Tokai region: Investigation of a mountain disaster caused by heavy rain in three prefectures; Aichi, Gifu and Nagano. Jour. Natural Disaster Sci., v.24,pp.51–59.

Shruti Naidua dkk, (2018), Early warning system for shallow landslides using rainfall threshold and slope stability analysis, Geoscience Frontiers 9 2018, 1871e1882, ScienDirect Journal.

T.Adrin dkk, (2007), Laboratory Rainfall-Induced Slope Failure with Moisture Content Measurement, Journal of Geotechnical and Geoenvironmental Engineering /Volume 133, Issue 5 , ASCE Journal 2007.

Taha, M.R. and Kabir, M.H, (2005), Tropical residual soil as compacted soil liners, Environmental Geology, SpringerVerlag,Berlin, v.47,pp.375-381.

Saparas, I., Rahardjo, H., Toll, D.G. and Leong, E.C. (2002) Controlling parameters for rainfall-induced landslides. Computers and Geotechnics. v.29, pp.1–27.

Wilkinson, P.L., Anderson, M.G. and Lloyd, D.M. (2002), An integrated hydrological model for rain-induced landslide prediction. Earth Surface Processes and Landforms, v.27, pp.1285–1297.

Y.Somjai dkk, (2016), Influence Factors Involving Rainfall-Induced Shallow Slope,Failure: Numerical Study, Int. J. Geomech., 04016158.2016, ASCE Journal 2016.

Young-Suk Song dkk, (2020), Laboratory Experiment and Numerical Analysis on the Precursory,Hydraulic Process of Rainfall-Induced Slope Failure Stability, jurnal Advances in Civil EngineeringVolume 2020, Article ID 2717356, 12 pages https: // doi.org / 10.1155 / 2020 / 2717356,Hindawi Journal

F. V. De Blasio, *Introduction to the Physics of Landslides*, 1st ed. New York, (2011).

Shujian Li, ,Yisha Pan,, Chongyang Wang,Dongming Zhang , Bin Zhang.and Ziyang Xiong, Stability Analysis of a Water-Rich Slope Under Seismic Disturbance, Wiley Advances in Civil Engineering Volume 2024, Article ID 8894948, 13 pages https://doi.org/10.1155/2024/8894948.

Usman Musa Sjahrain, Steeva G. Rondonuwu2, Herawaty Riogilang, ANALISIS POTENSI LIKUIFAKSI DENGAN MENGGUNAKAN

PARAMETER KUAT GESER TANAH LEMPUNG ,Jurnal Ilmiah Media Engineering Vol.11 No.3, November 2021 (189-198), ISSN: 2087-9334

T. Li, Y. Wang, and F. Wu, "Anti-Erosion Influences of Surface Roughness on Sloping Agricultural Land in the Loess Plateau, Northwest China," *Sustain.*, vol. 14, no. 10, 2022, doi: 10.3390/su14106246.

Muhammad Nasih A hasbi1, Agata Iwan Candra, Mohamad Agus Fajar Wibowo , Rahmat Heru, Arif Rivianto , Menentukan tingkat kelonsoran tanah dengan metoda kuat geser langsung, Jurnal Spektran Vol. 10, No. 2022, Hal. 64 - 69 e-ISSN: 2302-2590 doi: https://doi.org/10.24843/SPEKTRAN.2022.v10.i02.p01.

G. Luetzenburg, M. J. Bittner, A. Calsamiglia, C. S. Renschler, J. Estrany, and R. Poeppl, "Climate and land use change effects on soil erosion in two small agricultural catchment systems Fugnitz – Austria, Can Revull – Spain," *Sci. Total Environ.*, vol. 704, 2020, doi: 10.1016/j.scitotenv.2019.135389.

Shaochun Ma , Yudi Yao , Peng Bao , and Chengchao Guo, Effects of moisture content on strength and compression properties of foundation soils of cultural relics in areas flooded by the Yellow River, OPEN ACCESS EDITED BY Tadeusz Hryniewicz, Koszalin University of Technology, Poland, DOI 10.3389/fmats.2023.1186750.

LI Zhi-peng,at.al, The Analysis of The Impact of Liquid Limit on Mechanical Properties of Clayey Soil, IOP Conf. Series: Earth and Environmental Science 525 (2020) 012036, doi:10.1088/1755-1315/525/1/012036

Kuanyao Zhao ,Wanlin Chen , Qiang Xu , Fangzhou Liu , Denghui Gao , Dalei Peng, Centrifuge modeling of loess slope failure induced by rising water level utilizing intact sample, journal homepage: www.elsevier.com/locate/engfailanal,.https://doi.org/10.1016/j.engfailanal.2024.108572, Accepted 14 June 2024.

Xiaoliang Liu and Mei Su,Double Strength Reduction Method for Slope Stability Analysis Based on Water Content Variation: A Study and Engineering Application, Water 2023, 15, 1194. https://doi.org/10.3390/w15061194.

Zhang, X., Yang, Q., & Zhao, L, *Effects of Water Content and Plasticity Index on the Stability of Slopes: A Laboratory Investigation*. Geotechnical Testing Journal, 40(5), 928-940,2017.

Sigit, M,at.al (2018). Dalam, *Peran Likut Limit dalam Memprediksi Potensi Kelonsoran Lereng Tanah Lempung*. Jurnal Geoteknik Indonesia, 21(1), 33-40

Muhamad Rizki Rinaldi,at.al (2020), Analisa Kelongsorang Lereng Akibat Dari Peningkatan Kadar Air Yang Tinggi, JRSDD, joernal Edisi September 2020,Vol.8, No.3,Hal:463–468 (p-ISSN:2303-0011) (e-ISSN:2715-0690)

Tyas Budiasih1,dkk, Analisis pengaruh Batas Cair dan Angka Pori Terhadap Indeks Pemampatan Primer. Jurnal Smart Teknologi Vol. 4, No. 6 (2023) Halaman 827 – 833 ISSN: 2774-1702, http://jurnal.unmuhjember.ac.id/index.php/JST.

Vishal Ghutke, Sarika Modak , Tejas Saratkar , Abhijeet Ade , Prashant Bodalkar , Experimental Study of Model on Soil Slope Failure Subjected to Artificial Rainfall, International Journal for Research in Applied Science & Engineering Technology (IJRASET) , ISSN: 2321-9653; Volume 12 Issue V May 2024- Available at www.ijraset.com

Ali Fawaz , Elias Farah , Fadi Hagechehade, Slope stability analysis using numerical modelling, American Journal of Civil Engineering 2014; 2(3): 60-67 Published online April 30, 2014 (http://www.sciencepublishinggroup.com/j/ajce) , doi: 10.11648/j.ajce.20140203.11

LAMPIRAN

I. Publikasi jurnal internasional I (Pablis)
II. Publikasi jurnal internasional II (Accepted)
III. Publikasi prosiding Conference nasional (publis)
IV. Publikasi jurnal sinta 2 (Pablis)

PERBAIKAN DARI SEMINAR PROGRES 3

Pada bagian ini dijelaskan bagian – bagian perbaikan yang dilakukan pada laporan ini terhadap saran, masukan , dan komentar dari tim penguji di seminar progress :

Tanggal : 4 Juni 2025

Penguji :

1. Prof. Dr.Eng. Fauzan, S.T, M.Sc (Eng),
2. Prof. Abdul Hakam, M.T, Ph.D,
3. Prof.Dr. Bambang Istijono, M.E,
4. Prof Dr.Aprisal, M.S,
5. Dr. Andriani Setiawan,S.T, M.T
6. Dr.Nurhamidah, S.T, M.T, M.Eng.Sc.

No	Saran	Perbaikan
1	Gunakan standar vector untuk pemadatan	Sudah diperbaiki
2	Buatkan grafik data hasil percobaan	Sudah diperbaiki
3	Buatkan hasil analisis percobaan	Sudah diperbaiki
3	Beberapa salah ketik	Sudah diperbaiki

ANALYSIS OF THE EFFECT OF RAINFALL INTENSITY AND SLOPE STEEPNESS ON LANDSLIDE DISASTER

NOFRIZAL[1,2], FAUZAN[3], HAKAM.A[3,*], ISTIJONO.B[3], APRISAL[4]

[1] Civil Engineering Doctoral Student, Andalas University, Indonesia.
[2] Padang Institute of Technology, West Sumatera, Indonesia.
[3] Department of Civil Engineering, Faculty of Engineering, Andalas University, Indonesia.
[4] Soil Science Department of Agriculture Faculty, Andalas University, Indonesia.
[*] Corresponding author: ahakam@eng.unand.ac.id

Abstract

Soil erosion and landslide events pose significant threats to sustainable agriculture and human safety. Varying rainfall intensities play a crucial role in runoff, sediment yield, and slope stability. Factors such as soil properties, topography, and vegetation cover interact with rainfall to influence landslide vulnerability. A comprehensive investigation integrating both laboratory test modeling and numerical modeling was conducted to elucidate the mechanisms precipitating slope failure during precipitation events. Through the execution of landslide experiments employing laboratory modeling, wherein artificial rainfall is administered to uniform clay slopes, the timing and characteristics of various failures were delineated. Moreover, the volumetric moisture content is quantified in real time utilizing monitoring sensors alongside laboratory assessments. The acquired volumetric water content data subsequently serves to corroborate the outcomes of the numerical modeling efforts. The validated numerical simulations of laboratory-scale slope failures yield valuable insights into the hydraulic conditions that instigate landslides. Based on the numerical modeling outcomes, the diminished slope in laboratory assessments became saturated to an extent whereby the wet front initially progressed downward, subsequently resulting in the accumulation of rainwater at the slope's apex, which induced a water surface advancing towards the crest. Research on slope failure modeling under different rainfall intensities and slope inclinations provides valuable insights

Keywords:

Landslide;
Rainfall intensity;
Slope failure;
Safety factor;
Water content.

1 Introduction

Soil erosion is a significant environmental issue that threatens sustainable agriculture globally [1–4]. One major contributor to soil erosion is sloped farmland [5]. The effectiveness of various tillage methods in reducing runoff and sediment differs depending on rainfall intensity [6]. Even with the implementation of conservation tillage, severe soil erosion can occur on sloped farmland during periods of intense rainfall [7, 8]. Therefore, the varying rainfall intensities become a crucial factor relate with runoff and soil erosion. This can be the basis for landslide management policies or actions in the future.

Hillside collapse, or landslide, also threatens human safety and infrastructure, particularly in areas prone to heavy rainfall. Intense rainfall can saturate soil layers, reducing their stability and increasing the likelihood of slope failure [9]. It involves various interrelated factors such as soil properties, topography, vegetation cover, and especially rainfall intensity and duration [10, 11]. Furthermore, rainfall factors, including surface runoff, infiltration, and debris flow, can trigger changes in soil pore-water pressure, soil moisture content, or soil pressure on slopes, directly reducing the soil's shear strength. As rainfall intensity increases, infiltration rates also rise, which can lead to slope failure.

Soil permeability and texture are key determinants of landslide vulnerability. High permeability and specific soil textures increase the risk of landslides, especially on steep slopes (25-45%) [12]. The internal friction angle and cohesion of soil are critical in determining slope stability. As these properties increase, the safety factor of the slope also increases, indicating greater stability [13]. Continuous heavy rainfall leads to the formation of a saturated zone, where lateral seepage and air resistance delay infiltration, affecting slope stability. The safety factor decreases with increased slope angle and initial moisture content [14]. Rainfall-induced toppling in loess regions is exacerbated by surface runoff gathering in cracks, increasing hydrostatic pressure and reducing soil strength, leading to collapse. Despite rainfall is a primary trigger for landslides, it is essential to consider the complex interplay of various factors such as soil properties, slope characteristics, and vegetation. Effective landslide mitigation strategies, such as terracing and minimum tillage, can help manage these risks in agricultural and hilly areas [12].

Given the complexity of landslide triggers, it is essential to assess how rainfall interacts with other slope-related factors. Prolonged rainfall can saturate soil layers, weakening their structure and increasing pore-water pressure, especially in clay-rich soils. Vegetation loss further reduces slope stability by decreasing root reinforcement and increasing surface runoff. These combined effects show that rainfall intensity must be evaluated alongside slope geometry, soil characteristics, and land cover to accurately understand and mitigate landslide risks.

Current research [15] investigates the tillage methods in controlling rainwater partitioning and soil erosion in sloped farmland. It revealed that tillage altered rainwater distribution into depression storage, infiltration, and runoff. Tillage reduces runoff and increases infiltration. The soil surface properties under simulated rainfall with examines effects of surface roughness on runoff and infiltration has been discussed by [16]. Anti-erosion influences of several typical tillage practices were presented by [17]. Rainfall simulation experiments were performed with path analysis to analyse the interactive effects of the slope gradient, rainfall intensity, and surface roughness on the sediment yield and runoff volume. According to our findings, the gradient of a slope and the intensity of the rainfall both had a positive effect, while the surface roughness had a negative effect.

The Talamau Plateau in Pasaman Regency, West Sumatra, is one of the landslide-prone areas examined in this paper, as illustrated in Figure 1. The highest rainfall recorded between 2020 and 2021 ranged from 4,730.70 mm to 5,332.30 mm. Additionally, the slope inclination of 15–30° contributes to the occurrence of landslides. Based on these factors, a laboratory test of slope failure was modeled, taking into account the rainfall intensity and slope inclination, using soil samples characteristic of the Talamau Plateau. This approach aims to study landslide events as a means for future mitigation and preventive actions. The parameters contributing to slope failure are examined by analyzing the impact of rainfall intensity and duration on soil moisture content and their influence on slope collapse. Understanding how the behavior of slope failure changes with increasing rainfall intensity and soil moisture levels is essential, as these factors directly affect slope stability and safety. Furthermore, the study considers how the density of the underlying soil, particularly clay soil within the Atterberg limit zones, affects slope failure. This comprehensive examination of various factors provides valuable insights into the conditions that lead to slope failure, enabling more effective prevention and stabilization measure.

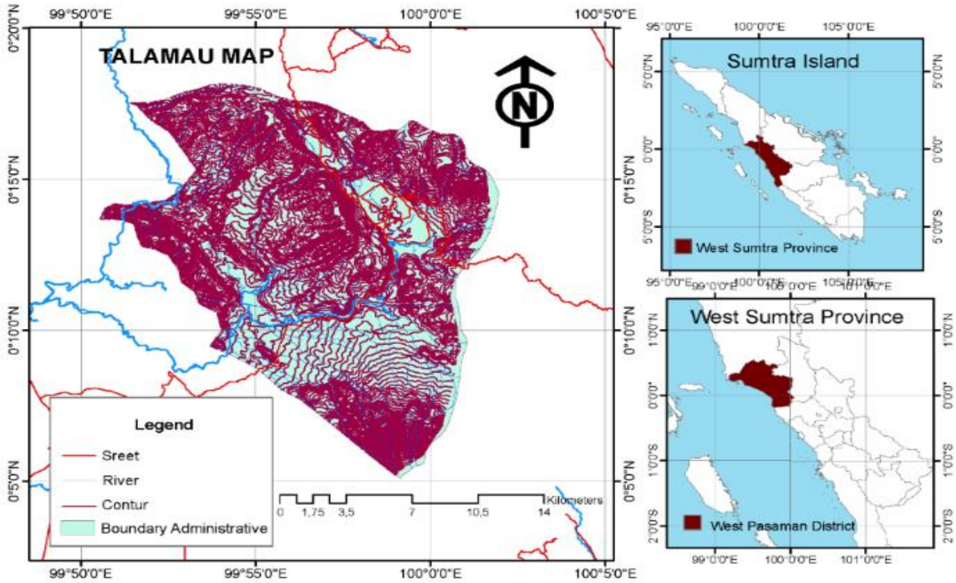

Fig. 1: Geographical Location of the Talamau Plateau Landslide Area in West Sumatra.

2 Methodology
2.1 Experimental Model Preparation

This research investigated the landslide-prone area in the Talamu sub-district, Pasaman Regency. Silty clay soil samples were taken at several points in landslide-prone areas to be analyzed by simulating the proposed model. Modelling and testing were carried out at the Civil Engineering Geotechnical Laboratory, Andalas University and Padang Institute of Technology. According to [18], slopes exceeding 5 degrees are identified as the primary contributors to soil erosion, as demonstrated in the case study conducted on the Loess Plateau. Meanwhile, in the case study of the Talamau Plateau, slopes reaching 30 degrees significantly contribute to landslide disasters during heavy rainfall, with the surface soil characteristics for this study are listed in Table 1.

The slope was constructed as a semi-3D model in the laboratory at a physical scale of 1:100. The slope model was built with four different slope angles: 30°, 45°, 60°, and 90°. The height of the slope model is 34 cm. The base width of the slope model is 30 cm, while the top width varies depending on the slope angle. The reviewed slope width is 30 cm. The slope model was made from layers of soil samples taken from the field, using soil parameters obtained from laboratory tests, and compacted to 90% of the dry density value (γd g/cm³) and its corresponding water content (%). The soil was then placed into the testing model to form slopes with the desired angles, as shown in Figure 2a. A watering device with oscillating nozzles, a rainfall controller, and a water storage tank. The rainfall controller enables precise adjustment of rainfall intensity. There are 10 water spraying nozzles that have been configured with a water discharge which represents rainfall in the Talamau area as illustrated in Figure 2b.

Additionally, a data observation system is integrated to monitor and record hydrological changes on slopes during simulated rainfall events. This system includes an outflow meter calibrated to measure rain intensity and duration, sensors to monitor soil water content variations, and a computer for data collection and analysis. A specialized soil moisture sensor is also employed to track changes in soil volumetric water content over time.

Table 1: The surface soil characteristics for the Talamau Plateau.

Experiment	Parameters	Value	Unit
Water content	w	60.594	%
Bulk density	γ	1.558	[gram/cm3]
Specific gravity	Gs	2.627	
Sieve analysis	Gravel	0.000	%
	Sand	34.067	%
	Clay	65.933	%
Atterberg limit	SL	64.885	%
	PL	46.974	%
	PI	17.911	%
Direct shear	c	0.218	[kg/cm2]
	φ	22.835	o
Compaction	w opt	48.455	[gram/cm3]
	γ dry max	1.235	[gram/cm3]

Note: SL = Shrinkage Limits, PL = Non-elastic Limits, PI = Non-elastic Index, c = cohesion, φ = Internal shear angle,
w opt = Optimum water contents, γ dry max = specific dry soil grafity.

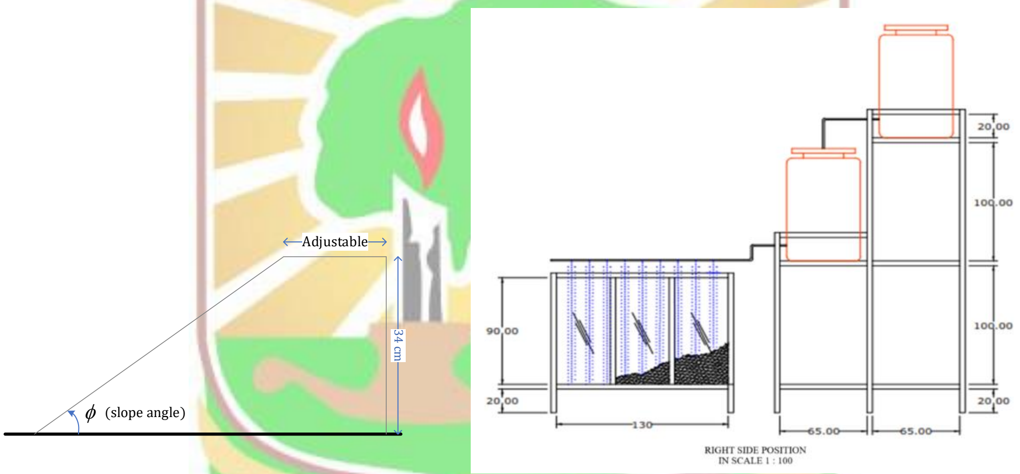

(a) (b)

Fig. 2: The Proposed Model for the Landslide Test Under Laboratory Experimental. (a) Landslide Model Sizing, (b) Proposed Model Construction.

2.2 Experimental Procedure and Parameter Measurement

This study focuses on examining the mechanisms of slope erosion failure in silt-clay and sandy-clay soils caused by the effects of rainfall intensity and duration. Testing includes determining the critical rainfall runoff rate and water infiltration in soil layers using a slope experiment apparatus. The analysis of slope failure due to erosion is conducted in four stages:

Stage 1: This phase represents the initial testing of soil samples, focusing on evaluating their physical properties, key soil parameters, and erodibility. The analysis includes determining characteristics such as specific gravity, which measures the soil's density relative to water, and bulk density, which represents the mass of soil per unit volume, including the spaces between particles. Additionally, the particle size distribution is assessed to identify the proportions of sand, silt, and clay, as this influences soil drainage and compaction properties. The soil's moisture content is also measured to determine the amount of water present, which is essential for plant growth, engineering applications, and understanding soil behavior in various conditions. Finally, erodibility is examined to gauge the soil's susceptibility to erosion caused by water or wind, a factor influenced by its texture, structure, and composition.

Stage 2: This stage involves testing the behavior of slope failure caused by rainfall intensity and duration at varying levels, including low (0 – 100 mm/hours), medium (100 – 300 mm/hours), and high, (300 – 500 mm/hours). The testing focuses on monitoring changes in soil moisture content over a specific period until slope failure occurs. The goal is to understand the degree of wetting caused by water infiltration resulting from the intensity and duration of rainfall. By simulating different rainfall conditions, the experiment replicates natural scenarios that lead to slope instability. As water infiltrates the slope, it increases soil saturation, weakening its structure and ultimately triggering failure. This process provides essential insights into the relationship between rainfall characteristics and slope stability, which are critical for predicting and mitigating landslide risks in vulnerable areas.

Stage 3: Verification of the experimental results is carried out under various soil layer conditions on slopes using the GeoSlope or GeoStudio software application. This process involves simulating the experimental scenarios within the software to replicate real-world slope configurations and validate the findings. GeoSlope and GeoStudio are advanced geotechnical tools designed to analyze slope stability, model soil behavior, and assess the interactions between soil layers under different conditions. By inputting the experimental data into the software, detailed analyses can be performed, considering factors such as soil strength, moisture content, pore water pressure, and external forces.

Stage 4: The discussion focuses on analyzing the influence of rainfall intensity and duration, as well as changes in soil moisture content, on the behavior of slope failure in underlying soil layers with varying slope angles and soil densities. This investigation aims to understand how different rainfall characteristics interact with the soil's moisture dynamics to affect slope stability. Rainfall intensity determines the rate of water infiltration, while its duration influences the total amount of water absorbed by the soil. These changes in moisture content can alter the soil's weight, cohesion, and internal friction, directly impacting its stability. Additionally, the slope angle affects the gravitational forces acting on the soil, and the density of the soil influences its resistance to deformation.

2.3 Numerical modelling configuration

Numerical modeling was conducted to study how rainfall intensity and water seepage affect landslide behavior, as observed in small-scale experiments. The purpose of this modeling is to generate accurate and reliable data on hydraulic variables at specific points within the experimental setup. This data helps to better understand the complex hydraulic processes that lead to landslides, which laboratory experiments alone cannot fully capture.

Using the Darcy-Buckingham equation, the movement of water in unsaturated soil—both horizontally and vertically—can be described by the following expressions for horizontal (q_x) and vertical (q_z) water fluxes:

$$q_x = -K(\psi)\left(\frac{d\psi}{dx}\right) \tag{1}$$

$$q_z = -K(\psi)\left(\frac{d\psi}{dx} + 1\right) \tag{2}$$

where, $K(\psi)$ represents the hydraulic conductivity, which varies depending on the capillary pressure, ψ. The water continuity equation is given by the following expression:

$$\frac{\partial\theta}{\partial t} = -\left(\frac{\partial q_x}{\partial x} + \frac{\partial q_z}{\partial z}\right) \tag{3}$$

In this context, θ refers to the soil water content, and t represents time. By modifying equations (1) and (2), equation (3) is derived, resulting in two-dimensional equations that describe both vertical and horizontal groundwater flow, known as Richards' Equation.

$$C(\psi)\frac{\partial\psi}{\partial t} = \frac{\partial}{\partial x}\left[K(\psi)\frac{\partial\psi}{\partial x}\right] + \frac{\partial}{\partial z}\left[K(\psi)\frac{\partial\psi}{\partial z}\right] + \frac{\partial}{\partial z}K(\psi) \quad (4)$$

In this case, $C(\psi)$ is the water capacity function, which is determined by the slope of the soil water retention curve. Equation (4) is solved using models that characterize the soil's water retention and hydraulic conductivity.

Soil Hydraulic Properties

The Lognormal (LN) model, developed by [19], is applied to solve Equation (4). This model is based on the assumption that the distribution of soil pore sizes follows a lognormal pattern. Using the LN model, key hydraulic properties such as effective saturation $S_e(\psi)$ and water capacity $C(\psi)$ are derived and expressed in the following equations.

$$S_e(\psi) = \frac{\theta-\theta_r}{\theta_s-\theta_r} = Q[ln(\psi/\psi_m)/\sigma] \quad (5)$$

$$C(\psi) = \frac{\theta_s-\theta_r}{\sqrt{2\pi\sigma(-\psi)}} exp\left[-\frac{\{ln(\psi/\psi_m)\}^2}{2\sigma^2}\right] \quad (6)$$

The parameters θ_s and θ_r represent the saturated and residual water contents, respectively. The dimensionless parameter σ characterizes specific system properties, while ψ_m denotes the main capillary pressure, which is associated with the average pore radius (expressed in centimeters). Additionally, Q refers to the complementary normal distribution function, mathematically defined as:

$$Q(x)\frac{\partial\psi}{\partial t} = (2\pi)^{-1/2}\int_K^{(x)} exp(-x^2/2)dx \quad (7)$$

$$K(S_e) = K_s S_e^{\alpha} Q[Q^{-1}(S_e) + \beta\sigma] \quad (8)$$

$$K(\psi) = K_s Q^a\left[\frac{1}{\sigma} ln\left(\frac{\psi}{\psi_m}\right)\right] Q\left[\frac{1}{\sigma} ln\left(\frac{\psi}{\psi_m}\right) + \beta\sigma\right] \quad (9)$$

In this context, K is linked to S_e and ψ, as described by [20]. Here, K_s represents the saturated hydraulic conductivity, while α and β are dimensionless parameters that describe the tortuosity of soil pores. The LN modeling framework defines soil hydraulic properties using seven key parameters: θ_s, θ_r, ψ_m, σ, K_s, α, and β.

2.4 Geometry and Boundary Conditions

The conventional slope used for numerical analysis consists of two distinct soil strata: the surface layer and the subsurface layer, as illustrated in Figure 2(a). This slope spans a total length of 80 centimeters and is inclined at an angle of 45 degrees. The cumulative thickness of the soil layers measures 34 centimeters, with the depths of the surface and subsurface layers assumed to be equal. This specific thickness reflects conditions typical of many clay-rich regions in Japan, where landslide activity is common. Such regions, characterized by soil depths ranging from 50 to 100 centimeters, have been extensively studied, including the observations by [21], which provide critical insights into the geotechnical factors influencing slope stability in these areas.

The no-flux boundary condition is applied at the interface beneath the soil layer, based on the assumption of an impermeable bedrock substrate underlying the subsurface layer. This ensures that no water flux occurs at the base of the soil profile. Similarly, the no-flux condition is imposed at the boundaries of the upper slope (separation ridge) and the lower slope (basin), effectively confining water movement within the defined domain. Precipitation infiltrates the soil surface, and when the ground surface becomes saturated, the resulting discharge is calculated. This process corresponds to the application of the seepage front boundary condition at the soil surface. The governing flow dynamics are modeled using the Richards equation (Equation (4)), which is solved numerically through the finite element method, as described by [22]. The computational discretization framework, shown in Figure 3, utilizes triangular finite elements to accurately capture the spatial variability of the system and ensure robust numerical analysis.

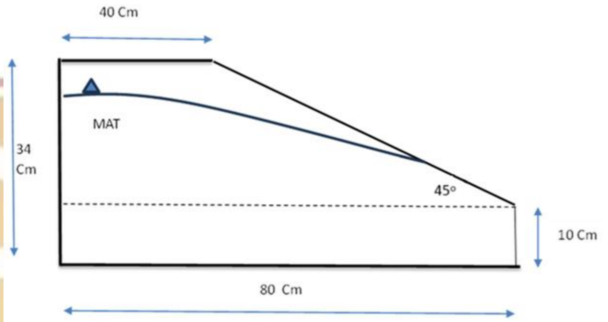

Fig. 3: Slope Geometry Section.

2.5 Slope Stability Analysis

The Bishop method is a widely recognized approach for assessing slope stability, particularly effective in determining the safety factor by analyzing the equilibrium of forces within a shear circle. Similar to [23] approach, it focuses on balancing the driving and resisting forces acting on a slope, which is essential for predicting potential landslides. The safety factor (FS) is calculated by comparing resisting forces, such as soil shear strength, to driving forces like gravity and external loads.

$$Fs = \frac{1}{\sum_{i=1}^{I} W_i \sin \delta_i} \sum_{i=1}^{I} \left[\frac{c_i G_i + (W_i - u_i G_i) \tan \phi_i}{\cos \delta_i + \sin \delta_i \tan \phi_i / Fs} \right] \quad (8)$$

Here, I represents the total number of slices within the sliding circle, U_i (cm) denotes the positive pore water pressure at the base of slice i, W_i(g) is the weight of slice i, G_i (cm) corresponds to the horizontal length of slice i, δ_i (º) is the inclination of the slice's base i, ϕ_i (º) is the internal friction angle, and c_i (gf cm^{-2}) represents the cohesion intercept.

Studies have shown that an FS greater than 1.25 indicates a stable slope, while values below this threshold suggest instability [24]. Research highlights that 2D analyses often produce more conservative FS estimates compared to 3D analyses, which offer a more realistic depiction of complex slope geometries [25]. The choice between 2D and 3D methods is critical, especially in heterogeneous soil conditions [26]. The Bishop method has proven effective in diverse geological settings, such as clay and sand slopes, demonstrating reliability in estimating FS despite uncertainties in soil properties [26]. Case studies, such as those in West Lombok, underscore its practical utility in preventing landslides and protecting critical infrastructure [24, 27]. However, it is important to recognize the limitations of limit equilibrium methods, as they rely on assumptions that may underestimate risks in certain soil types, such as clay, which can exhibit greater variability in stability assessments [26].

3 Results and Discussion

Two scenarios were used for numerical simulations, as shown in Table 2. The first scenario examines how prior rainfall affects drainage over 24, 48, and 96 hours. This period helps set the starting conditions before a small rainfall event begins (three hours after the Hougawachi rainstorm). The soil thickness was set to 34 cm, and the slope angle was 40 degrees. The effective soil porosity for surface and subsurface layers was set to the average of the observed values [28, 29], as listed in Tables 2.

Table 2: Overview of the Parameters for Each Numerical Simulation Scenario Total of vehicles for each entrance.

Scenarios	Rainfall period [Minute]	Soil thickness [cm]	Slope Gradient (degree)	Main rainfall [mm/hour]	Conditions analyzed
1	24, 48, 90	34	40	Low	1, 2, 3
2	24, 48, 90	34	40	High	1, 2, 3

3.1 Soil Grain Distribution

Table 3 provides data on soil grain distribution for a landslide area, analyzed using a sieve test. It lists the sieve number, retained weight, cumulative retained weight, and calculates the percentage retained and passing for different grain diameters. Coarse grains are captured in larger sieves, with 18.13% retained at a 4.75 mm diameter and progressively higher percentages retained in smaller sieves, reaching 100% retention in the pan (finer than 0.075 mm). This distribution highlights the soil's gradation and particle size distribution, crucial for assessing stability and susceptibility to landslides.

Table 3: Data for Soil Grain Distribution.

Sieve number	Retained weight	Total retained weight [g]	Percent retained (%)	Percent passing (%)	Grain diameter [mm]	Soil Classification
4	54.400	54.400	18.13	81.87	4.750	Gravel
10	26.000	80.400	26.80	73.20	2.000	Sand
20	28.200	108.600	36.20	63.80	0.840	Sand
40	23.300	131.900	43.97	56.03	0.420	Sand
100	34.500	166.400	55.47	44.53	0.150	Sand
200	11.100	177.500	59.17	40.83	0.075	Sand
PAN	122.500	300.000	100.00	0.00		Clay

The grain size distribution graph in Figure 4 provides insight into the soil's characteristics and its potential influence on landslide susceptibility. The gradual slope of the curve indicates a well-graded soil with a mix of fine and coarse particles, suggesting moderate drainage properties and good compaction potential. However, the presence of finer particles, such as silt and clay, as reflected in the higher percentage passing at smaller diameters, may lead to reduced permeability and higher water retention. These conditions can increase pore water pressure during heavy rainfall or saturation, reducing shear strength and making the soil more prone to instability and landslides. Additionally, the finer particles may lead to liquefaction or surface erosion under stress, further exacerbating slope failure risks. Thus, this soil's composition and drainage behavior are critical factors in assessing and mitigating landslide hazards.

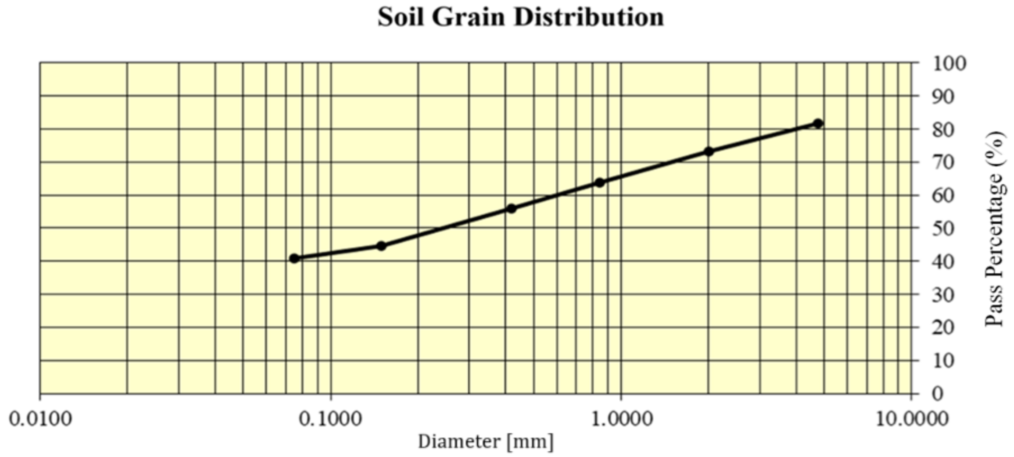

Fig. 4: Graph of the grain soil distribution.

A classification of the soil layers based on the grain size distribution data from Table 3, which is essential for modeling slopes in landslide-prone areas. The table categorizes the soil into three primary types: gravel, sand, and clay, with each category linked to specific sieve analysis results. Gravel comprises 18.13% of the soil, corresponding to the material retained on the sieve with a 4.75 mm aperture, representing the coarsest particles in the sample. Sand accounts for 41.03% of the soil, derived from the cumulative material retained on sieves down to the 0.075 mm aperture (sieve 200), highlighting medium-sized grains that play a crucial role in drainage and shear strength. Clay makes up 40.83% of the soil, representing the finest particles that pass through the 0.075 mm sieve. These fine particles contribute to soil cohesion and water retention, significantly influencing slope stability. This classification helps engineers and geologists evaluate soil properties, predict slope behavior, and design effective landslide mitigation strategies.

3.2 Density of the Slope Foundation Soil

Figure 5 illustrates the hardware preparation for the density of the slope foundation soil. It was carried out based on standard [30–32]. The results are listed in Table 4 which highlights variations in soil properties across different slope angles. There are four different slope angles depicted in Figure 6. As the slope angle decreases from 90° to 30°, significant changes are observed in soil weight, volume, and density (γd). For instance, the soil density varies from 1.13 g/cm³ at 90° to 1.75 g/cm³ at 30°, indicating that lower slope angles may result in more compacted soil. Initial moisture content, ranging from 0.07% to 0.25%, also influences these variations, as higher moisture content tends to reduce soil density. These relationships underscore the interdependence of slope geometry, soil compaction, and moisture in determining soil stability and suitability for foundation support.

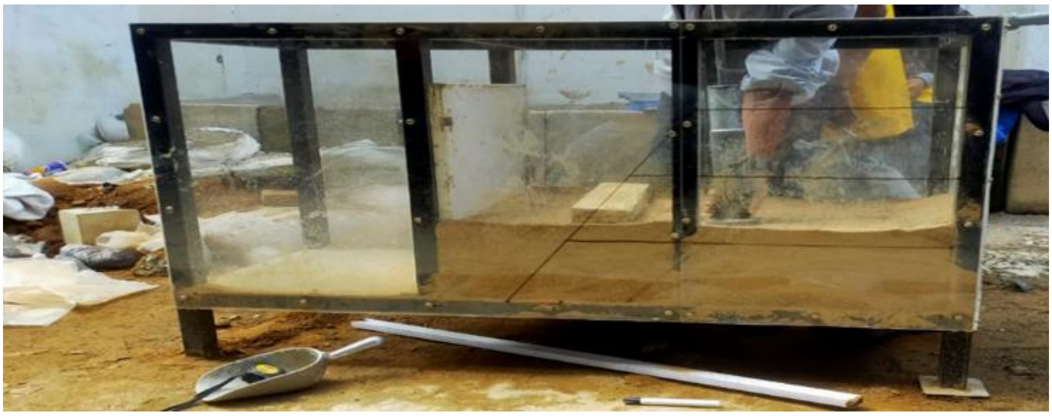

Fig. 5: Preparing hardware simulation for the density of the slope foundation soil.

Table 4: The Density Data of the Sope Foundation Soil.

No.	Slope angle magnitude (°)	Weight of the soil layer [gr]	Dimension (cm)	Volume [cm³]	Initial moisture content (%)	Soil density γd $\left[\frac{(gr/cm^3)}{1+W(gr/cm^3)}\right]$
1	90	49550.0	$V = L \times W \times H$ $V = 40 \times 34 \times 28$	38080.0	0.15	1.13
2	60	60755.0	$V = \frac{(a+b)}{2} \times W \times H$ $V = \frac{(43+63)}{2} \times 34 \times 30$	54060.0	0.07	1.05
3	45	96105.0	$V = \frac{(a+b)}{2} \times W \times H$ $V = \frac{(30+66)}{2} \times 34 \times 34$	72828.0	0.25	1.06
4	30	82195.0	$V = \frac{(a+b)}{2} \times W \times H$ $V = \frac{(16+62)}{2} \times 30 \times 34$	39780.0	0.18	1.75

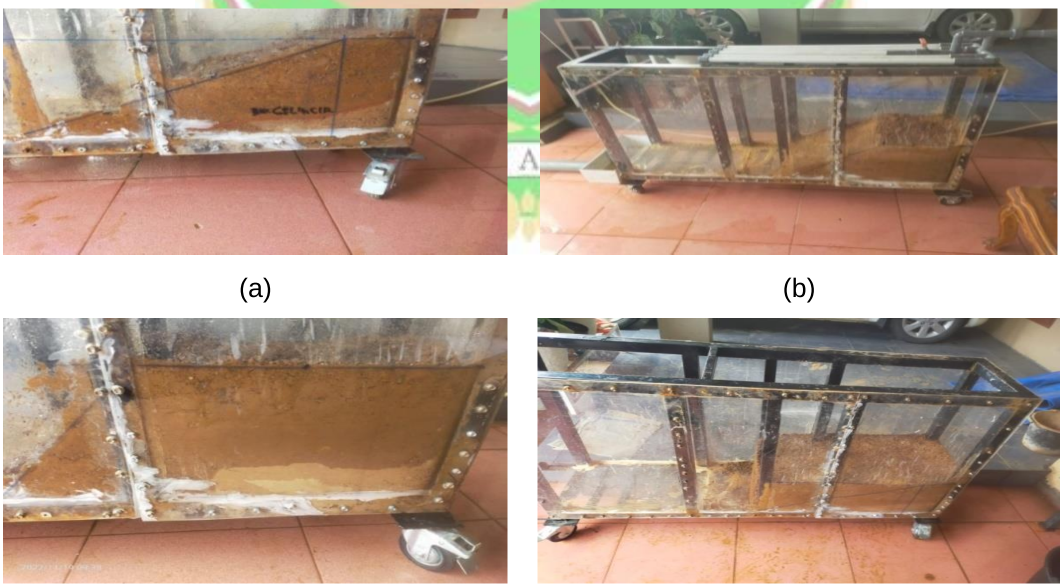

(a) (b)

(c) (d)

Fig. 6: Hardware simulation setup in varies slope, (a) 30°, (b) 45°, (c) 60°, (d) 90°.

3.3 Slope Failure experiment under different hillside degree

The landslide simulation unfolds in a sequence of events as shown in Table 5. Beginning with seepage flow entering the slope layers at minute 10, where water infiltration gradually saturates the soil, reducing its shear strength and triggering early signs of instability. By minute 20, deformation becomes evident on the slope surface, as subtle shifts in soil indicate the increasing loss of structural integrity. At minute 30, a slip plane begins to form deep within the slope, delineating a critical failure zone as water continues to seep into the soil layers. By minute 40, the seepage flow reaches the slope base, exerting hydrostatic pressure and further weakening the foundation.

This culminates in the initial collapse of the slope toe at minute 50, where the stress is most concentrated. Over the next 10 minutes, the collapse intensifies, spreading upwards and destabilizing larger portions of the slope. By minute 70, the slope heel becomes increasingly unstable, with prominent cracks and displacements appearing as the collapse accelerates toward the slope's upper sections. The culmination of these processes occurs at minute 80, as the slope toe experiences total failure, resulting in a full-scale landslide that displaces significant volumes of soil. By minute 90, the movement ceases, with the landslide halting due to stagnation as the forces driving the collapse diminish, leaving the slope in a state of post-failure equilibrium.

Table 5: Landslide Simulation on a 30-Degree Hillside Slope.

Time [Minute]	Intensity (I) [mm/hour]	Rainfall threshold [mm/hour]	Water content after rain (%)	Slope condition behavior
0	0	0	17.67	The experiment begins
10	113.12	12.63	48.56	Seepage flow enters the slope layers
20	22.12	21.83	50.63	Deformation occurs on the slope surface
30	15.08	30.07	30.30	A slip plane begins to form
40	5.66	37.75	59.92	Seepage flow starts reaching the base
50	9.05	45.02	62.50	Collapse begins at the slope toe
60	7.54	52.00	52.12	The collapse continues to increase
70	9.70	58.73	46.96	The slope heel becomes increasingly unstable to collapse
80	8.48	65.27	52.52	The slope toe experiences total failure (landslide)
90	5.03	71.63	55.51	The landslide has stopped due to stagnation

(1.75 (gr/cm3) slope density and 17.67 % Initial water content)

As listed in Table 6, the landslide simulation begins with the gradual onset of deformation on the slope surface. First observed at minute 10, subtle shifts in the soil indicate the initial signs of instability. By minute 20, the deformation spreads further, affecting larger portions of the slope and signaling an escalation of instability. At minute 30, the slope head collapses, marking the first significant structural failure. This collapse becomes more pronounced by minute 40, as the slope head displaces and loses cohesion. At minute 50, an initial slip plane begins to form, identifying the zone of weakness where further failure is concentrated. By minute 60, the slip plane deepens, intensifying the landslide and accelerating soil movement. At minute 70, the landslide area expands towards the flat section at the slope head, increasing the affected zone and the scale of the failure. By minute 80, the slip plane extends to halfway up the slope, indicating the progression of the failure towards the upper regions. Finally, at minute 90, the landslide depth approaches the slip plane, and the collapse ceases due to stagnation, leaving the slope in a state of post-failure stability.

Table 6: Landslide simulation on a 45-degree hillside slope.

Time [Minute]	Intensity (I) [mm/hour]	Rainfall threshold [mm/hour]	Water content after rain (%)	Slope condition behavior
0	0	0	25.00	The experiment begins
10	90.50	12.63	11.52	Deformation occurs on the slope surface
20	33.94	21.83	43.75	The deformation spreads further on the slope
30	22.62	30.07	68.75	The slope head begins to collapse
40	11.31	37.75	45.83	The slope head collapses further
50	13.57	45.02	46.15	The initial slip plane begins to form
60	22.62	52.00	50.00	The slip plane deepens, and the landslide intensifies
70	25.86	58.73	43.48	The landslide area expands towards the flat section at the slope head
80	22.62	65.27	52.17	The slip plane reaches halfway up the slope
90	7.54	71.63	13.74	The depth of the landslide has approached the slip plane, and the collapse has stagnated.

(1.06 (gr/cm3) slope density and 25.00 % Initial water content)

The result in Table 7 shows the simulation begins with the introduction of seepage flow into the slope layers, initiating the process that will lead to failure. In Minute 10, deformation begins to occur on the slope surface as the soil starts to shift due to the infiltration of water. By Minute 20, the deformation spreads further across the slope, signifying an increasing loss of stability. In Minute 30, the slope head begins to collapse, with the upper portion of the slope losing cohesion under the pressure of the displaced soil. This collapse intensifies by Minute 40, causing further destabilization of the slope head. In Minute 50, the initial slip plane begins to form as a clear zone of weakness develops within the slope, leading to localized failure. By Minute 60, the slip plane deepens, and the landslide accelerates, displacing larger volumes of soil and causing the collapse to intensify. In Minute 70, the landslide area expands towards the flatter section at the slope head, further increasing the scale of the failure. By Minute 80, the slip plane reaches halfway up the slope, signifying that the failure zone has propagated significantly. Finally, in Minute 90, the depth of the landslide approaches the slip plane, and the collapse stagnates, as the system reaches equilibrium and the movement of soil stops.

The simulation begins with the introduction of seepage flow into the slope, causing an increase in pore water pressure and initiating soil instability as described in Table 8. In 10 minutes, deformation begins to occur on the slope surface as the soil shifts due to the weakening of the material from infiltrating water. By 20 minutes, the slope starts to collapse along its surface, as the soil begins to lose its cohesion and slide downward under the influence of gravity. At 30 minutes, the slip plane extends beyond half the height of the slope, signaling a deeper and more widespread failure zone that threatens the stability of the entire slope. The collapse at the slope head intensifies, and by 40 minutes, the slope head continues to fail, ultimately leading to a total collapse at the uppermost portion of the slope. As the collapse progresses, it nears the maximum failure point by 50 minutes, with the failure zone spreading and deepening. Finally, at 60 minutes, the collapse stops, with the optimum failure occurring in the slope head area, where the majority of the displacement and collapse have concentrated, marking the end of the event as the system reaches a post-failure equilibrium.

Table 7: Landslide simulation on a 60-degree hillside slope.

Time [Minute]	Intensity (I) [mm/hour]	Rainfall threshold [mm/hour]	Water content after rain (%)	Slope condition behavior
0	0	0	7,41	The experiment begins
10	90,50	12,63	28,00	Seepage flow begins
20	56,56	21,83	57,14	Deformation starts to occur on the slope
30	22,62	30,07	33,33	The slope head begins to collapse
40	33,94	37,75	38,46	The slip plane reaches halfway up the slope
50	18,10	45,02	50,00	The initial slip plane starts to form
60	15,08	52,00	67,62	The slope crest experiences increased landslides
70	16,16	58,73	42,86	The landslide area expands towards the flat section at the slope head
80	14,14	65,27	45,00	The slip plane reaches the base of the slope
90	7,54	71,63	42,86	The collapse has stopped, with the optimum collapse occurring in the slope head area.

(1.05 (gr/cm3) slope density and 7.41 % Initial water content)

Table 8: Landslide simulation on a 90-degree hillside slope.

Time [Minute]	Intensity (I) [mm/hour]	Rainfall threshold [mm/hour]	Water content after rain (%)	Slope condition behavior
0	0	0	9,64	The experiment begins
10	101,81	12,63	29,17	Deformation occurs on the slope surface
20	56,56	21,83	26,09	The slope begins to collapse along its surface
30	22,62	30,07	21,43	The slip plane has exceeded half the height of the slope
40	33,94	37,75	34,62	The slope head continues to collapse, leading to total collapse at the slope head
50	20,36	45,02	32,69	The collapse is approaching the maximum failure point
60	11,31	52,00	30,77	The collapse has stopped, with the optimum collapse occurring in the slope head area

(1.13 (gr/cm3) slope density and 9.64 % Initial water content)

3.4 Slope failure experiment in different rainfall intensity

Simulation has been configured for the hillside slope 45-degree with 1.06 (gr/cm3) slope density and 25.00 % Initial water content. Different rainfall intensities have been simulated to validate the landslide event. Three different rainfall intensities have been set for 131 mm/hour, 167 mm/hour, and 183 mm/hour. Figure 7 illustrates the relationship between rainfall intensity (131 mm/hour) and the duration of rainfall, along with the corresponding changes in post-rainfall water content in the slope. The rainfall intensity remains constant at 131 mm/hour throughout the period, while the water content exhibits fluctuations over time. Initially, the soil's water content was 25.00% before rainfall began. During the experiment, the water content fluctuated, showing a steady increase, reaching 59.92% at around the 40th minute. At this point, the soil significantly reducing slope stability. The water content peaked at 62.50% around the 50th minute, followed by a decline to 46.96%. Towards the end of the observation period, the water content stabilized between 52–55%. At the 80th minute, the water content reached 55.52%, and the slope was no longer stable, leading to maximum collapse. By the 90th minute, the slope failure had ceased, with the final water content recorded at 55.51%.These fluctuations highlight the dynamic interaction between rainfall and soil's water retention capacity, suggesting that prolonged rainfall at high intensities could lead to critical saturation levels and increased risk of slope instability.

Figure 8 shows the relationship between rainfall intensity (167 mm/hour) and the duration of rainfall, along with changes in the slope's post-rainfall water content. The rainfall intensity remains constant throughout the observation period, while the water content undergoes significant variations. At the start of the experiment, the initial soil water content was 25.00%. As rainfall was applied, water infiltrated the soil, and the water content rose steadily, reaching a peak of 68.75% at around the 30th minute. This peak indicates that the soil had undergone significant saturation, approaching or even exceeding its liquid limit, which led to a notable reduction in shear strength and a transition toward a more fluid soil state.

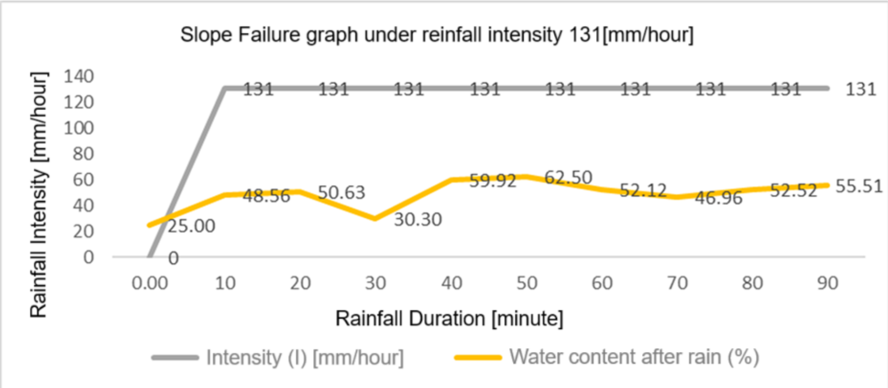

Fig. 7: Landslide Simulation for 131 mm/hour Rainfall Intensity.

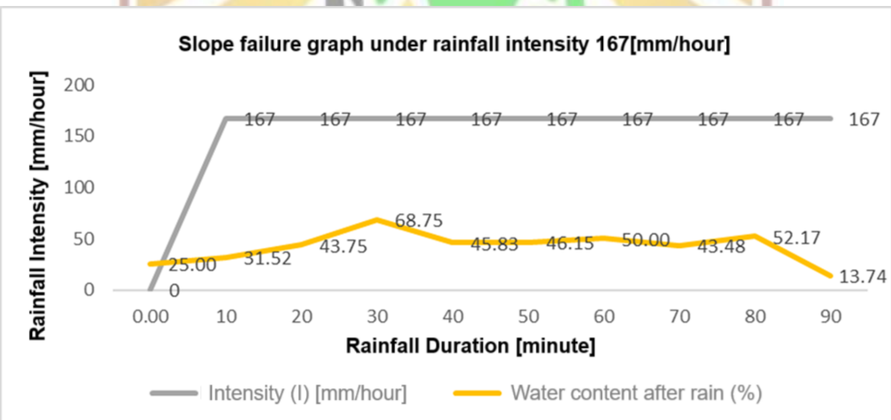

Fig. 8: Landslide Simulation for 167 mm/hour Rainfall Intensity.

Following this peak, the water content decreased gradually to approximately 46.15% by the 50th minute, suggesting the onset of soil movement or drainage processes within the slope model. Between the 60th and 80th minutes, the slope experienced progressive failure, culminating in maximum collapse at the 80th minute when the water content was recorded at 52.17%. This value signifies that even though the water content had reduced from the peak, it remained sufficiently high to maintain the soil in an unstable, near-liquid condition, allowing large-scale movement. After the collapse event, the water content sharply dropped to 13.74% by the 90th minute, indicating rapid loss of pore water due to slope failure and potential surface runoff. Therefore, the critical influence of sustained, high-intensity rainfall can be triggering slope instability. The behavior observed reflects typical landslide mechanisms, where prolonged saturation weakens soil structure, lowers resistance to shear stress, and ultimately leads to sudden, massive slope failure.

Figure 9 illustrates the relationship between rainfall intensity and soil water content during a landslide model experiment conducted under a constant rainfall intensity of 183 mm/hour. The gray line shows that the rainfall intensity quickly rises and then remains steady at 183 mm/hour throughout the 90-minute duration. Meanwhile, the yellow line represents the change in soil water content over time. Initially, the soil's water content starts at 25.00%. As rainfall continues, the water content steadily increases, reaching 28.00% at 10 minutes and peaking sharply at 57.14% by 20 minutes. This rapid rise reflects quick infiltration of water into the slope material. However, after reaching this early peak, the water content drops significantly to 33.33% by the 30th minute, suggesting partial drainage or redistribution of water within the slope. Between 30 and 60 minutes, the water content fluctuates slightly but generally trends upwards, reaching another peak at 67.62% around the 60th minute. This second, higher peak indicates critical saturation conditions, where the soil's internal structure is weakened, and the slope becomes highly unstable. Afterward, the water content decreases again, stabilizing between 42.86% and 45.00% from 70 to 90 minutes.

These water content variations indicate different phases of the slope response under continuous heavy rainfall. The initial sharp rise and later saturation phase demonstrate the increased vulnerability of the slope to failure as the soil loses shear strength. The stabilization of water content towards the end suggests that after major slope movement or failure, the soil structure and water pathways changed, possibly leading to improved drainage. Overall, this figure highlights the critical role of prolonged heavy rainfall in triggering slope failures through progressive soil saturation and strength reduction.

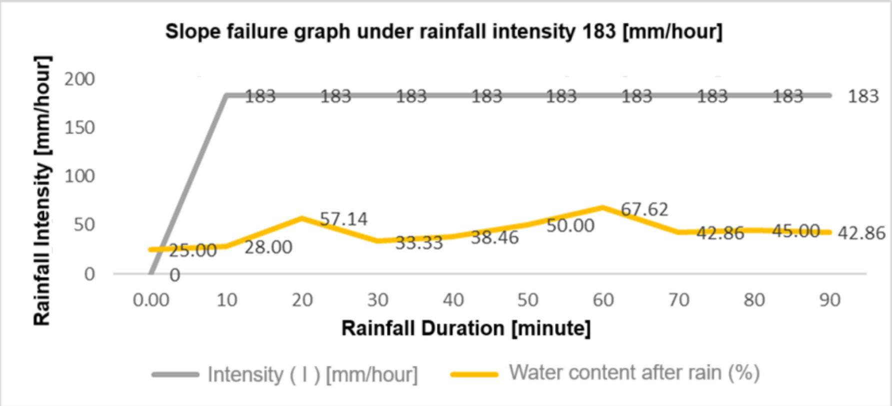

Fig. 9: Landslide Simulation for 183 mm/hour Rainfall Intensity.

3.5 Discussion

The experimental results provide critical insights into slope stability under varying rainfall intensities, soil properties, and slope geometries. The simulation with 183 mm/hour rainfall intensity highlights that soil water content rises sharply from 25% to a peak of 67.62% at around 60 minutes, indicating rapid infiltration and saturation. This peak marks a critical saturation point, after which water content slightly declines and stabilizes between 42.86% and 45%. Such behavior suggests that prolonged rainfall leads to the accumulation of pore water pressure, reducing shear strength and increasing the likelihood of slope instability. Furthermore, the gradual stabilization of water content implies partial drainage or redistribution of moisture within the soil layers, which can either delay or mitigate the onset of failure depending on soil permeability and slope geometry.

These observations underscore the importance of understanding infiltration dynamics to predict and manage landslide risks effectively.

The soil grain distribution analysis reveals a composition with 18.13% gravel, 41.03% sand, and 40.83% clay, highlighting a well-graded mixture that combines drainage efficiency with water retention properties. While the coarser particles contribute to structural stability and drainage, the finer particles, especially clay, increase cohesion but also raise the potential for water retention, leading to elevated pore pressure under saturated conditions. The density variations across slope angles further emphasize the role of compaction, as lower angles (30°) exhibit higher densities (1.75 g/cm³) compared to steeper slopes (90°) with lower densities (1.13 g/cm³). These findings align with the slope failure experiment, where water infiltration triggers deformation, slip plane formation, and eventual collapse over a 90-minute timeline. The sequence of failure highlights the gradual weakening of structural integrity due to hydrostatic pressure and soil displacement, culminating in complete failure. These insights emphasize the interplay of rainfall intensity, soil composition, and slope geometry in landslide initiation, providing a foundation for designing effective slope stabilization and drainage systems to mitigate risks.

4 Conclusion

This study highlights the critical influence of rainfall intensity and slope steepness on landslide occurrences, emphasizing the interplay of soil properties, infiltration dynamics, and slope geometry. The experimental results demonstrate that increasing rainfall intensity leads to rapid infiltration, saturation, and rising pore water pressure, which reduce soil shear strength and trigger slope instability. Key findings include the observation that water content peaks within the first 60 minutes of rainfall exposure, followed by partial stabilization, indicating a transition from saturation to drainage and redistribution processes. The soil grain distribution analysis revealed a well-graded mixture comprising 18.13% gravel, 41.03% sand, and 40.83% clay, which affects water retention and permeability. While coarser particles enhance drainage, finer particles, particularly clay, increase cohesion but also elevate pore pressure under saturated conditions, contributing to slope failure risk. Variations in soil density further underscore the role of slope geometry, with lower slope angles exhibiting higher compaction and stability compared to steeper slopes. Simulated rainfall experiments validated these findings by replicating the progression of slope failure, starting with surface deformation, slip plane formation, and culminating in full-scale collapse over a 90-minute period. The sequence of failure events demonstrated that water infiltration gradually compromises slope stability, highlighting the importance of hydrostatic pressure and soil displacement mechanisms in landslide processes. This is highlighting the need for comprehensive landslide mitigation strategies, including soil reinforcement, terracing, and effective drainage systems. Future studies should focus on integrating vegetation cover and advanced soil stabilization techniques to further improve slope resilience against intense rainfall events. This research provides a foundation for informed decision-making in disaster prevention and sustainable land management practices in landslide-prone regions.

Acknowledgement

Here you can write the acknowledgement.

References

[1] G. LUETZENBURG, M. J. BITTNER, A. CALSAMIGLIA, C. S. RENSCHLER, J. ESTRANY, and R. POEPPL, "Climate and land use change effects on soil erosion in two small agricultural catchment systems Fugnitz – Austria, Can Revull – Spain,"

Sci. Total Environ., vol. 704, 2020, doi: 10.1016/j.scitotenv.2019.135389.
[2] R. MA, F. HU, C. XU, J. LIU, and S. ZHAO, "Response of soil aggregate stability and splash erosion to different breakdown mechanisms along natural vegetation restoration," *Catena*, vol. 208, no. 26, 2022, doi: 10.1016/j.catena.2021.105775.
[3] J. ZHAO, Z. WANG, Y. DONG, Z. YANG, and G. GOVERS, "How soil erosion and runoff are related to land use, topography and annual precipitation: Insights from a meta-analysis of erosion plots in China," *Sci. Total Environ.*, vol. 802, 2022, doi: 10.1016/j.scitotenv.2021.149665.
[4] A. BELMANA, M. MELLAS, and V. CAVALEIRO, "Assessment of Coarse Soil'S Stability Towards Internal Erosion Case of Biskra'S Dam Soil," *Civ. Environ. Eng.*, vol. 20, no. 1, pp. 332–348, 2024, doi: 10.2478/cee-2024-0026.
[5] L. WANG, B. MA, and F. WU, "Effects of wheat stubble on runoff, infiltration, and erosion of farmland on the Loess Plateau, China, subjected to simulated rainfall," *Solid Earth*, vol. 8, no. 2, pp. 281–290, 2017, doi: 10.5194/se-8-281-2017.
[6] L. ZHAO, Q. FANG, R. HOU, and F. WU, "Effect of rainfall intensity and duration on soil erosion on slopes with different microrelief patterns," *Geoderma*, vol. 396, no. January, 2021, doi: 10.1016/j.geoderma.2021.115085.
[7] D. DEUSCHLE, J. P. G. MINELLA, T. DE A. N. HÖRBE, A. L. LONDERO, and F. J. A. SCHNEIDER, "Erosion and hydrological response in no-tillage subjected to crop rotation intensification in southern Brazil," *Geoderma*, vol. 340, no. July 2018, pp. 157–163, 2019, doi: 10.1016/j.geoderma.2019.01.010.
[8] M. YUAN, Y. ZHANG, Y. ZHAO, and J. DENG, "Effect of rainfall gradient and vegetation restoration on gully initiation under a large-scale extreme rainfall event on the hilly Loess Plateau: A case study from the Wuding River basin, China," *Science of the Total Environment*, vol. 739. 2020. doi: 10.1016/j.scitotenv.2020.140066.
[9] R. BULKO and S. MASAROVIČOVÁ, "Effect of Lime Filling on the Compactibility of Clay Soils," *Civ. Environ. Eng.*, vol. 18, no. 2, pp. 501–506, 2022, doi: 10.2478/cee-2022-0047.
[10] X. JING, Y. CHEN, C. PAN, T. YIN, W. WANG, and X. FAN, "Erosion failure of a soil slope by heavy rain: Laboratory investigation and modified GA model of soil slope failure," *Int. J. Environ. Res. Public Health*, vol. 16, no. 6, 2019, doi: 10.3390/ijerph16061075.
[11] A. SALIMAH, M. AMMAR, D. RAHMAWATI, YELVI, and S. TRI WIDYA, "Landslide Analysis Study and Cisewu Countermeasures in District, Garut Regency, West Java," *IOP Conf. Ser. Mater. Sci. Eng.*, vol. 771, no. 1, pp. 0–8, 2020, doi: 10.1088/1757-899X/771/1/012046.
[12] MUJIYO, T. M. PRATINGKAS, O. CAHYONO, and D. P. ARIYANTO, "Landslides Hazard Assessment Using Soil Physics Approaches as a Determinant Factor on Agricultural Land in Hilly Area," *Jurnal Pengelolaan Sumberdaya Alam dan Lingkungan*, vol. 14, no. 3. pp. 566–577, 2024. doi: 10.29244/jpsl.14.3.566.
[13] Y. ZENG *et al.*, "A case study on soil slope landslide failure and parameter analysis of influencing factors for safety factor based on strength reduction method and orthogonal experimental design," *PLoS One*, vol. 19, no. 5 May, pp. 1–20, 2024, doi: 10.1371/journal.pone.0300586.
[14] L. LI *et al.*, "Stability analysis of rainfall-induced landslide considering air resistance delay effect and lateral seepage," *Sci. Rep.*, vol. 14, no. 1, pp. 1–10, 2024, doi: 10.1038/s41598-024-59121-4.
[15] X. ZHAO, X. SONG, L. LI, D. WANG, P. MENG, and H. LI, "Effect of microrelief features of tillage methods under different rainfall intensities on runoff and soil erosion in slopes," *Int. Soil Water Conserv. Res.*, vol. 12, no. 2, pp. 351–364, 2024, doi: 10.1016/j.iswcr.2023.10.001.
[16] S. BAHDDOU, W. OTTEN, W. R. WHALLEY, H. C. SHIN, M. EL GHAROUS, and R. J. RICKSON, "Changes in soil surface properties under simulated rainfall and the effect of surface roughness on runoff, infiltration and soil loss," *Geoderma*, vol. 431, no. February, 2023, doi: 10.1016/j.geoderma.2023.116341.

[17] T. LI, Y. WANG, and F. WU, "Anti-Erosion Influences of Surface Roughness on Sloping Agricultural Land in the Loess Plateau, Northwest China," *Sustain.*, vol. 14, no. 10, 2022, doi: 10.3390/su14106246.
[18] L. WU, M. PENG, S. QIAO, and X. YI MA, "Effects of rainfall intensity and slope gradient on runoff and sediment yield characteristics of bare loess soil," *Environ. Sci. Pollut. Res.*, vol. 25, no. 4, pp. 3480–3487, 2018, doi: 10.1007/s11356-017-0713-8.
[19] K. KOSUGI, "Lognormal distribution model for unsaturated soil hydraulic properties," *Water Resour. Res.*, vol. 32, no. 9, pp. 2697–2703, 1996.
[20] J. A. P. POLLACCO *et al.*, "HyPix: 1D physically based hydrological model with novel adaptive time-stepping management and smoothing dynamic criterion for controlling Newton–Raphson step," *Environ. Model. Softw.*, vol. 153, no. January, 2022, doi: 10.1016/j.envsoft.2022.105386.
[21] C. FANG, H. SHIMIZU, T. NISHIYAMA, and S. I. NISHIMURA, "Determination of residual strength of soils for slope stability analysis: State of the art review," *Rev. Agric. Sci.*, vol. 8, no. 1971, pp. 46–57, 2020, doi: 10.7831/ras.8.0_46.
[22] J. B. CLEMENT, F. GOLAY, M. ERSON, and D. SOUS, "Adaptive Discontinuous Galerkin Method for Richard Equation," in *Topical Problems of Fluid Mechanics 2020*, 2020, pp. 27–34. doi: https://doi.org/10.14311/TPFM.2020.004.
[23] A. GUTIÉRREZ-MARTÍN, M. ÁNGEL HERRADA, J. I. YENES, and R. CASTEDO, "Development and validation of the terrain stability model for assessing landslide instability during heavy rain infiltration," *Nat. Hazards Earth Syst. Sci.*, vol. 19, no. 4, pp. 721–736, 2019, doi: 10.5194/nhess-19-721-2019.
[24] N. A. PUTRI, AZWALANAS, AHAMID, HARDITIA, ALPIANA, and HIDAYATI, "An Analysis of Single Slope Stability at Pemenang Road Using Bishop Method," *IOP Conf. Ser. Earth Environ. Sci.*, vol. 1175, no. 1, 2023, doi: 10.1088/1755-1315/1175/1/012006.
[25] S. KUMAR, A. KUMAR, B. RAO, S. S. CHOUDHARY, and A. BURMAN, "Analysis of 2D and 3D Slope Stability Using the Bishop Simplified Method," *IOP Conf. Ser. Earth Environ. Sci.*, vol. 1326, no. 1, 2024, doi: 10.1088/1755-1315/1326/1/012117.
[26] N. S. DOAN, "Reliability analysis and uncertainty quantification of clay and sand slopes stability evaluated by Fellenius and Bishop's simplified methods," *Int. J. Geo-Engineering*, vol. 14, no. 1, 2023, doi: 10.1186/s40703-023-00200-2.
[27] M. A. MAODIN, FARYANSAH, S. D. ARIADI, G. S. VERLANDI, ALPIANA, and HIDAYATI, "Analysis of Andesite Rock Slope Stability with Bishop Method," *IOP Conf. Ser. Earth Environ. Sci.*, vol. 1175, no. 1, 2023, doi: 10.1088/1755-1315/1175/1/012007.
[28] R. R. WEIL and NYLE C. BRADLY, *The Nature and Properties of Soil*, vol. 11, no. 1. 2017. [Online]. Available: http://scioteca.caf.com/bitstream/handle/123456789/1091/RED2017-Eng-8ene.pdf?sequence=12&isAllowed=y%0Ahttp://dx.doi.org/10.1016/j.regsciurbeco.2008.06.005%0Ahttps://www.researchgate.net/publication/305320484_SISTEM_PEMBETUNGAN_TERPUSAT_STRATEGI_MELESTARI
[29] DANIEL HILLEL, *Environmental Soil Physics*. Academic Press, Inc., 1998.
[30] ASDM D2937, *Standard Test Method for Density of Soil in Place by the Drive-Cylinder Method*, vol. 4, no. June. 2000, pp. 1–2.
[31] ASTM D698, *Standard Test Methods for Laboratory Compaction Characteristics of Soil Using Standard Effort (12,400 ft-lbf/ft3 (600 kN-m/m3))1*, no. Reapproved 1989. 2021, pp. 1–2. doi: 10.1520/C1709-18.
[32] ASTM D1557, *Standard Test Methods for Laboratory Compaction Characteristics of Soil Using Modified Effort (56,000 ft-lbf/ft3 (2,700 kN-m/m3))1*, vol. 08, no. Reapproved 2021. 2021, pp. 1–2. doi: 10.1520/C1709-18.

EFFECTS OF INCREASING SOIL WATER CONTENT ON LIQUIDITY INDEX AND SLOPE FAILURE POTENTIAL THROUGH LABORATORY MODELLING

Nofrizal[1,2], * Fauzan[3], Abdul Hakam.[3] ,Bambang Istijono.[3], Andriani [3],and Aprisal[4]

[1] Civil Engineering Doctoral Student, Andalas University
[2] Padang Institute of Technology
[3] Department of Civil Engineering, Faculty of Engineering, Andalas University
[4] Department of Soil Science, Faculty of Agriculture, Andalas University

Corresponding Author :* fauzan@eng.unand.ac.id, **Received: :00 Oct. 2018, Revised: 00 Nov. 2018, Accepted: 00 Dec. 2018**

ABSTRACT: This study investigates the influence of increasing soil moisture content on the Liquid Limit (LL), Liquidity Index (LI), and their subsequent effects on slope stability through controlled laboratory-scale physical modelling. Soil samples obtained from a landslide-prone area were initially characterized by index and consistency tests to determine their physical properties. The construction of slope models replicated the actual field condition at angles of 30°, 45°, and 60°, and was stimulated with a rainfall-induced failure scheme by progressive saturation. The main challenge found in the study was that changes in the Atterberg limits and Liquidity Index with rising moisture content in conventional slope stability assessment were frequently overlooked. Experimental results reveal that an increase in water content markedly elevates the Liquidity Index, with slope failures predominantly occurring when LI >1. Slopes with steeper angles, particularly those greater than 45°, indicates a significant reduction in shear strength and cohesion under the saturation stimulation, resulting in a high risk of instability. Furthermore, the results indicate that when water content exceeds the Liquid Limit, the soil structure rapidly degrades and transitions into a fluid-like state, causing it more vulnerable to flow-type failures. Also, the study provides empirical evidence encouraging the use of the Liquidity Index as a practical metric for assessing slope failure risk in fine-grained soils. By integrating Atterberg limit parameters with physical slope modeling, the study has managed to establish a simple, reliable, and cost-effective framework for evaluating rainfall-triggered landslide. In addition, the findings emphasize the critical importance of monitoring LI and LL values in steep, moisture-sensitive terrains as early warning indicators of slope instability.
Keywords: Indek propertis soil,Water content, liquid limit,slop angle, slope failure

1.

1. INTRODUCTION

Slope stability is the main concern in geotechnical engineering, specifically in the planning and design of infrastructure; highways, embankments, retaining structures, open-pit mines, and earth dams [1], [2]. Slope failures can lead to severe consequences, including structural damage, causalities, environmental harm, and substantial economic losses [3]–[5]. Therefore, a reliable slope stability assessment is essential to mitigate these risks and ensure the durability and safety of the structures [6].

One of the primary factors contributing to slope instability is soil moisture variation, especially in regions with intense rainfall and poor drainage 7], [8]. Changes in water content strongly influence the mechanical behavior of soils by modifying effective stress, shear strength, deformation characteristics, and pore water pressure conditions [9]–[11]. In cohesive soils, particularly clays, an increase in moisture content can significantly degrade mechanical strength and stiffness, making slopes more susceptible to failure.

For fine-grained soils, the consistency and plasticity properties are typically assessed through the Atterberg limits, which include the Liquid Limit (LL), Plastic Limit (PL), and Shrinkage Limit (SL) [13], [14]. These parameters provide crucial information about how the soil behaves under different moisture levels. The Liquidity Index (LI), derived from the Atterberg limits, is a key indicator of soil consistency relative to its plastic range. When LI exceeds unity, the soil will be in the liquid-like state, indicated by extremely shear strength and an increased risk of slope failure **[15].**

Numerous studies have highlighted the role of water content and pore water pressure in triggering slope instability. Feng [16] reported significant reductions in residual shear strength for cohesive soils when subjected to oversaturation conditions. Troncone et al. [17] developed topographic models that correlat the occurrence of shallow landslides with elevated groundwater levels. Other studies emphasized the importance of matric suction and unsaturatedsoil mechanics in slope stability analyses [18]–[20]. Rahardjo et al. [21] experimentally demonstrated that increasing saturation reduces suction effects, thereby accelerating slope failure in clayey soils. Similarly, Sugimoto and Ishizuka [22] and Nofrizal et al. [23] showed that rainfall infiltration and groundwater fluctuations play a critical role in reducing slope safety factors and initiating landslides.

Despite advances in numerical modelling techniques and slope stability frameworks, the influence of moisture-induced changes in Atterberg limits and the Liquidity Index has been insufficiently explored in physical modeling studies. Conventional analyses typically assume invariant soil consistency parameters, thereby neglecting the progressive degradation of soil strength associated with increasing water content. To address this gap, the present study conducts controlled laboratory experiments to investigate the relationship between soil water content, Liquidity Index, and slope failure behavior.

The study focuses on soils from the Talamau Plateau in Pasaman Regency, West Sumatra, an area frequently affected by landslides due to its geological condition and substantial annual rainfall [24], [25]. Annual precipitation in the region ranges between approximately 4,730 and 5,332 mm, combined with slope inclinations commonly exceeding 15°–30°, generating highly unfavorable stability conditions. These conditions make the Talamau region an ideal case study for examining rainfall-induced slope failure mechanisms.

Physical slope models were constructed at a 1:100 scale using field soil samples and tested under controlled rainfall conditions. The experiments were aimed to identify critical moisture thresholds, particularly when the Liquidity Index exceeds 1, and to evaluate the resulting deformation and failure mechanisms across different slope geometries. By establishing an empirical relationship of consistency parameters with slope behavior, this study provides a practical and field-applicable approach for assessing landslide susceptibility in fine-grained soils.

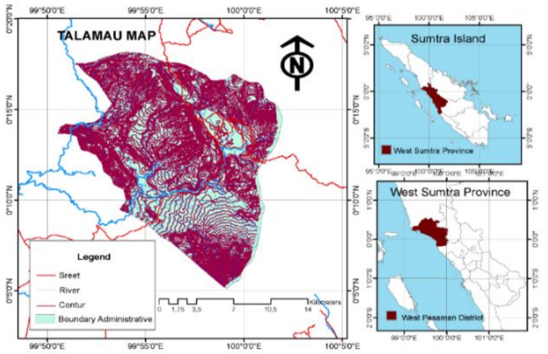

Fig.1 Geographical location of the Talamau Plateau landslide area of West Sumatra

2. RESEARCH SIGNIFICANT

The primary significance of this study resides in the experimental verification of the Liquidity Index (LI) greater than 1 as a reliable and practical indicator of slope failure in fine-grained soils. By establishing a direct correlation between Atterberg limit parameters from the laboratory testing and the actual physical manifestation of slope failure, this research bridges the gap between conventional index testing and real-world slope instability phenomena.

Unlike traditional slope stability assessments that assume constant soil consistency parameters, this study explicitly demonstrates how increasing soil water content alters the Liquidity Index and accelerates the transition from stable to unstable slope conditions.

3. MATERIAL AND METHOD

3.1 Study Area and Soil Sampling

This research was conducted on soils collected from landslide-susceptible zones in the Talamau Sub-district, Pasaman Regency, West Sumatra, Indonesia. The region is characterized by steep terrain, complex geological structures, and high annual rainfall, making it highly vulnerable to rainfall-induced slope failures. Field investigations identified critical unstable locations where silty clay soils dominate the near-surface layers**.**

Soil samples were collected using hand augers and core samplers at depths ranging between 0 and 1.5 m, representing the most weathered and failure-prone soil strata. The samples were transported to the Geotechnical Engineering Laboratory of Andalas University and the Soil Mechanics Laboratory of Padang Institute of Technology for comprehensive testing. Prior to laboratory analysis, the soils were air-dried, cleared of organic matter and coarse fragments, and sieved through a 2 mm mesh.

Index and physical property tests were conducted following ASTM standards, including natural water content (ASTM D2216), specific gravity (ASTM D854), unit weight, and Atterberg limits (ASTM

D4318). The Liquid Limit (LL) and Plastic Limit (PL) values were subsequently used to calculate the Liquidity Index (LI), which serves as an indicator of soil consistency and its response to increasing moisture content. The physical and mechanical properties of the tested soils are shown in Table 1.

Table 1. Values of soil characteristics of test samples

Experiment	Parameters	Value	Units
Water content	w	60.594	%
Volume weight	γ	1,558	gram/cm3
Specific gravity	Gs	2.627	
Sieve analysis	Gravel	0.000	%
	Sand	34.067	%
	Clay	65.933	%
Atterberg limit	SL	64.885	%
	PL	46.974	%
	PI	17.911	%
Direct shear	c	0.218	kg/cm2
	φ	22.835	°
Compaction	w opt	48.455	gram/cm3
	γ dry max	1.235	gram/cm3

Note: SL = Shrinkage Limit, PL = Non-elastic Limit, PI = Non-elastic Index, c = cohesion, φ = Inner shear angle, w opt = Optimum water content, γ dry max = dry soil specific gravity.

3.2 Physical Slope Modelling

Semi-three-dimensional physical slope models were constructed at a scale of 1:100, with a uniform height of 34 cm and a base width of 30 cm. The models utilized the field soil compacted to 90% of the maximum dry density under dry conditions. Slope geometries of 30°, 45°, 60°, and 90° were selected to represent both natural and anthropogenic slopes commonly found in the study area.

Rainfall was simulated with a calibrated rainfall simulator equipped with ten oscillating nozzles, specifically designed to replicate local rainfall intensities. Throughout the experimental procedures, water infiltration, surface deformation, and slope failure mechanisms were continuously monitored. Soil moisture content was measured at regular intervals, and additional soil samples were collected during the tests to reassess Atterberg limits and calculate the corresponding Liquidity Index values. The slope model configuration and rainfall simulation setup are illustrated in Fig. 2(a) and Fig. 2(b), respectively.

3.3 Experimental Framework

The experimental study was conducted to investigate the failure mechanisms of silty clay soils subjected to progressively increasing moisture conditions. The research methodology consisted of three primary stages.

Stage 1: Soil Characterization: This stage involved determining the physical and mechanical properties of the soil, including particle size distribution, specific gravity, bulk and dry unit weights, moisture content, and Atterberg limits (LL, PL, and PI). These parameters provided the fundamental basis for understanding soil consistency, plasticity, and moisture-induced behavior relevant to slope stability.

Stage 2: Slope Model Construction and RainfallSimulation: In this stage, compacted soil samples were employed to construct slope models at specified angles. Controlled artificial rainfall was applied to simulate infiltration and saturation processes. Changes in soil moisture content were monitored over time, and soil consistency parameters were re-evaluated to assess the progression toward liquefaction and slope instability.

Stage 3: Stability Assessment and Failure Analysis: The final stage focused on evaluating the relationship between increasing water content, Liquidity Index evolution, and slope failure behavior. Changes in shear strength, cohesion, and internal friction were inferred from soil consistency transitions. The combined effects of moisture content, soil density, and slope geometry were analyzed to identify critical thresholds leading to deformation and collapse.

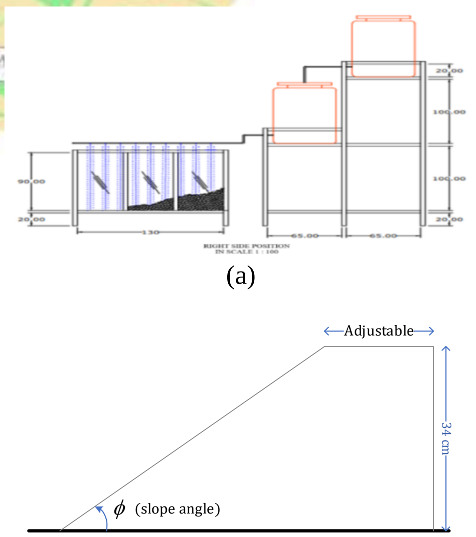

(a)

(b)

Fig. 2 Slope model. (a) Size of Landslide Model, (b) Slope Model Dimension

3.4 Water Content-Liquidity Index Relationship

In slope stability analysis, the interaction between water content, Liquid Limit, and soil mechanical properties is particularly critical for fine-grained soils. As water content increases and approaches or exceeds the Liquid Limit, soil cohesion and internal friction angle decrease significantly due to reduced particle bonding and loss of matric suction. This behavior is quantitatively captured by the Liquidity Index (LI), defined as:

$$LI = \frac{w-PL}{LL-PL} \qquad (1)$$

where w is the natural water content, PL is the plastic limit, and LL is the liquid limit. Values of LI less than zero indicate stiff or semi-solid soil, values between 0 and 1 correspond to plastic behavior, and values exceeding 1 represent a liquid-like state. Variations in LI during rainfall simulation directly reflect the degradation of soil shear strength and play a critical role in slope failure initiation.

The variations of LI significantly affect soil unit weight, cohesion, and internal friction, and are therefore critical for evaluating slope stability under rainfall infiltration conditions. The temporal evolution of the Liquidity Index (LI) during rainfall simulations is illustrated in Fig. 3, highlighting the progressive relationship between increasing moisture content and soil liquidity. The corresponding LI values for different soil conditions and slope configurations can be seen in Table 2, providing a quantitative basis for assessing slope failure susceptibility in landslide-prone areas.

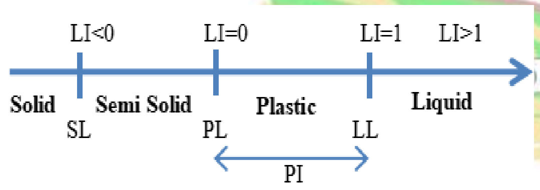

Fig. 3 Soil Liquidity Index Graph

Table 2. Quantitative basis for assessing slope failure susceptibility

Items	Description
LI< 1	Semi-solid soil, high strength
0< LI < 1	Plastic state soil, medium strength, soil is a kind of plastic material
LI > 1	Soil begins to lose consistency, approaching liquid state, soil is liquefiable.
LI > 1.5	Very soft/liquid soil means that the water content of the soil is higher than its liquidity limit, so the soil behaves like a liquid and loses its cohesion.

4. RESULTS AND DISCUSSION

4.1 Soil Properties and Grain Size Distribution

The results of the sieve analysis on the soil samples used in the slope modelling experiments are presented in Table 4. Particle size distribution plays a critical role in evaluating soil behavior, particularly concerning permeability, plasticity, and susceptibility to slope failure. The soil samples were in grain sizes ranging from 4.75 mm to 0.075 mm, with no particles retained on the No. 4 sieve, indicating the absence of gravel-sized material.

Soil retention began at the No. 10 sieve (2.0 mm), accounting for 1.43% of the total mass, and increased significantly at the No. 20 and No. 40 sieves, with cumulative retention values of 8.83% and 19.60%, respectively. The maximum retention occurred at the No. 100 sieve (0.15 mm), representing 32.30% of the sample. A substantial proportion of the soil (65.93%) passed the No. 200 sieve, confirming the dominance of fine-grained particles.

The corresponding grain size distribution curve (Fig. 5) displays a smooth and continuous profile, indicating a relatively uniform gradation without abrupt changes in particle size. The steep slope observed within the fine fraction range suggests a high content of clay and silt, which is typically associated with low permeability and high-water retention capacity. These characteristics strongly influence slope stability by facilitating pore water pressure buildup during rainfall infiltration. Based on the gradation data in Table 5, the soil is composed of 34.07% sand and 65.93% clay, with no gravel content. This classification confirms that the soil is fine-grained and plastic in nature, making it highly sensitive to moisture variations and prone to strength degradation under saturated conditions.

Table 3. Soil Grain Size Distribution Data

Sieve number	Retained weight	Total retained weight [g]	Percent retained (%)	Escaped (%)	Grain diameter [mm]
4	0.0	0.000	0.00	100.00	4.75
10	4.3	4.300	1.43	98.57	2
20	22.2	26.500	8.83	91.17	0.84
40	32.3	58.800	19.60	80.40	0.42
100	38.1	96.900	32.30	67.70	0.15
200	5.3	102.200	34.07	65.93	0.075
PAN	197.8	300	100.00	0.00	

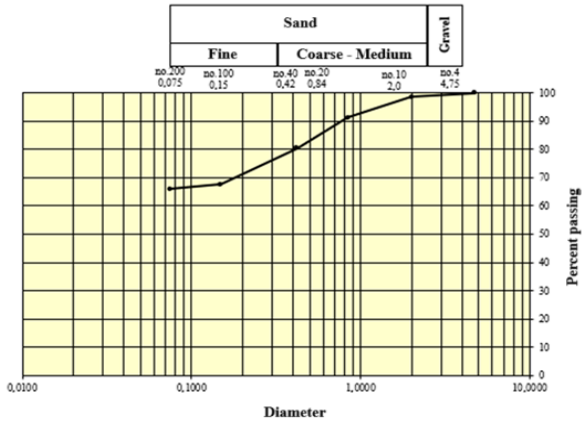

Fig.4 Soil grain distribution graph

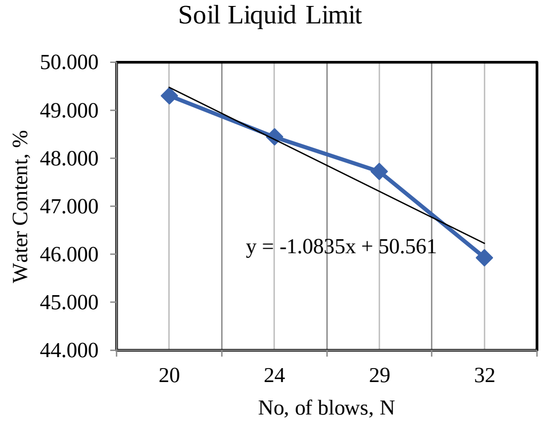

Fig.5 Liquid limit test results

Table 4. Summary of Soil Gradation Percentages

No	Soil type	Percentage (%)
1	Gravel	0
2	Sand	34.07
3	Clay	65.93

4.2 Effects of Increasing Water Content on Liquid Limit and Mechanical Properties

The influence of water content on soil consistency and mechanical behaviour was evaluated through laboratory testing and physical slope modelling. Slope deformation and failure processes were continuously recorded using video documentation. Meanwhile, soil moisture content was measured at different stages of rainfall simulation.

The results indicate that increasing water content significantly affects the Liquid Limit (LL) and Plastic Limit (PL) values, leading to changes in soil plasticity and shear strength. As moisture content approached the Liquid Limit, soil stiffness decreased noticeably. resulting in progressive deformation. Once the water content exceeded the LL, the soil transitioned into a viscous, fluid-like state indicated by a significant loss of cohesion and internal friction

The experimental data presented in Table 6 show that the average reduction of water content was approximately 47.85%. which closely corresponds to the measured Liquid Limit. This observation confirms that slope failure initiation is strongly correlated with moisture content near or exceeding the LL. Furthermore, the correlation between water content and the number of blows in the Casagrande test illustrated in Fig. 6, follows a logarithmic trend, further validating the consistency limits obtained.

Table 5. Liquid Limit and Plastic Limit Test Results

Type of Inspection		Liquid Limit				Plastic Limit	
No	Many of strokes	20	24	29	32	A	B
1	Weight of Cup + Wet Soil	8.55	7.54	8.05	10.23	6.94	7.07
2	Weight of Cup + Dry Soil	7.13	6.45	6.79	8.31	6.21	6.52
3	Weight of Water: (1-2)	1.42	1.09	1.26	1.92	0.73	0.55
4	Weight of Cup	4.25	4.2	4.15	4.13	4.24	5.14
5	Weight of Dry Soil: (2-4)	2.88	2.25	2.64	4.18	1.97	1.38
6	Water content: (3 : 5) x 100 (%)	49.306	48.444	47.727	45.933	37.056	39.855
7	Average collapse water content (%) :	47.853				38.455	

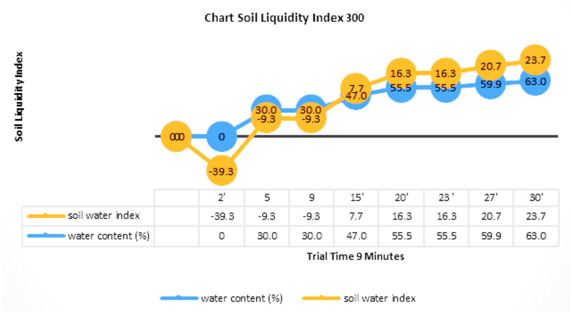

Fig.6 Soil liquidity index for slope 30º

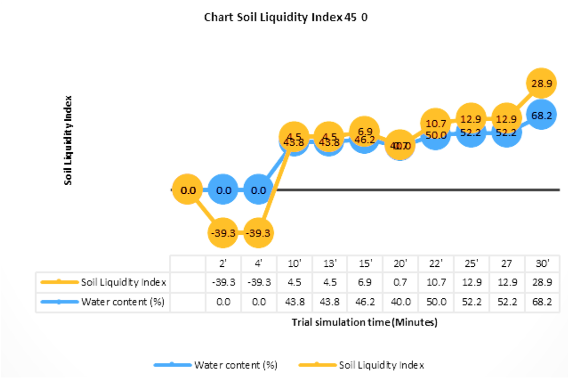

Fig.7 Soil liquidity index for slope 45º

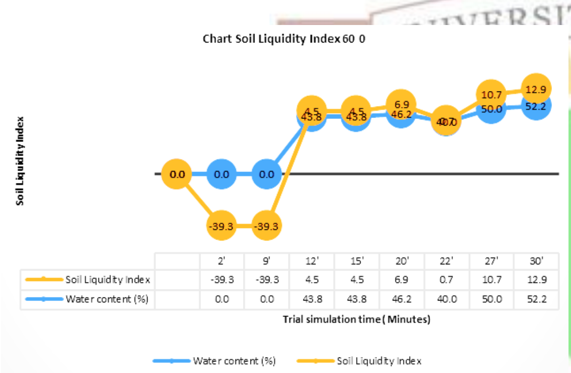

Fig.8 Soil liquidity index for slope 60º

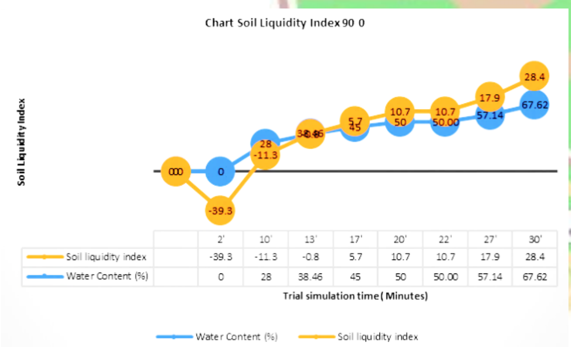

Fig.9 Soil liquidity index for slope 90º

4.3 Liquidity Index Evolution and Slope Failure Behavior

The results of the Liquidity Index (LI) tests obtained in this experiment are presented in Figs. 7–10. A detailed discussion of the observed test results is provided in the following section.

The Liquidity Index (LI) demonstrated considerable efficacy as parameter for indicating the progression of soil behavior from a stable to an unstable state. Across all slope configurations, LI values increased sharply as water content rose during rainfall simulation. Slope failure consistently occurred when LI exceeded unity indicating a transition to liquid-like state.

For the slope inclined at 30°, failure was initiated once the moisture content exceeded the soil's Liquid Limit, with LI values rapidly increasing beyond unity. Continued saturation resulted in a quasi-liquid state, ultimately leading to total slope collapse. Although gentler slopes required higher moisture content to fail, the results demonstrate that even moderate slopes can become unstable once the soil reaches a liquid consistency.

In the 45° slope model, deformation occurred at lower moisture contents compared to the 30° slope, highlighting the combined influence of slope geometry and soil consistency. Partial failure began before the Liquid Limit was reached while the total collapse occurred once LI exceeded 1, indicating a plastic-to-liquid transition.

The models with slopes of 60° and 90° demonstrated extreme sensitivity to moisture increase. In these cases, small increments in water content caused rapid increases in LI and immediate reductions in shear strength. Failure occurred abruptly once the Liquid Limit was exceeded, with LI values reaching as high as 12.9 for the 60° slope and 28.4 for the vertical slope. These results demonstrate that steep slopes are particularly vulnerable to rainfall-induced liquefaction and flow-type failures.

4.4 Effect of Slope Geometry on Failure

Slope geometry significantly influences both the timing and mode of failure. Gentler slopes tend to experience progressive deformation and delayed collapse whereas steeper slopes fail rapidly once critical moisture thresholds are exceeded. As slope angle increases gravitational forces intensify the effects of reduced shear strength making failure more sudden and severe.

The experimental results show that for steep slopes the Liquidity Index increases more rapidly with moisture content accelerating the loss of soil structure. This interaction between slope angle and soil liquidity underscores the importance of incorporating both geometric and hydraulic factors in slope stability assessments.

4.5 Mechanism of Rainfall-Induced Slope Failure

The dominant failure mechanism observed in this study is moisture-induced liquefaction resulting from excessive pore water pressure. As water infiltrates the soil matrix, matric suction decreases, particle bonding weakens, and effective stress is reduced. When the water content exceeds the Liquid Limit, soil particles lose contact, cohesion approaches zero, and the soil behaves as a viscous fluid.

Under these conditions. even minimal gravitational forces can initiate slope movement. particularly on steep slopes. Additionally, external disturbances such as prolonged rainfall or seismic vibrations can further accelerate failure leading to rapid flow-type landslides.

5. CONCLUSIONS

This study demonstrates that soil moisture content and slope geometry are the primary factors influencing slope failure mechanisms in fine-grained soils. Laboratory-scale physical modelling confirms that increasing water content significantly alters soil consistency leading to reductions in shear strength and cohesion as the Liquid Limit is approached and surpassed.

Experimental data consistently show that slope failure occurs when the Liquidity Index exceeds 1. marking the transition from plastic to liquid soil behaviour. Steep slopes (60° and 90°) exhibit particularly high vulnerability with abrupt failure occurring at relatively small increases in moisture content. The maximum recorded Liquidity Index reached 28.4 for the vertical slope indicating complete soil liquefaction and total loss of structural resistance.

The findings validate the Liquidity Index as a reliable and practical indicator for assessing rainfall-induced slope failure risk in cohesive soils. Incorporating LI into slope monitoring and early warning systems provides a simple, cost-effective. and field-applicable approach for identifying critical moisture thresholds. This research contributes to have a better understanding of slope instability mechanisms and offers valuable guidance for geotechnical risk assessment and landslide mitigation in moisture-prone terrains.

6. ACKNOWLEDGMENTS

The author expresses their deepest gratitude for the moral and financial support provided by Andalas University through the PDD Grant with the Contract No.: 28/UN16.19/PT.01.03/PDD/ 2024. on July 17. 2024.

7. REFERENCES

1. G. Wang. B. Zhao. B. Wu. C. Zhang. and W. Liu. “Intelligent prediction of slope stability based on visual exploratory data analysis of 77 in situ cases.” Int. J. Min. Sci. Technol.. vol. 33. no. 1. pp. 47–59. 2023. doi: 10.1016/j.ijmst.2022.07.002.
2. O. H. Jasim and M. Tonaroğlu. “Using Geogrid Encased Granular Columns for Embankment’s Slope Protection: 3D-Finite Difference Analysis.” *Appl. Sci.*. vol. 13. no. 4. 2023. doi: 10.3390/app13042448.
3. G. Vasudha and J. Deepa. “Landslide Vulnerability of Urban slums: Case of Warje Slum. Pune. Maharashtra.” Disaster Adv.. vol. 16. no. 3. pp. 44–51. 2023.
4. P. Sestras and S Bilasco. “Multi-Instrumental Approach to Slope Failure Monitoring in a Landslide Susceptible Newly Built-Up Area: Topo-Geodetic Survey. UAV 3D Modelling and Ground-Penetrating Radar.” Remote Sens.. vol. 14. no. 22. 2022. doi: 10.3390/rs14225822.
5. J. Ma, and J.Sheng. “Machine Learning Models for Slope Stability Classification of Circular Mode Failure: An Updated Database and Automated Machine Learning (AutoML) Approach.” *Sensors*. vol. 22. no. 23. 2022. doi: 10.3390/s22239166.
6. K. B. Jyothi and U. K. Singh. “Static and pseudo-static stability analysis of right earthen embankment of nagarjuna sagar dam by geostudio.” E3S Web Conf.. vol. 391. 2023. doi: 10.1051/e3sconf/202339101018.
7. Z. Zhang. L. Qin. G. Ye. W. Wang. and J. Zhang. “Physical Modeling and Intelligent Prediction for Instability of High Backfill Slope Moisturized under the Influence of Rainfall Disasters.” *Appl. Sci.*. vol. 13. no. 7. 2023. doi: 10.3390/app13074218.
8. X. Liu and M. Su. “Double Strength Reduction Method for Slope Stability Analysis Based on Water Content Variation: A Study and Engineering Application.” Water (Switzerland). vol. 15. no. 6. 2023. doi: 10.3390/w15061194.
9. D. Artykbaev. A. Jumabayev. A. Tleubayeva. and G. Tleulenova. “Method for Earthquake-Resistant Slope Steepness : An Integrated Experimental-Numerical Approach.” Int. J. GEOMATE. vol. 29. no. 131. pp. 67–75. 2025.
10 Q. Kang. Y. Xia. X. Li. W. Zhang. and C. Feng. “Study on the Effect of Moisture Content and Dry Density on Shear Strength of Silty Clay Based on Direct Shear Test.” *Adv. Civ. Eng.*. vol. 2022. 2022. doi: 10.1155/2022/2213363.
11. W. Ahmad and T. Uchimura. “The Effect of Moisture Content at Compaction and Grain Size Distribution on the Shear Strength of Unsaturated Soils.” *Sustain.*. vol. 15. no. 6. 2023. doi: 10.3390/su15065123.
12. R. A. Murison. S. W. Jacobsz. T. A. V. Gaspar. T. S. Da Silva Burke. and A. S. Osman. “Drying and wetting soil-water retention behaviour of a highly expansive clay under varying initial density.” E3S Web Conf.. vol. 382. 2023. doi: 10.1051/e3sconf/202338209005.
13. Y. Xu. X. Zhang. G. Wang. X. Liu. and A.

Yang. “Role of Diatom Microstructure in Determining the Atterberg Limits of Fine-`Grained Diatomaceous Soil.” *Appl. Sci.*. vol. 13. no. 4. 2023. doi: 10.3390/app13042287.
14. B. C. O’Kelly. J. Alonso-Azcárate. and J. M. Moreno-Maroto. “A Comprehensive Review of Soil Remolding Toughness Determination and Its Use in the Classification of Fine-Grained Soils.” Appl. Sci.. vol. 13. no. 9. 2023. doi: 10.3390/app13095711.
15. J. J. Jiang and Z. D. Cui. “Instability of High Liquid Limit Soil Slope for the Expressway Induced by Rainfall.” Appl. Sci.. vol. 12. no. 21. 2022. doi: 10.3390/app122110857.
16. X. Feng. “Effect of Shear Rate on the Residual Strength of Clayey Soils.” Journal of Electrical Systems. vol. 20. no. 3. pp. 1835–1841. 2024. doi: 10.52783/jes.3749.
17. A. Troncone. L. Pugliese. and E. Conte. “Rainfall Threshold for Shallow Landslide Triggering Due to Rising Water Table.” *Water (Switzerland)*. vol. 14. no. 19. 2022. doi: 10.3390/w14192966.
18. M. R. Hakro. Z. Almani. M. A. Channa. and J. Jokhio. “Numerical Modelling of Matric Suction in Unsaturated Soil under Shallow Foundation Under Varying Soil and Hydrological Conditions.” *J. Kejuruter.*. vol. 36. no. 2. pp. 569–580. 2024. doi: 10.17576/jkukm-2024-36(2)-17.
19. J. Ling. X. Li. S. Lin. Y. Cen. and C. Li. “Laboratory Study on Entire Range Suction Measurement and Microstructure Change of Granite Residual Soil.” *Transp. Res. Rec.*. vol. 2677. no. 10. pp. 191–203. 2023. doi: 10.1177/03611981231160546.
20. G. A. Adiguna. M. Wijaya. P. P. Rahardjo. A. Sugianto. A. Satyanaga. and A. H. Hamdany. “Practical Approach for Assessing Wetting-Induced Slope Failure.” *Appl. Sci.*. vol. 13. no. 3. 2023. doi: 10.3390/app13031811.
21. H. Rahardjo. T. H. Ong. R. B. Rezaur. and E. C. Leong. “Factors Controlling Instability of Homogeneous Soil Slopes under Rainfall.” *J. Geotech. Geoenvironmental Eng.*. vol. 133. no. 12. pp. 1532–1543. 2007. doi: 10.1061/(asce)1090-0241(2007)133:12(1532).
22. S. Sugimoto and Y. Ishizuka. “Slope Deformation Monitoring Using Wireless Sensor Network and Evaluation of Mechanical Stability By Fdm Simulation.” *Int. J. GEOMATE*. vol. 22. no. 94. pp. 13–20. 2022. doi: 10.21660/2022.94.97.
23. Nofrizal. Fauzan. A. Hakam. B. Istijono. and Aprisal. “Analysis of the Effect of Rainfall Intensity and Slope Steepness on Landslide Disaster.” *Civ. Environ. Eng.*. vol. 0. no. 0. 2025. doi: 10.2478/cee-2025-0073.
24. B. G. Dewanto, R.Priadi. “The 2022 Mw 6.1 Pasaman Barat. Indonesia Earthquake. Confirmed the Existence of the Talamau Segment Fault Based on Teleseismic and Satellite Gravity Data.” Quaternary. vol. 5. no. 4. 2022. doi: 10.3390/quat5040045.
25. P. V. Hoa. N. Q. Tuan. P. V. Hong. G. T. P. Thao. and N. A. Binh. “GIS-based modeling of landslide susceptibility zonation by integrating the frequency ratio and objective–subjective weighting approach: a case study in a tropical monsoon climate region.” *Front. Environ. Sci.*. vol. 11. no. May. pp. 1–20. 2023. doi: 10.3389/fenvs.2023.1175567.
26 Das. B. M. Principles of Geotechnical Engineering. 7th ed.. Cengage Learning. Stamford. CT. USA. 2010,write it as ”pp 1 – 665

On the last page, both columns must be the same height from top or bottom. Please do not change the journal and authors’ information.

Please do not change the format of this template.

List of references: Follow the template strictly. Missing pp.??-?? is not acceptable.

Book references need the page number, publisher name, place of publication, Year, pp, etc. If a book contains a total of 500 pages, then it must be written as pp.1-500.

Last name, First name. “Article Title”. Newspaper Title, Month Date, Year of publication.

According to the Chicago Manual of

JPPIPA 9(1) (2023)

Journal of Science Education Research

Journal of Research in Science Education

http://jppipa.unram.ac.id/index.php/jppipa/index

Laboratory Study of Geotechnical Characteristics of Soil in Landslide-Prone Zone in Talamau District, West Pasaman Regency

Nofrizal[1,2], Fauzan[3]*, Abdul Hakam[3]. Bambang Istijono[3], Andriani Setiawan [3], Aprisal[4]

1 Civil Engineering Doctoral Student, Andalas University
2 Padang Institute of Technology
3 Department of Civil Engineering, Faculty of Engineering, Andalas University
4 Department of Soil Science, Faculty of Agriculture, Andalas University

Received:
Revised:
Accepted:
Published:

Corresponding Author:
Fauzan
fauzan@eng.unand.ac.id

DOI:

Phone*: +62 896-0296-9366

Abstract: The main triggering factor for landslides is high rainfall intensity, especially during the rainy season. Excessive rainfall can cause an increase in water content in the soil, which in turn will reduce the shear strength of the soil and increase the volume weight of the soil.The method used is a laboratory experiment by taking samples from the field. The sample of this study was sandy clay soil taken from a landslide-prone area located in Talamau District, West Pasaman Regency. Based on the results of soil geotechnical laboratory tests in the landslide-prone zone in Talamau District, West Pasaman Regency, it can be concluded that the soil sample has moderate plasticity characteristics with a Liquid Limit of 59.39%, Plastic Limit of 49.77%, and Plasticity Index of 9.62%. The soil reaches a maximum dry density of 1.37 gr/cm³ at an optimum water content of 500 ml, with a grain size distribution dominated by the sand fraction (83.978% retained on sieve No. 4-20) and a very low fine material content (1.234%). The results of the triaxial test showed soil behavior that varied from brittle to strain-hardening depending on the level of cell stress. Overall, the soil can be classified as well-graded sand with good drainage but low cohesion, thus requiring additional stabilization for construction applications in landslide-prone areas.

Keywords: Laboratory Study, Landslide Prone, West Pasaman

Introduction

Indonesia is an archipelagic country with diverse topographic conditions, ranging from lowlands to mountains with steep slopes (Centeno, 2024). These geographical conditions, combined with a tropical climate with high rainfall, make Indonesia one of the countries prone to landslides (Heo et al., 2024; Rakuasa et al., 2025). The landslide phenomenon not only threatens the safety of people's lives and property, but also causes significant economic losses and infrastructure damage that can hamper regional development (Kumar, 2024).

West Sumatra, as one of the provinces with hilly and mountainous topography, faces serious challenges related to the threat of landslides (Kausarian et al., 2024). West Pasaman Regency, located in the northern part of West Sumatra, has geographical characteristics dominated by hills with varying slope gradients (Usman & Sumantyo, 2022). This condition is exacerbated by high tectonic activity due to its position in the Indo-Australian and Eurasian subduction zones, increasing the potential for slope instability in the region (Hutchings & Mooney, 2021).

Talamau District is one of the districts in West Pasaman Regency that has a relatively high level of landslide vulnerability (Bari et al., 2023). This area is characterized by undulating to hilly topography with fairly steep slopes, especially in areas bordering rivers (Bian et al., 2025). Local geological conditions dominated by sedimentary and volcanic rocks that have undergone intensive weathering form residual soil with complex and varied geotechnical characteristics (Islam et al., 2024).

The main triggering factor for landslides in Talamau District is high rainfall intensity, especially during the rainy season (Guzzetti et al., 2022). Excessive rainfall can cause an increase in water content in the soil, which in turn will reduce the shear strength of the soil and increase the volume weight of the soil (Das et al., 2022). These conditions, combined with unstable slope geometry, create conditions conducive to landslides (McColl, 2022). In addition, human activities such as land clearing for agriculture, infrastructure development, and mining that do not pay attention to slope stability aspects also contribute to increasing the risk of landslides (Alcantara-Ayala, 2025).

A deep understanding of the geotechnical characteristics of soil is the main key in efforts to mitigate landslide disaster risks (Bilal et al., 2025). Geotechnical characteristics of soil include various parameters such as physical properties, mechanical properties, and soil behavior to changes in environmental conditions (Momeni et al., 2022). These parameters include grain size distribution, Atterberg limits, specific gravity, water content, shear strength, compressibility, and soil permeability. Each parameter has an important role in determining slope stability and the potential for landslides (Woldesenbet et al., 2023).

Laboratory studies are the most accurate and reliable method for determining the geotechnical characteristics of soil (Jastrzębska, 2021). Through a series of standard and calibrated laboratory tests, precise and reliable geotechnical parameter data can be obtained for slope stability analysis (Innocenti et al., 2023). Laboratory tests relevant to this study include soil physical properties tests such as sieve analysis, liquid limit and plastic limit tests, specific gravity tests, and soil mechanical properties tests such as direct shear strength tests, triaxial tests, and permeability tests (Afolagboye et al., 2021).

Previous studies conducted in various landslide-prone areas in Indonesia have shown that the geotechnical characteristics of soil have high variability, even in a relatively small location (Nguyen et al., 2023). This variability is influenced by factors such as the type of parent rock, weathering level, drainage conditions, and loading history. Therefore, studies of the geotechnical characteristics of soil need to be carried out specifically for each location, taking into account local geological and environmental conditions (Daud et al., 2025).

The results of laboratory studies of soil geotechnical characteristics can be used as a basis for various practical applications in landslide risk mitigation (Pasierb et al., 2019). The geotechnical parameter data obtained can be used for slope stability analysis, design of retaining structures, drainage systems, and safe spatial planning. In addition, understanding the geotechnical characteristics of soil is also important for the development of an effective and accurate landslide early warning system (Lin et al., 2025).

Given the high risk of landslides in Talamau District and the absence of a comprehensive study on the geotechnical characteristics of the soil in the area, this study is very important to conduct. This study is expected to provide a significant contribution to efforts to mitigate the risk of landslides through a better understanding of the geotechnical characteristics of the soil in landslide-prone zones. The results of this study can also be a reference for local governments in planning sustainable and safe development from the risk of landslides (Muhiddin et al., 2021).

This study will focus on the geotechnical characterization of soil through a series of comprehensive laboratory tests, with the aim of obtaining an accurate and reliable geotechnical parameter database. The data obtained will be statistically analyzed to understand the variability and distribution of geotechnical parameters, as well as the relationship between parameters that can affect slope stability. The results of this study are expected to provide practical recommendations for landslide risk mitigation and become a basis for further research in the field of geotechnics and disaster mitigation.

Method

In this study, the method used is the laboratory experiment method by taking samples from the field. The sample of this study was sandy clay soil taken from a landslide-prone area located in Talamau District, West Pasaman Regency, and the soil property value was tested in the laboratory. For laboratory testing, it was carried out in the Geotechnical Laboratory of Civil Engineering, Unand and the Padang Institute of Technology. The specific gravity of the samples in this study can be seen in table 1 below.

Table 1. Specific Gravity of Sample

Pycnometer Number			1	2
Weight of empty pycnometer	W1	=	30.87	30.9
Weight of pycnometer + dry soil	W2	=	40.87	40.9
Weight of bare soil	Wt	=	10	10
Weight of pycnometer+water+soil at temperature 20o	W3	=	132.59	132.17
Temperature toC		=	28	
Weight of pycnometer + water at temperature 20o	W4	=	126.45	125.75
W5 = Wt + W4		=	136.45	135.75
Fill the land	W5-W3	=	3.86	3.58
Specific gravity Gs = Wt/ (W5-W3)		=	2.59	2.79
Average specific gravity		=	2.69	

Results and Discussion

Atterberg Test

The Atterberg test is a laboratory test to determine the consistency limits of fine-grained soil, especially clay and silt, which consists of liquid limit, plastic limit, and shrinkage limit tests. This test is important for classifying soil and understanding its mechanical properties under various water content conditions (O'Kelly, 2021).

The liquid limit test steps begin with preparing a soil sample that passes sieve No. 40, then mixing it with distilled water until it has a paste-like consistency. The sample is placed in a Casagrande bowl and leveled, then a groove is made in the middle using a groove maker. The bowl is tapped at a speed of 2 taps per second until the groove is closed by 13 mm, and the number of taps and water content are recorded. This process is repeated with variations in water content to obtain a flow curve and determine the liquid limit up to 35 taps.

For the plastic limit test, a soil sample with a water content close to the plastic limit is formed into a small ball, then rolled on a glass plate to form a rod with a diameter of 3 mm. The rolling process is repeated until the rod begins to crack or break, which indicates the plastic limit has been reached. The water content at this condition is recorded as the plastic limit. The plasticity index is then calculated by subtracting the plastic limit from the liquid limit, which provides information about the water content range over which the soil is plastic and can be used for soil classification and geotechnical planning. The Atterberg test results can be seen in table 2 below.

Table 2. Atterberg Test

Types of Examination			Liquid Limit				Plastic Limit	
Many Punches			35	28	23	11		
Cup Number			AR1	AR2	AR3	AR4	A	L
Weight of cup + wet soil		grams =	11	12.65	13.03	16.06	8.44	8.3
Weight of cup + dry soil		grams =	9.51	10.3	10.6	11.58	6.74	6.7
Water weight	(1-2)	grams =	1.49	2.35	2.43	4.48	1.69	1.6
Cup weight		grams =	6.42	6.06	6.91	6.01	3.41	3.42
Dry soil weight	(2-4)	grams =	3.09	4.24	3.69	5.57	3.33	3.28
Water content	(3:5)x100%		48.22	55.85	65.85	80.43	50.75	48.78
Average (%)		=					49.77	

Information :
Liquid Limit (LL) = Liquid limit graph equation

$$LL = y = -27.29 \ln(x) + 147.23$$
$$LL = 59.39\ \%$$
$$PL = 49.77\ \%$$
$$PI = LL - PL = 9.62\ \%$$
$$SL = 28.78\ \%$$

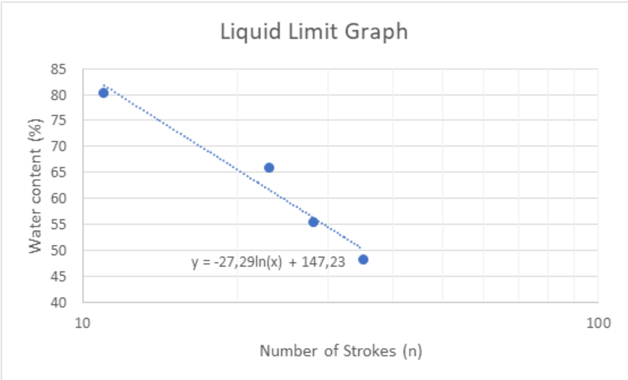

Figure 1. Liquid Limit Graph

Based on the Atterberg Test data presented, the results of the study indicate the characteristics of soil plasticity that can be categorized as soil with moderate plasticity. The Liquid Limit (LL) value of 59.39% indicates that the soil requires a fairly high water content to reach a liquid state, while the Plastic Limit (PL) of 49.77% indicates the lower limit where the soil can still be formed without cracking. The relatively small difference between these two values results in a Plasticity Index (PI) of 9.62%, indicating a limited range of soil plasticity. The concept of Atterberg limits first introduced by Albert Atterberg in 1911 has become a standard in the characterization of fine-grained soils, and the results of this study are consistent with the basic principles that have been established in the geotechnical literature (Ouyang & Mayne, 2023).

Further analysis of the water content data at various blow rates showed a correlation consistent with the principle of the liquid limit test. At 35 blows, the water content was recorded at 48.22%, then increased gradually to 80.43% at 11 blows. This pattern is in accordance with the theory put forward by Casagrande that the fewer blows required to close the groove, the higher the water content of the soil. The graph equation $y = -27.29 \ln(x) + 147.23$ shows a good logarithmic relationship between the number of blows and the water content, confirming the validity of the test results. Previous studies by various geotechnical experts have shown that this logarithmic relationship is a common characteristic in liquid limit testing, reflecting the rheological properties of clay soils (Carriere et al., 2018).

Based on the USCS (Unified Soil Classification System) classification, soil with a PI between 4-7% is categorized as low plasticity soil, while a PI of 7-17% indicates moderate plasticity. With a PI of 9.62%, this soil sample is included in the moderate plasticity category, indicating that the soil has a moderate ability to deform without losing cohesion. The Shrinkage Limit (SL) value of 28.78% indicates that the soil will experience significant volume shrinkage when the water content decreases below that value. A study conducted by Onyelowe et al. (2022) showed that soils with similar characteristics generally have predictable behavior in engineering applications, although they require special attention to changes in moisture conditions.

Soil with moderate plasticity characteristics requires special attention in construction design. Research conducted by Ahmad et al. (2024) showed that soil with PI in the range of 7-17% is generally suitable for light to medium construction, but requires a good drainage system to prevent volumetric stability problems. The Atterberg limits values obtained also indicate that this soil has a moderate clay mineral content, which is in accordance with the findings of Niu et al. (2024) on the relationship between soil mineralogy and plasticity properties. Soil with similar characteristics can be used as construction materials with appropriate treatment, such as chemical or mechanical stabilization to improve long-term performance.

Compaction

Soil compaction is the process of adding energy to the soil to reduce the volume of air pores, thereby increasing the density and strength of the soil. Water content testing is a fundamental step in compaction because the optimum water content greatly affects the effectiveness of compaction. Water content testing is carried out using the oven method, where wet soil samples are weighed, then dried in an oven at a temperature of 105-110 ° C for 24 hours or until constant weight, then reweighed to calculate the percentage of water content to the dry weight of the soil (Frene et al., 2024).

Compaction checks are carried out to determine the relationship between water content and dry density of soil at certain compaction energies. The testing procedure includes preparing soil samples with varying water content, then each sample is compacted in a cylindrical mold with three or five layers using a pestle with a predetermined weight and drop height. The test results are in the form of a relationship curve between water content and dry density which shows the optimum water content and maximum dry density. Optimum water content is the water content at which the soil reaches maximum dry density with a certain compaction energy, while maximum dry density is the highest density value that can be achieved at that optimum water content (Shimobe et al., 2021). The compaction results can be seen in tables 3 and 4 below.

Table 3. Water Content Check

Sample Number		1		2		3		4		5		6	
Cup Number		A	B	RA1	RA2	RA3	RA4	AR1	AR2	AR3	AR4	D1	D2
Amount of water	ml	200		300		400		500		600		700	
Weight of cup + wet soil	gr	33.72	32.55	29.68	33.12	30.69	22.42	25.35	29.18	34.14	34.24	21.53	21.67
Cup weight +dry land	gr	30.29	29.2	25.85	28.79	25.95	19.09	21.02	23.51	26.99	26.63	17.05	16.94
Water weight	gr	3.43	3.35	3.83	4.33	4.74	3.33	4.33	5.67	7.15	7.61	4.48	4.73
Cup weight	gr	5.33	5.42	6.22	6.98	6.66	6.09	6.44	6.07	6.93	6.81	5.91	5.39
Dry soil weight	gr	24.96	23.78	19.63	21.81	19.29	13	14.58	17.44	20.06	19.82	11.55	11.55
Water content	%	13.74	14.09	19.51	19.85	24.57	25.62	29.70	3.51	35.64	38.40	40.22	40.95
Average water content	%	13.91		19.68		25.09		31.10		37.02		40.58	

Table 4. Density Check

Mold weight	gr	3380	3380	3380	3380	3380	3380
Weight of mold + wet soil	gr	4740	4805	4905	5010	5075	5040
Wet soil weight	gr	1360	1425	1525	1630	1695	1660
Wet volume weight (ᵞb)	gr/cm3	1.49	1.56	1.67	1.79	1.86	1.82
Dry volume weight (ᵞd)	gr/cm3	1.31	1.31	1.34	1.37	1.36	1.30

Optimum Water Content = Highest value of dry density (ᵞd)

= 1.37 gr/cm3

= 500 ml (seen from the water content used at the highest value ᵞd)

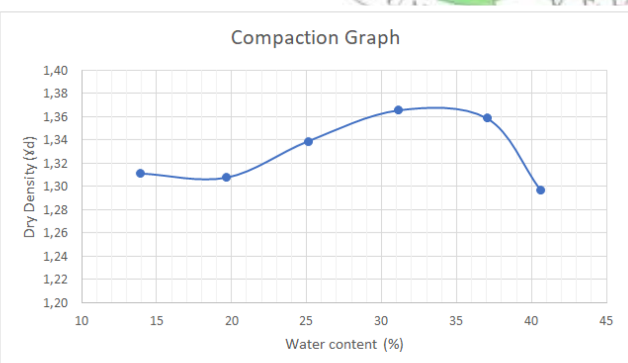

Figure 2. Compaction Graph

The results of the water content test showed significant variations along with the addition of water volume from 200 ml to 700 ml. The average water content increased gradually from 13.91% at 200 ml of water addition to 40.58% at 700 ml of water addition. This increasing pattern shows a consistent relationship between the volume of water added and the resulting water content in the soil sample. The variation in water content between samples at each level of water addition was relatively small, indicating consistency in the testing procedure and the homogeneity of the soil samples used.

The density data shows that the wet unit weight (γb) increases with the addition of water, starting from 1.49 gr/cm³ to a peak of 1.86 gr/cm³ at 600 ml of water addition, then decreasing to 1.82 gr/cm³ at 700 ml. This pattern indicates that the addition of water initially helps compaction by lubricating the soil particles, but after reaching the optimum point, the excess water actually reduces the density because it fills the space that should be occupied by solid soil particles. This phenomenon is a normal characteristic in laboratory soil compaction testing.

The test results showed that the maximum dry density (γd) was achieved at a value of 1.37 gr/cm³ with an optimum water content of around 500 ml. Although there were small fluctuations in the dry density values at various levels of water content (ranging from 1.30-1.37 gr/cm³), the highest value of 1.37 gr/cm³ was obtained at optimum water content conditions. This condition indicates the ideal balance point between sufficient water content to facilitate compaction and not excessive so as to reduce the effective density of the soil (Brempong et al., 2023).

These findings have important implications in practical applications of construction and geotechnical engineering. The maximum dry density of 1.37 gr/cm³ with an optimum water content of 500 ml provides a guideline for achieving optimal soil compaction in the field. The compaction curve formed shows a classic relationship between water content and density, where increasing water content from dry conditions will increase density to a peak, then decrease if the water content is excessive. These data can be used as a reference to determine the appropriate compaction procedure in construction projects to ensure optimal soil stability and bearing capacity (Vitali et al., 2022).

Sieve Analysis

Sieve analysis or sieve analysis is a laboratory test method to determine the particle size distribution of soil based on the percentage of grains by weight that pass through a series of sieves with different hole sizes (Svensson et al., 2022). This test is an important part of soil classification and is used for coarse-grained soils such as gravel and sand. Sieve analysis provides information about soil gradation which is very useful in determining engineering soil properties such as permeability, shear strength, and compressibility (Sohel et al., 2024).

The sieve analysis procedure begins with preparing a representative dry soil sample, then weighing the total weight of the sample. The sample is placed on a sieve stack arranged sequentially from the largest hole at the top to the smallest at the bottom, with a collection pan at the bottom. The sieve stack is then shaken mechanically or manually for a certain time (usually 10-15 minutes) until no more particles pass through. After sieving is complete, the material retained on each sieve is weighed and recorded. The results of the sieve analysis are presented in the form of a grain size distribution curve that describes the relationship between grain size and the percentage of weight that passes through. The results of the sieve analysis can be seen in table 5 below.

Table 5. Sieve Analysis

Filter number	Filter hole diameter	Weight of soil sieved	% by weight of filtered soil	% cumulative ground sieve	% of soil passing through the sieve
1	2	3	4 [(3)/W] x 100	5	6 100 – (5)
4	4.75	0	0	0	100
10	2	265.85	53.17	53.17	46.83
20	0.85	154.04	30,808	83,978	16,022
40	0.425	41.35	8.27	92.248	7,752
60	0.25	15.4	3.08	95,328	4,672
140	0.106	10.2	2.04	97,368	2,632
200	0.075	6.99	1,398	98,766	1.234
PAN	-	4.52			
Total weight W1		498.35			

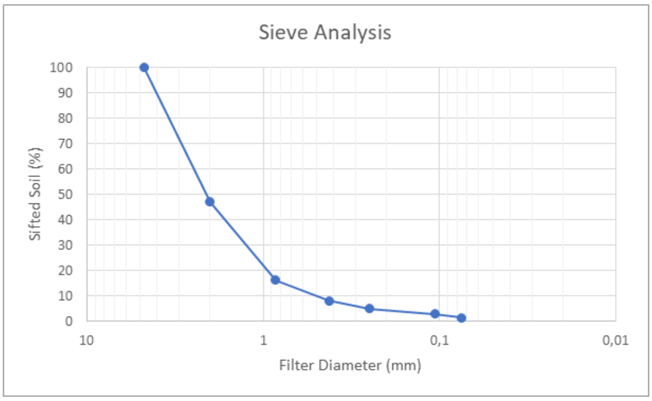

Figure 3. Sieve Analysis

The results of the sieve analysis showed that the soil samples had a fairly diverse grain size distribution with a dominance of medium sizes. Of the total sample weight of 498.35 grams, the highest percentage was retained on sieve No. 10 (2 mm diameter) at 53.17%, followed by sieve No. 20 (0.85 mm diameter) at 30.808%. This distribution indicates that most of the soil particles are between 0.85-2 mm in size, which is included in the coarse to medium sand category. The distribution pattern that decreases gradually from large to small grain sizes indicates relatively good gradation, although there is dominance in certain fractions. Sieve analysis determines the particle size distribution of a given soil sample and thus helps in easy identification of the mechanical properties of the soil, which supports the finding that grain distribution characteristics play an important role in determining the engineering properties of the material (Polakowski et al., 2021).

Based on the cumulative percentage passing the sieve, it can be identified that 46.83% of the material passed the No. 10 sieve, 16.022% passed the No. 20 sieve, and only 1.234% passed the No. 200 sieve. This data shows that the fine material (which passed the No. 200 sieve) is very little, which is less than 2%, which classifies this soil as a coarse-grained soil with a very low fines content. Soil gradation is an important aspect of soil mechanics and geotechnical engineering because it is an indicator of other engineering properties such as compressibility, shear strength, and hydraulic conductivity. This characteristic indicates that the soil has relatively high permeability and good drainage, but may have low cohesion due to the minimal content of fine particles such as clay and silt(Shimobe & Spagnoli, 2022).

Based on the obtained grain size distribution, the soil can be classified as well-graded sand according to the soil classification system. Well-graded sand (SW) consists of fine, medium, and coarse grains of sand, which is in accordance with the findings of this study where the material is distributed in a variety of size ranges (Chen et al., 2022). With a dominance of particles measuring 0.85-4.75 mm (83.978% retained on the sieve range Number 4 to Number 20) and a very low fines content (1.234%), this soil has technical characteristics suitable for construction applications that require good drainage such as pavement base layers or filter materials. Good soils are well-graded dense gravel, gravelly sand, silty gravel, excess compacted clay, and rocks, which support the potential application of this material in construction (Wazoh & Mallo, 2021).

Previous studies have shown that soil gradation has a significant effect on the mechanical properties of the material. Test results show that higher shear strength is obtained for gap-graded (GG) soil compared to well-graded (WG) and uniformly graded (UG), although in the context of general construction applications, well-graded sand remains the preferred choice due to its stability. For applications requiring high stability or high bearing capacity, additional stabilization or blending with a binder may be required due to the lack of fine particles that act as natural binders between grains. Fines become significant to the engineering properties and characteristics of the soil when they are contained at least 5% by weight, while the sample in this study only contained 1.234% fines, thus requiring special attention in applications requiring high cohesion (Pande et al., 2020).

Triaxial Testing

Triaxial testing is one of the most important geotechnical testing methods to determine soil shear strength parameters, namely cohesion (c) and internal friction angle (φ) (Ghoreishi et al., 2021). This test is carried out using a triaxial device consisting of a triaxial cell filled with water or pressurized air, where a cylindrical soil sample is placed in a rubber membrane and given cell pressure (confining pressure) from all directions. The main advantage of the triaxial test is its ability to control drainage conditions and measure stress and strain accurately, so that it can simulate stress conditions that occur in the field (Xie et al., 2020).

The triaxial testing procedure begins with the preparation of cylindrical soil samples with a height to diameter ratio of 2:1, then the samples are wrapped with rubber membranes and placed in triaxial cells. The cell pressure is applied gradually while measuring the vertical and horizontal deformation of the sample. Axial loading is applied until the sample fails or reaches a certain strain. The test results are in the form of stress-strain curves and Mohr circles which are used to determine the failure envelope and soil shear strength parameters. This data is very important for slope stability analysis, foundation bearing capacity, and other geotechnical structure designs. The triaxial test results can be seen in table 6 and Mohr Circle Diagrams in table 7 below.

Table 6. Triaxial Test Data

∑ (%)	Reading Dial	Proving Ring		
		Voltage 0.5	**Tension 1**	**Voltage 1.5**
0	0	0	0	0
0.1	7.15	6	3	6
0.2	14.3	10	7	8
0.3	21.45	12	9	10
0.4	28.6	14	10	12
0.5	35.75	16	11	14
1	71.5	25	19	23
1.5	107.25	32	24	30
2.5	178.75	41	31	40
3	214.5	44	35	45
4	286	49	41	51
5	357.5	52	45	57
6	429	54	48	61
7	500.5	54	50	64
8	572	48	51	67
9	643.5	-	49	68
10	715	-	-	64
12	858	-	-	-
14	1001	-	-	-
16	1144	-	-	-
18	1287	-	-	-
20	1430	-	-	-

Table 7. Mohr Circle Diagrams

Mohr Circle Diagrams						Corner
0.5		**1**		**1.5**		
x	**y**	**x**	**y**	**x**	**y**	
0.5000	0.0000	1.0000	0.0000	1.5000	0.0000	0
0.5600	0.6863	1.0615	0.7035	1.6012	1.1568	10
0.7383	1.3517	1.2443	1.3855	1.9017	2.2784	20
1.0295	1.9760	1.5427	2.0255	2.3925	3.3308	30
1.4246	2.5403	1.9478	2.6040	3.0585	4.2820	40
1.9117	3.0274	2.4471	3.1033	3.8796	5.1031	50
2.4760	3.4225	3.0255	3.5083	4.8308	5.7692	60
3.1003	3.7137	3.6655	3.8067	5.8832	6.2599	70

3.7657	3.8919	4.3476	3.9895	7.0049	6.5605	80
4.4520	3.9520	5.0510	4.0510	8.1617	6.6617	90
5.1382	3.8919	5.7545	3.9895	9.3184	6.5605	100
5.8036	3.7137	6.4366	3.8067	10.4401	6.2599	110
6.4280	3.4225	7.0766	3.5083	11.4925	5.7692	120
6.9923	3.0274	7.6550	3.1033	12.4437	5.1031	130
7.4794	2.5403	8.1543	2.6040	13.2648	4.2820	140
7.8745	1.9760	8.5593	2.0255	13.9308	3.3308	150
8.1656	1.3517	8.8578	1.3855	14.4216	2.2784	160
8.3439	0.6863	9.0405	0.7035	14.7221	1.1568	170
8.4040	0.0000	9.1021	0.0000	14.8233	0.0000	180

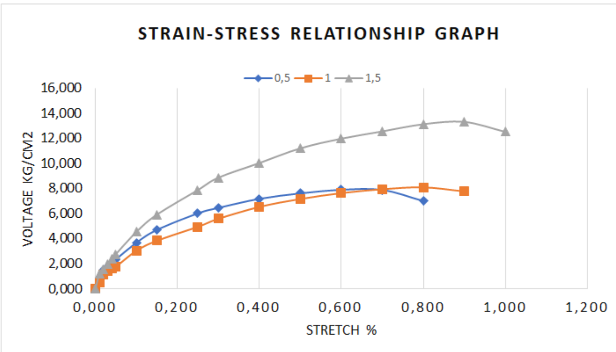

Figure 4. Strain – Stress Relationship Graph

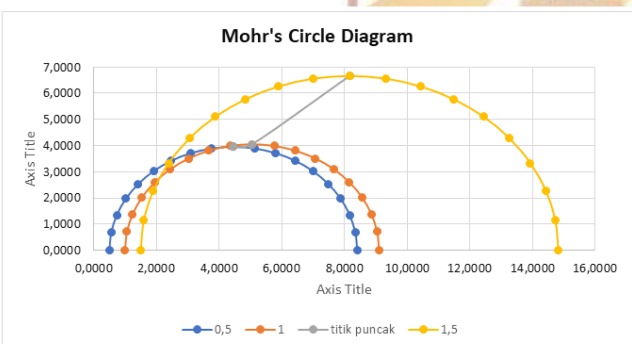

Figure 5. VisualMohr Circle Diagrams

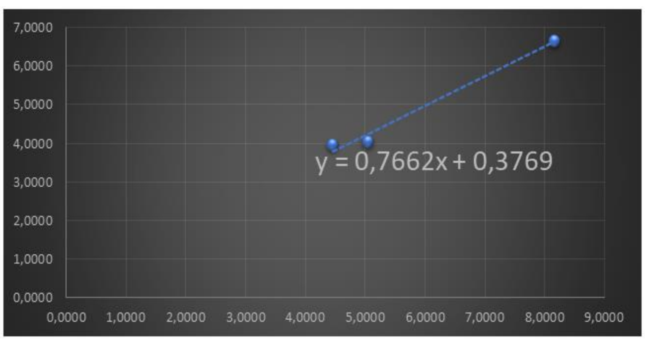

Figure 6. Linear Regression Graph

The triaxial tests performed demonstrate the application of a well-established methodology standard in geotechnics to determine soil shear strength parameters. Triaxial shear testing is the most versatile of all methods for testing soil shear strength and finding cohesion (c) and angle of internal friction (φ) (Yin et al., 2022). The test data show three different cell stress levels (0.5; 1.0; and 1.5 kg/cm²) with dial and proving ring readings reflecting the soil response to gradually increasing axial loads. A typical triaxial test involves confining a sealed cylindrical soil specimen, with a height-to-diameter ratio of 2:1, into a pressure cell to simulate defined stress conditions. This methodology allows a comprehensive evaluation of the mechanical properties of the soil under controlled conditions.

Based on the data obtained, the stress-strain response pattern shows characteristics that are consistent with the theory of soil mechanics. At a cell stress of 0.5 kg/cm², the sample reaches a maximum value of proving ring 54 at a strain of 6-7%, then decreases to 48 at a strain of 8%. For a cell stress of 1.0 kg/cm², the peak strength is reached at proving ring 51 at a strain of 8%, while at a cell stress of 1.5 kg/cm², the response continues to increase to proving ring 68 at a strain of 9%. The purpose of these procedures is to measure the triaxial shear strength of soil specimens subjected to different drainage conditions in the field. This pattern indicates that the soil exhibits strain-softening behavior at low cell stress and strain-hardening at high cell stress.

The Mohr circle diagram data shows a systematic stress distribution for each cell stress level. The marked values (4.4520; 3.9520) for stress 0.5 and (5.0510; 4.0510) for stress 1.0 probably represent the failure conditions or maximum points in the analysis. The angle α of the considered plane appears as the angle 2 α in the Mohr circle. From the Mohr-Coulomb theory, we can conclude two key things: the Mohr circle represents the stress state in the soil at a point, while the Mohr envelope represents the shear strength of the soil. The x and y coordinates in the table represent the normal and shear stresses which vary with the angle of the failure plane from 0° to 180°.

Previous studies have confirmed that from triaxial test data, it is possible to extract fundamental material parameters about the sample, including the angle of shear resistance, apparent cohesion, and dilatancy angle (Gong et al., 2020). The results of this test are in line with the principles established in the geotechnical literature. Mohr's circle is used to calculate the angle of soil internal friction and soil shear strength (Rasti et al., 2021). Shear strength is a measure of the resistance of the soil to shift or shear along its plane, where soil with higher shear strength has stronger cohesion between particles. The data obtained allows the determination of the parameters c and φ which are essential for stability analysis and geotechnical design (Doan et al., 2023).

Comparison of soil response at three cell stress levels shows behavior consistent with consolidation and shear strength theory. At a cell stress of 0.5 kg/cm², the soil exhibits brittle behavior with a decrease in strength after reaching a peak. At a cell stress of 1.0 kg/cm², the behavior becomes more ductile with a longer plateau. While at a cell stress of 1.5 kg/cm², the soil exhibits continuous strain-hardening behavior. Mohr's circle is used to determine which principal stresses will produce this combination of shear and normal stresses, and the plane angle at which this will occur. These variations in behavior reflect the influence of effective stress on soil failure mechanisms, which is very important for practical applications in foundation design and slope stability analysis (Chanyshev, 2023).

The results of this triaxial test provide a strong basis for geotechnical design parameters. Triaxial shear test is the most versatile of all shear test methods to obtain soil shear strength i.e. Cohesion (C) and Internal Friction Angle (Ø). The data obtained can be used to determine soil bearing capacity, slope stability, and retaining structure design. The different behavior patterns at each cell stress level indicate the importance of considering in-situ stress conditions in the analysis. The shear strength parameters obtained from this test should be validated with field conditions and used in numerical analysis for prediction of soil behavior on a larger scale (Patil & Pusadkar, 2022).

Conclusion

Based on the results of soil geotechnical laboratory tests in landslide-prone zones in Talamau District, West Pasaman Regency, it can be concluded that the soil sample has moderate plasticity characteristics with a Liquid Limit of 59.39%, Plastic Limit of 49.77%, and Plasticity Index of 9.62%. The soil reaches a maximum dry density of 1.37 gr/cm³ at an optimum water content of 500 ml, with a grain size distribution dominated by the sand fraction (83.978% retained on sieve No. 4-20) and a very low fine material content (1.234%). The triaxial test results show soil behavior that varies from brittle to strain-hardening depending on the level of cell stress. Overall, the soil can be classified as well-graded sand with good drainage but low cohesion, thus requiring additional stabilization for construction applications in landslide-prone areas.

Acknowledgements

The author expresses their deepest gratitude for the moral and financial support provided by Andalas University through the PDD Grant in the fiscal year 2024 (Contract No.: 28/UN16.19/PT.01.03/PDD/2024, Date: July 17, 2024).

During the research, the author received a lot of support, guidance, direction and input from various parties, therefore on this occasion the author would like to thank colleagues and lecturers in the Civil Engineering Department, Faculty of Engineering, Andalas University.

Author Contribution

N: preparation of original draft, results, discussion, methodology, conclusion; F, B. I, S. A and A: analysis, review, proofreading and editing.

Funding

This research did not receive any external funding.

Conflict of Interest

The authors declare that there is no conflict of interest regarding the publication of this paper.

References

Ahmad, S., Ghazi, M. S. A., Syed, M., & Al-Osta, M. A. (2024). Utilization of fly ash with and without secondary additives for stabilizing expansive soils: A review. Results in Engineering, 102079. https://doi.org/10.1016/j.rineng.2024.102079

Afolagboye, LO, Abdu-Raheem, YA, Ajayi, DE, & Talabi, AO (2021). A comparison between the consistency limits of lateritic fraction soils passing through sieve numbers 40 and 200. Innovative Infrastructure Solutions, 6, 1-8. https://doi.org/10.1007/s41062-020-00427-3

Alcántara-Ayala, I. (2025). Landslides in a changing world. Landslides, 1-15. tps://doi.org/10.1007/s10346-024-02451-1

Brempong, M.B., Amankwaa-Yeboah, P., Yeboah, S., Owusu Danquah, E., Agyeman, K., Keteku, A.K., ... & Adomako, J. (2023). Soil and water conservation measures to adapt cropping systems to climate change facilitated water stresses in Africa. Frontiers in Sustainable Food Systems, 6, 1091665. https://doi.org/10.3389/fsufs.2022.1091665

Bian, M., Qiu, H., & Chen, X. (2025). The Distribution Characteristics of Large Landslides Along the Daduhe River in the Eastern Tibetan Plateau and Their Effects on Landscape Evolution. Remote Sensing, 17(7), 1133. https://doi.org/10.3390/rs17071133

Bari, F., Istijono, B., Yuhendra, R., Hakam, A., Noer, M., & Ophiyandri, T. (2023, May). Potential debris flow after earthquake in Mount Talamau Pasaman district and West Pasaman district. In IOP Conference Series: Earth and Environmental Science (Vol. 1173, No. 1, p. 012069). IOP Publishing. DOI 10.1088/1755-1315/1173/1/012069

Bilal, M., Xing, A., & Hazarika, H. (2025). The Chinese loess plateau, earthquakes, and flowslides: the need to enhance geotechnical disaster resilience. https://doi.org/10.1007/s10346-024-02430-6

Chanyshev, A. (2023). A way to determine the positive direction of the shear force on the elemental area. Geohazard Mechanics, 1(2), 179-184. https://doi.org/10.1016/j.ghm.2023.04.004

Centeno, D.D. (2024, August). Socio-Spatial Analysis of Indigenous Cultural Tourism Sites: A Comparative Study of Kampoeng Wisata Cinangneng, Bogor, Indonesia and Tam-Awan Village, Baguio City, Philippines. In IOP Conference Series: Earth and Environmental Science (Vol. 1384, No. 1, p. 012023). IOP Publishing. DOI 10.1088/1755-1315/1384/1/012023

Carrière, S.R., Jongmans, D., Chambon, G., Bièvre, G., Lanson, B., Bertello, L., ... & Chambers, J.E. (2018). Rheological properties of clayey soils originating from flow-like landslides. Landslides, 15, 1615-1630. https://doi.org/10.1007/s10346-018-0972-6

Chen, J. N., Ren, X., Xu, H., Zhang, C., & Xia, L. (2022). Effects of grain size and moisture content on the strength of geogrid-reinforced sand in direct shear mode. International Journal of Geomechanics, 22(4), 04022006. https://doi.org/10.1061/(ASCE)GM.1943-5622.0002309

Doan, T., Indraratna, B., Nguyen, T.T., & Rujikiatkamjorn, C. (2023). Interactive role of rolling friction and cohesion on the angle of repose through a microscale assessment. International Journal of Geomechanics, 23(1), 04022250. https://doi.org/10.1061/(ASCE)GM.1943-5622.0002632

Das, T., Rao, V.D., & Choudhury, D. (2022). Numerical investigation of the stability of landslide-affected slopes in Kerala, India, under extreme rainfall event. Natural Hazards, 114(1), 751-785. https://doi.org/10.1007/s11069-022-05411-x

Daud, AY, Syafri, S., & Jaya, B. (2025). Landslide Disaster Mitigation Analysis in Kalukku District, Mamuju Regency. Urban and Regional Studies Journal, 7(2), 190-203. https://doi.org/10.35965/ursj.v7i2.6043

Frene, J. P., Pandey, B. K., & Castrillo, G. (2024). Under pressure: elucidating soil compaction and its effect on soil functions. Plant and Soil, 502(1), 267-278. https://doi.org/10.1007/s11104-024-06573-2

Ghoreishi, B., Khaleghi Esfahani, M., Alizadeh Lushabi, N., Amini, O., Aghamolaie, I., Hashim, NAAN, & Alizadeh, SMS (2021). Assessment of geotechnical properties and determination of shear strength parameters. Geotechnical and Geological Engineering, 39, 461-478. https://doi.org/10.1007/s10706-020-01504-1

Guzzetti, F., Gariano, S.L., Peruccacci, S., Brunetti, M.T., & Melillo, M. (2022). Rainfall and landslide initiation. In Rainfall (pp. 427-450). Elsevier. https://doi.org/10.1016/B978-0-12-822544-8.00012-3

Gong, F., Luo, S., Lin, G., & Li, X. (2020). Evaluation of shear strength parameters of rocks by preset angle shear, direct shear and triaxial compression tests. Rock Mechanics and Rock Engineering, 53, 2505-2519. https://doi.org/10.1007/s00603-020-02050-1

Hutchings, S. J., & Mooney, W. D. (2021). The seismicity of Indonesia and tectonic implications. Geochemistry, Geophysics, Geosystems, 22(9), e2021GC009812. https://doi.org/10.1029/2021GC009812

Heo, S., Sohn, W., Park, S., & Lee, D. K. (2024). Multi-hazard assessment for flood and Landslide risk in Kalimantan and Sumatra: Implications for Nusantara, Indonesia's new capital. Heliyon, 10(18). DOI: 10.1016/j.heliyon.2024.e37789

Islam, I., Ahmed, W., Rizwan, M., Ullah, S., Orakzai, A.U., & Petrounias, P. (2024). Investigating the role of geochemistry and geotechnical properties in landslide characterization and triggering mechanisms: A case study from Dir Upper, Khyber Pakhtunkhwa Pakistan. Physics and Chemistry of the Earth, Parts A/B/C, 135, 103636. https://doi.org/10.1016/j.pce.2024.103636

Innocenti, A., Rosi, A., Tofani, V., Pazzi, V., Gargini, E., Masi, E. B., ... & Casagli, N. (2023). Geophysical surveys for geotechnical model reconstruction and slope stability modeling. Remote Sensing, 15(8), 2159. https://doi.org/10.3390/rs15082159

Jastrzębska, M. (2021). Modern displacement measuring systems used in geotechnical laboratories: Advantages and disadvantages. Sensors, 21(12), 4139. https://doi.org/10.3390/s21124139

Kumar, P. (2024). Social and Economic Impact in the Landslide Prone Zones and Related Policies. In Landslides in the Himalayan Region: Risk Assessment and Mitigation Strategy for Sustainable Management (pp. 499-529). Singapore: Springer Nature Singapore. https://doi.org/10.1007/978-981-97-4680-4_22

Kausarian, H., Illahi, RR, Suryadi, A., & Sumantyo, JTS (2024, July). Soil Movement Vulnerability Zones Determination Based on RS/GIS Analysis and Geological Mapping in Koto Tinggi Area, Limapuluh Kota, West Sumatra. In IGARSS 2024-2024 IEEE International Geoscience and Remote Sensing Symposium (pp. 4864-4867). IEEE. DOI: 10.1109/IGARSS53475.2024.10642317

Lin, S., Liang, Z., Guo, H., Hu, Q., Cao, X., & Zheng, H. (2025). Application of machine learning in early warning systems of geotechnical disasters: a systematic and comprehensive review. Artificial Intelligence Review, 58(6), 168. https://doi.org/10.1007/s10462-025-11175-0

McColl, S.T. (2022). Landslide causes and triggers. In Landslide hazards, risks, and disasters (pp. 13-41). Elsevier. https://doi.org/10.1016/B978-0-12-818464-6.00011-1

Momeni, M., Bayat, M., & Ajalloeian, R. (2022). Laboratory investigation on the effects of pH-induced changes on geotechnical characteristics of clay soil. Geomechanics and Geoengineering, 17(1), 188-196. https://doi.org/10.1080/17486025.2020.1716084

Muhiddin, AB, Nur, SH, Harianto, T., Djamaluddin, R., Arsyad, A., & Suprapti, A. (2021). Dissemination of disaster mitigation in landslide-prone areas. JURNAL TEPAT: Applied Technology for Community Service, 4(2), 129-136. https://doi.org/10.25042/jurnal_tepat.v4i2.191

Nguyen, T.S., Ngamcharoen, K., & Likitlersuang, S. (2023). Statistical characterization of the geotechnical properties of Bangkok subsoil. Geotechnical and Geological Engineering, 41(3), 2043-2063. https://doi.org/10.1007/s10706-023-02390-z

Niu, W., Guo, B., Li, K., Ren, Z., Zheng, Y., Liu, J., ... & Men, X. (2024). Cementitous material based stabilization of soft soils by stabilizer: Feasibility and durability assessment. Construction and Building Materials, 425, 136046. https://doi.org/10.1016/j.conbuildmat.2024.136046

Onyelowe, KC, Mojtahedi, FF, Azizi, S., Mahdi, HA, Sujatha, ER, Ebid, AM, ... & Aneke, FI (2022). Innovative overview of SWRC applications in modeling geotechnical engineering problems. Designs, 6(5), 69. https://doi.org/10.3390/designs6050069

O'Kelly, B.C. (2021). Review of recent developments and understanding of Atterberg limits determinations. Geotechnics, 1(1), 59-75. DOI. 10.3390/geotechnics1010004

Ouyang, Z., & Mayne, P. W. (2023). Evaluating friction angles for clays: piezocone tests compared with Atterberg limits. Proceedings of the Institution of Civil Engineers-Geotechnical Engineering, 177(2), 147-157. https://doi.org/10.1680/jgeen.22.00135

Pasierb, B., Grodecki, M., & Gwóźdź, R. (2019). Geophysical and geotechnical approaches to a landslide stability assessment: a case study. Acta Geophysica, 67(6), 1823-1834. https://doi.org/10.1007/s11600-019-00338-7

Patil, LB, & Pusadkar, SS (2022, December). Performance of Black Cotton Soil Reinforced with Randomly Distributed Banana Fibers. In Indian Geotechnical Conference (pp. 27-33). Singapore: Springer Nature Singapore. https://doi.org/10.1007/978-981-97-1745-3_3

Polakowski, C., Ryżak, M., Sochan, A., Beczek, M., Mazur, R., & Bieganowski, A. (2021). Particle size distribution of various soil materials measured by laser diffraction—the problem of reproducibility. Minerals, 11(5), 465. https://doi.org/10.3390/min11050465

Pande, G. N., Pietruszczak, S., & Wang, M. (2020). Role of gradation curve in description of mechanical behavior of unsaturated soils. International Journal of Geomechanics, 20(2), 04019159. https://doi.org/10.1061/(ASCE)GM.1943-5622.0001551

Rasti, A., Adarmanabadi, H.R., Pineda, M., & Reinikainen, J. (2021). Evaluating the effect of soil particle characterization on internal friction angle. American Journal of Engineering and Applied Sciences. DOI: 10.3844/ajeassp.2021.129.138

Rakuasa, H., Budnikov, V.V., & Latue, P.C. (2025). Application of GIS Technology for Landslide Prone Area Analysis in Ambon Island, Indonesia. Journal of Geographical Sciences and Education, 3(1), 19-28. https://doi.org/10.69606/geography.v3i1.170

Shimobe, S., Karakan, E., & Sezer, A. (2021). Improved dataset for establishing novel relationships between compaction characteristics and physical properties of soils. Bulletin of Engineering Geology and the Environment, 80(11), 8633-8663. https://doi.org/10.1007/s10064-021-02456-3

Svensson, D.N., Messing, I., & Barron, J. (2022). An investigation in laser diffraction soil particle size distribution analysis to obtain compatible results with sieve and pipette methods. Soil and Tillage Research, 223, 105450. https://doi.org/10.1016/j.still.2022.105450

Sohel, R., Nie, Z., Ali, S., & Ismail, AS (2024, May). Impact of Industrial Solid Waste on Soil Geotechnical Properties. In IOP Conference Series: Earth and Environmental Science (Vol. 1335, No. 1, p. 012030). IOP Publishing. DOI 10.1088/1755-1315/1335/1/012030

Shimobe, S., & Spagnoli, G. (2022). A general overview on the correlation of compression index of clays with some geotechnical index properties. Geotechnical and Geological Engineering, 40(1), 311-324. https://doi.org/10.1007/s10706-021-01888-8

Usman, F., & Sumantyo, JTS (2022). Prediction of Ground Surface Deformation Induced by Earthquake on Urban Area Using Machine Learning. Science and Technology Indonesia, 7(4), 435-442. https://doi.org/10.26554/sti.2022.7.4.435-442

Vitali, M., Corvaro, F., Marchetti, B., & Terenzi, A. (2022). Thermodynamic challenges for CO2 pipelines design: A critical review on the effects of impurities, water content, and low temperature. International Journal of Greenhouse Gas Control, 114, 103605. https://doi.org/10.1016/j.ijggc.2022.103605

Woldesenbet, T.T., Arefaine, HB, & Yesuf, MB (2023). Numerical stability analysis and geotechnical investigation of landslide prone area (the case of Gechi district, Western Ethiopia). Environmental Challenges, 13, 100762. https://doi.org/10.1007/s12665-023-11133-5

Wazoh, H.N., & Mallo, S.J. (2021). Implications of the engineering geological properties of soils in the Implementation of the Greater Jos Master Plan, North Central Nigeria. European Journal of Engineering and Technology Research, 6(5), 118-128. DOI. 10.24018/ejeng.2021.6.5.2530

Xie, H., Lu, J., Li, C., Li, M., & Gao, M. (2022). Experimental study on the mechanical and failure behaviors of deep rock subjected to true triaxial stress: A review. International Journal of Mining Science and Technology, 32(5), 915-950. https://doi.org/10.1016/j.ijmst.2022.05.006

Yin, Z., Zhang, Q., Zhang, X., Zhang, J., & Li, X. (2022). Shear strength of grouted clay: comparison of triaxial tests to direct shear tests. Bulletin of Engineering Geology and the Environment, 81(7), 261. https://doi.org/10.1007/s10064-022-02739-3

Dokumentasi Percobaan

Lampiran 1 Lokasi Pengambilan Sampel

Lampiran 2 Sampel setelah penjemuran

Lampiran 3 Pengujian Sampel di labortorium

Lampiran 4 Pemadatan lereng pada model percobaan

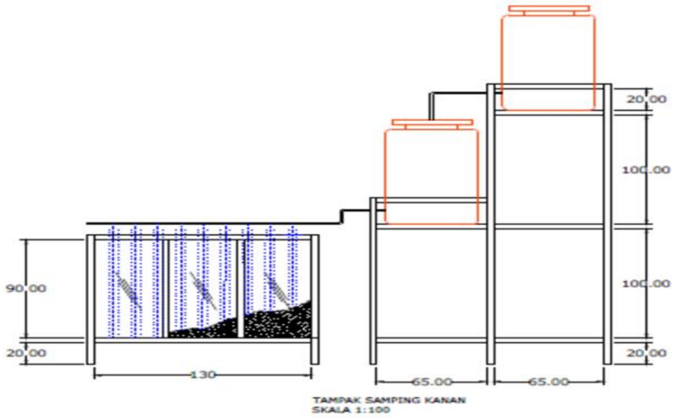

Lampiran 5 Model lereng dan simulator hujan

Lampiran 6 Dokumentasi percobaan keruntuhan untuk sudur lereng 45

Lampiran 7 Dokumentasi percobaan tren curah hujan pada